Changing Patterns of Tropospheric Variability in the North Atlantic Region

Dissertation
zur Erlangung des Doktorgrades
der Naturwissenschaften im Fachbereich
Geowissenschaften
der Universität Hamburg

vorgelegt von

Katrin Walter
aus
Hamburg

Hamburg
2003

Als Dissertation angenommen vom Fachbereich Geowissenschaften
der Universität Hamburg

auf Grund der Gutachten von Herrn Priv. Doz. Dr. H.-F. Graf
und Herrn Prof. Dr. K. Fraedrich

Hamburg, den 25.11.2003

Prof. Dr. H. Schleicher
Dekan des Fachbereichs Geowissenschaften

Abstract

The tropospheric variability in the winterly Northern Hemisphere is closely coupled to the variability in the stratosphere. Changes in the strength of the stratospheric polar vortex are related to changes in the planetary wave structure in the troposphere. The polar vortex strength is mainly characterized by two regimes: weak and strong. It is examined how this affects the structure of low frequency teleconnections in the North Atlantic region with regard to the North Atlantic Oscillation (NAO). Changes in the structure and the frequency domain of the NAO and the consequences for the covariability with North Atlantic sea surface temperature (SST) are studied. This is achieved by examining both reanalysis data from the U.S. National Centers for Environmental Prediction/National Center for Atmospheric Research (NCEP/NCAR) and the Kaplan SST dataset.

Teleconnections of North Atlantic mid to upper tropospheric geopotential height are examined separately for the two regimes of the stratospheric polar vortex. In both cases, the major teleconnection patterns have north-south dipole structures with opposing centers of action in subpolar and subtropical latitudes. The strong polar vortex case is characterized by a single pattern over the central North Atlantic, whereas there are two patterns in the weak vortex case: one over the western North Atlantic/northeastern Canada and one over the eastern North Atlantic. The growth of streamfunction anomalies related to these teleconnection patterns reveals to be characterized by different dynamical processes. In the weak vortex regime, the growth is mainly driven by transient eddy fluxes, whereas, in the strong vortex regime, forcing resulting from interaction of low frequency transients (periods ≥ 10 days) with stationary eddies is equally important. Composites of the North Atlantic storm track and monthly mean precipitation rates reveal to be dependent on both, the teleconnection pattern and its polarity. Hence, a large part of the tropospheric variability cannot be explained in the classical framework of the NAO without considering the polar vortex strength.

Evidence is presented that not only the structure of the teleconnection patterns but also the covariation between the winterly atmospheric flow and SST is not stationary in the North Atlantic region. During the recent decades since the late 1960s/early 1970s and during the first three decades of the 20th century, the North Atlantic SST is strongly connected with the regional atmospheric circulation in the North Atlantic sector, i.e. the NAO. During these periods the NAO index – defined as the difference of normalized sea level pressures at the Azores and Iceland – is characterized by pronounced decadal variability. In contrast, the NAO index is only weakly correlated with the North Atlantic SST from the 1930s to the early 1960s, when the NAO index is characterized by weak decadal variability. Remote influences, in particular from the tropical Pacific region, become important especially for the SST in the western tropical North Atlantic.

Contents

Chapter 1

Introduction

The wintertime circulation over the North Atlantic and western Europe is strongly influenced by the North Atlantic Oscillation (NAO). It is the dominant mode of variability in the North Atlantic region and is characterized by a meridional oscillation in atmospheric mass between centers of action near Iceland and over the subtropical Atlantic, leading to a concurrent variation in the strength of the Iceland low and the Azores high (Walker and Bliss, 1932; Glowienka-Hense, 1990; Hurrell, 1995; Hurrell and van Loon, 1997). The NAO shows variability on all timescales with pronounced low-frequency fluctuations. It is most noticeable during boreal winter and is associated with changes in speed and direction of the wind in the North Atlantic sector, and in particular with a meandering of the subtropical jet. Changes in the NAO affect heat and moisture transports between the North Atlantic ocean and the continents as well as the intensity, number and paths of synoptic disturbances. The NAO therefore strongly influences the weather in the North Atlantic region and in particular over Europe. Fluctuations in the NAO are furthermore related to changes in sea surface temperature (SST), ocean currents and their heat transport as well as to variations of sea ice cover in Arctic regions. Hence, the NAO is of strong interest for economy, agriculture and fishery in the North Atlantic region.

The climatic processes governing the NAO are not fully understood up to now. Several studies suggest that external parameters influence low-frequency variations of the NAO such as solar radiation (Cubasch et al., 1997) or volcanic eruptions (Graf et al., 1994), but also internal processes in the atmosphere (James and James, 1989) as well as interactions with other climate subsystems have the potential to induce low-frequency variability. Modeling experiments with coupled atmosphere-ocean general circulation models (GCMs) show that dynamic interactions between ocean and atmosphere (e.g. Latif and Barnett, 1994; 1996) as well as interactions between the troposphere and the stratosphere (Perlwitz

et al., 2000) may influence the low-frequency variability in the atmosphere.

Troposphere-stratosphere interaction

During winter, the circulation in the Northern Hemispheric lower to middle stratosphere is characterized by strong and almost zonally symmetric westerly flow in subpolar latitudes, whereas weaker easterly winds dominate during summer. The winterly flow pattern is referred to as the stratospheric polar vortex. It is mainly thermally driven owing to the cooling of the northern polar region which is associated with the substantial reduction of incoming solar radiation in winter. The vortex thus usually forms in early winter, whereas it normally decays in late winter to early spring ('Final Warmings') when the circulation changes back to the summer situation. However, the vortex may also be subject to disturbances during high winter. Such events are associated with warming of the polar stratosphere, i.e. with a reversal of the meridional temperature gradient, but do not always lead to a change towards easterly winds in the stratosphere, i.e. to a breakdown of the vortex. Warming events that cause such breakdowns are named 'Major Midwinter Warmings'. The center of the polar vortex is then often displaced to latitudes south of 60°–65°N or is splitted into several small vortices.

The strength of the winter mean stratospheric polar vortex is characterized by a regime-like behavior. In his examination of probability density Christiansen (2003) showed that the first Principal Component timeseries of winter mean geopotential heights in the middle and lower stratosphere — describing variations in the strength of the polar vortex — has a bimodal probability density distribution. This indicates that the strength of the stratospheric polar vortex is characterized by two regimes in which the vortex is either primarily strong or weak. Christiansen (2003) admits that the results are not as clear for monthly means, but Perlwitz and Graf (2001b) also reported bimodality in the distribution of anomaly correlations of the monthly mean zonal mean zonal wind at the 50 hPa level.

Fluctuations in the strength of the stratospheric polar vortex are assumed to be mainly caused by the interaction of upward propagating planetary waves from the troposphere with the (zonal) mean flow in the stratosphere (Matsuno, 1970). However, also several external factors have the potential to influence the intensity of the stratospheric polar vortex and the probability for the development of a Major Midwinter Warming. Fluctuations in solar radiation were found to be related to fluctuations in the stratosphere: Labitzke and van Loon (1988) detected a 10–12 year oscillation in lower stratospheric temperature and geopo-

tential height. This oscillation reveals to be in phase with the 11 year solar cycle. Labitzke (1987) furthermore reported an influence of the Quasi-Biennial Oscillation (QBO) on the probability for a breakdown of the vortex. The QBO is an almost 2 year-fluctuation between phases with either easterly of westerly winds in the tropical stratosphere. During a solar maximum, mid-winter breakdowns of the vortex appear to occur mainly if the QBO is in its westerly phase, whereas during a solar minimum breakdowns mainly happen in the easterly QBO phase (Labitzke, 1999). During the past 2–3 decades, the polar vortex significantly strengthened (Graf et al., 1995; Perlwitz and Graf, 1995; Kodera and Koide, 1997; Thompson and Wallace, 1998). This can at least in part be explained by the increasing anthropogenic emission of greenhouse gases: Sensitivity experiments with comprehensive climate models show that the polar vortex continously intensifies with increasing concentration of greenhouse gases (Graf et al., 1995; Shindell et al., 1999). A possible mechanism for the greenhouse-gas-induced modification of the polar vortex strength is presented by Perlwitz and Graf (1995): The polar vortex is initially intensified by the lifting of lower latitude geopotential height layers due to increasing temperature and humidity in tropospheric lower latitudes. Moreover, violent volcanic eruptions in the tropics may lead to a strengthened temperature gradient and, thus to a stronger vortex due to the absorption of long-wave and near-infrared radiation in the tropics (Labitzke and van Loon, 1996). Ramaswamy et al. (1996) and Graf et al. (1998) showed that an intensified vortex at the and of winter may also be related to the decrease in the stratospheric ozone concentration in lower latitudes.

It has been shown in numerous studies that the tropospheric variability is strongly coupled with the variability in the lower and middle stratosphere in winter. In their examination of Eliassen-Palm flux divergences (see Edmon et al., 1980) Chen et al. (2002) detected a close connection between the troposphere and the lower stratosphere in Northern Hemispheric midlatitudes, whereas the upper stratosphere reveals to be connected to the tropical troposphere, and in particular to that in the tropical Pacific region.

In order to isolate quasi-stationary modes of coupled stratospheric-tropospheric variability in the Northern Hemisphere extratropics, multivariate methods like Singular Value Decomposition (SVD) analysis (Baldwin et al., 1994; Perlwitz, 2000) and Canonical Correlation Analysis (CCA; Perlwitz and Graf, 1995) have been applied. Perlwitz and Graf (1995) found that, on the basis of monthly means, the linearly coupled variability of Northern Hemispheric 500- and 50 hPa geopotential height data can mainly be described by two modes. On the basis of winter mean data (December to March), however, Baldwin et al. (1994) showed that the leading mode dominates by far. The leading coupled variability mode for monthly or seasonal means describes a connection between the strength of the stratospheric polar vortex and a tropospheric geopotential height structure

which is characterized by a large degree of zonal symmetry. However, the tropospheric pattern also exhibits a wavetrain-like structure over the North Atlantic and Europe (Baldwin et al., 1994; Perlwitz and Graf, 1995). The second coupled mode describes a connection between a wavetrain in the troposphere reaching over the North Pacific and North America and a wave-like pattern in the stratosphere. The latter is associated with perturbations of the stratospheric polar vortex by waves of zonal wavenumbers 1 and 2. The second coupled mode reveals to be related to fluctuations of the SST in the tropical Pacific on interannual timescales (Perlwitz and Graf, 1995; Kodera et al., 1996).

The tropospheric pattern of geopotential height variability associated with the leading coupled mode strongly resembles the Northern Annular mode (NAM; Thompson and Wallace, 2000). The surface imprint of this mode is also often referred to as the Arctic Oscillation, which was derived by Thompson and Wallace (1998) as the leading coupled Empirical Orthogonal Function (EOF) of Northern Hemispheric sea level pressure. The horizontal structure of the NAM is characterized by a large degree of zonal symmetry, with a primary center of action governing the entire Arctic basin and opposing centers over the midlatitude North Atlantic and North Pacific. The vertical structure is mainly equivalent barotropic, while the zonally symmetric component amplifies from the surface up the the stratosphere (Thompson and Wallace, 2000). Thompson and Wallace (1998) suggested that the NAO may be part of the NAM (or the Arctic Oscillation). Deser (2000), however, presented evidence that for seasonal mean data the connection to the Pacific basin is negligible compared to the connection between the Atlantic and the polar region. This finding is supported by Castanheira and Graf (2003) who showed that sea level pressures on the Azores and in the North Pacific region are not significantly correlated all the time. They found a significant correlation only for winter months in which the stratospheric polar vortex is strong.

The leading coupled mode can be exaggerated by both, stratospheric and tropospheric processes (Graf et al., 1997). It is widely assumed in literature that the leading coupled mode of the Northern Hemispheric circulation in winter evolves from interactions between tropospheric planetary waves and the mean flow in the stratosphere described e.g. by Matsuno (1970). Planetary waves that are generated in the troposphere by heat sources and orography propagate upwards. They can change the stratospheric flow when they break and get absorbed. Evidence for downward propagation of low-frequency anomalies from the stratosphere to the surface was presented by Baldwin and Dunkerton (1999). The largest of such anomalies originate above 1 hPa and descend through the stratosphere within 1–2 weeks (Baldwin and Dunkerton, 2001). However, the analyses presented by Baldwin and Dunkerton (2001) also suggest that, in general, only the strongest anomalies of either sign appear to connect to the surface, whereas

weaker anomalies typically remain within the stratosphere. Hence, most high frequency variations in the troposphere appear to be unrelated to the stratosphere. This corresponds to the findings of Perlwitz (2000), indicating that a forecast potential for the phase of the NAO from the strength of the stratospheric polar vortex only exists when changes between the polar vortex regimes occur. Moreover, Castanheira et al. (2001) showed that the stratospheric polar vortex and the NAO constitute different normal modes of the atmosphere, which are only connected to some degree.

A mechanism for a downward influence linking the strength of the lower stratospheric polar vortex with NAM-like anomalies in the troposphere was suggested by Hartley et al. (1998), Ambaum and Hoskins (2002), and Black (2002). The mechanism is based on the fact that large-scale anomalies of potential vorticity in the lower stratosphere induce geopotential height perturbations in the polar troposphere through hydrostatic and geostrophic adjustment of the atmospheric column. A strong polar vortex in the lower stratosphere is then associated with anomalously low pressure in the troposphere near the pole. This represents a large-scale annular stirring of the troposphere from above.

Another mechanism by which the stratosphere can influence the tropospheric flow was proposed by Hines (1974). This mechanism is based on the idea that the zonal winds in the stratosphere strongly influence the refractive index and, thus, the propagation/reflection characteristics of upward propagating waves and their interaction with the mean flow (Charney and Drazin, 1961; Matsuno, 1970; Andrews et al., 1987). If the the zonal mean zonal wind in the stratosphere exceeds a critical velocity, planetary waves that propagate upward from the troposphere are reflected downward and in meridional direction. The reflected waves re-influence the planetary wave pattern in the troposphere. This may also induce changes in the zonal mean flow and in the transient eddy structure. The critical velocity depends on the wavenumber and the latitude, meaning that, under winter conditions, only very long waves have the possibility to reach the stratosphere in middle and high latitudes — if the critical velocity is not exceeded (Charney and Drazin, 1961; Perlwitz, 2000). Limpasuvan and Hartmann (2000) and Hu and Tung (2002) found that such reflection takes place near the tropopause rather than in the lower stratosphere. They showed that the vertical propagation of planetary waves with zonal wavenumber 1 is more effectively impeded near the tropopause in years with high phase of the NAM than in years with low NAM. Hu and Tung (2002) argued that this is associated with changes in the refractive index near the subpolar tropopause, which can be mainly attributed to changes in the strength of the zonal wind there. This means that, in the high NAM phase — characterized by strong westerly winds near the subpolar tropopause — a larger fraction of ultra-long planetary waves is reflected downward or in meridional direction (mainly equatorward) and therefore does

not reach the stratosphere, The stratospheric polar vortex is then less disturbed than in the low NAM phase. Limpasuvan and Hartmann (2000) concluded that, therefore, the high NAM phase is mostly related to a strong stratospheric polar vortex. Perlwitz and Harnik (2003) presented evidence for downward reflection in the upper stratosphere. They showed that a strong vertical curvature of the zonal wind profile associated with negative shear in the upper stratosphere is related to enhanced (downward) reflection of upward propagating waves with zonal wavenumber 1. The reflected waves do not disturb the polar vortex due to a clear meridional waveguide in the lower to middle stratosphere. This waveguide channels the reflected wave activity back to the high latitude troposphere and prevents it from getting absorbed in the stratosphere. Since Perlwitz and Harnik (2003) found that, on seasonal timescales, an enhanced negative wind shear in the upper stratosphere is related with a strong polar vortex in the lower stratosphere, they argued that there is more downward reflection in years with a strong polar vortex. This corresponds to the findings of Perlwitz and Graf (2001a), who detected a significant feedback between stratosphere and troposphere for waves with zonal wavenumber 1 only in years with extraordinarily strong vortex.

This thesis does not attempt to identify the atmospheric level at which the selective reflection is most effective. However, it may be assumed that a large fraction of the ultra-long planetary waves is reflected during periods in which the stratospheric polar vortex is strong, whereas this is less so in the weak vortex case. The modified reflection/transmission properties lead to changes in the tropospheric stationary wave pattern. This also affects the transient variability structure. Graf and Castanheira (2001) showed that the leading modes of monthly mean 500 hPa geopotential height variability in the Northern Hemisphere winter are characterized by very different structures in the strong and weak vortex regime. This implies that the interaction between troposphere and stratosphere may also influence the structure of the NAO.

Interaction between atmosphere and ocean

Many studies suggest that atmosphere-ocean interaction is a determining factor for both the atmospheric and the oceanic circulation in the North Atlantic region. It has long been recognized that fluctuations in sea surface temperature (SST) and NAO are related (Bjerknes, 1964). The atmospheric circulation can influence the ocean by changing surface fluxes of heat, momentum, and fresh water. Cayan (1992) analyzed composites of winter months characterized by positive and negative NAO. He concluded that the NAO is responsible for generating systematic large-amplitude anomalies of wind speed, latent and sensible heat fluxes, and hence of sea surface temperature over much of the extratropi-

cal North Atlantic. Deser and Blackmon (1993) and Kushnir (1994) found that the interannual to quasi-decadal SST variation in the North Atlantic is strongly correlated to the atmospheric circulation over that area. This conclusion is supported by experiments with an ocean general circulation model (OGCM) showing that realistic large-scale SST anomalies can be produced with prescribed observed atmospheric forcing (Luksch, 1996). Grötzner et al. (1998) suggested from a coupled GCM experiment that the wind driven circulation in the North Atlantic may be characterized by decadal cycles in the subtropical gyre, which incorporates the tropical and midlatitude North Atlantic Ocean. The atmospheric circulation may even have the potential to influence the thermohaline circulation (Timmermann et al., 1998; Delworth and Dixon, 2000).

However, uncertainty and ambiguity exists regarding the influence of the midlatitude ocean on the atmospheric circulation. Numerous experiments with more or less simplified atmospheric models and prescribed SST anomalies suggest that there might be some influence of the midlatitude ocean on the atmospheric circulation (e.g. Kushnir and Held, 1996; Peng et al., 1997; Peng and Whitaker, 1999; Walter et al., 2001), although the strength of the atmospheric response most likely depends on the atmospheric circulation itself, i.e. on the activity of synoptic eddies, and on the ability of the models to capture those fluctuations. Rodwell et al. (1999), Latif et al. (2000), and Mehta et al. (2000) were able to reconstruct especially the multiyear fluctuations of the NAO index in ensemble model experiments with prescribed observed SST anomalies, suggesting that the NAO would be predictable if the SST anomalies could be predicted. However, as stated by Mehta et al. (2000) those results are strongly influenced by the ensemble size. Bretherton and Battisti (2000) argue that one must be careful in using these AGCM runs with prescribed SST for interpreting the variability of the coupled system: The ensemble averaged surface energy fluxes in the prescribed-SST runs appear to damp the low-frequency SST anomalies, whereas in nature they act to drive them. Barsugli and Battisti (1998) presented evidence that coupling between atmosphere and ocean in midlatitudes acts to enhance the variance in both media and to decrease the energy flux between them.

The SST in the North Atlantic is not only influenced by the atmospheric NAO phenomenon. Numerous studies with observational or reanalysis data (e.g. Hastenrath et al., 1987; Curtis and Hastenrath, 1995; Nobre and Shukla, 1996; Enfield and Mayer, 1997; Hastenrath, 2000) and several modeling studies (Hameed et al., 1993; Saravanan and Chang, 2000) suggested that the El Niño/Southern Oscillation phenomenon (ENSO) considerably influences the SST in the tropical North Atlantic. Warm SST events in the tropical Pacific are accompanied by positive SST anomalies in the (western) tropical North Atlantic. Hastenrath (2000) and Nobre and Shukla (1996) presented evidence that the link between the tropical Pacific and the North Atlantic region might be ac-

complished — possibly through barotropic Rossby wave propagation (Hoskins and Karoly, 1981) — by a wavetrain-like teleconnection pattern extending from the equatorial Pacific across North America to the North Atlantic. Curtis and Hastenrath (1995) showed that, in January, the subtropical high over the North Atlantic and, thus, the meridional pressure gradient is weakened during Pacific warm phases, which implies weakened northeast tradewinds, and, as primary consequences, reduced latent heat fluxes in the tropical North Atlantic and anomalous Ekman downwelling (i.e. reduced upwelling) equatorward of 20°N. In the subsequent months this results in warm SST anomalies in the tropical North Atlantic.

In most studies, the correlation between oceanic and atmospheric variables in the North Atlantic region is regarded as stationary, i.e. not changing much with time. However, the atmospheric circulation in the North Atlantic region in terms of the variability of the NAO index has not been uniform since the beginning of the observations in the 19th century, and before, as can be inferred from proxy data (Appenzeller et al., 1998). Raible et al. (2001) presented evidence that the correlation between NAO and North Atlantic SST may not be independent of the structure of NAO variability. They found that, in a 600 year experiment with the coupled GCM ECHAM4/HOPE, the strength of the correlation between the NAO and the North Atlantic SST is sensitive to the decadal variability of the NAO. They detected two different regimes of North Atlantic atmosphere–ocean interaction connected with the strength of the decadal variability of NAO: During periods in which the NAO shows high variability on the decadal timescale the North Atlantic SST is strongly correlated to the NAO, whereas this correlation is weaker during periods characterized by weak decadal variability of the NAO. The latter mode is characterized by a strong PNA pattern linking the tropical Pacific region and the North Atlantic region.

A better understanding of the mechanisms influencing the spatio-temporal variability of the NAO on interannual to interdecadal timescales is required for improving the predictability in the North Atlantic region. This thesis concentrates on structural and temporal inhomogeneities of the wintertime NAO during the last four to five decades. The interaction between stratosphere and troposphere has the potential to induce structural changes of atmospheric teleconnection patterns. Structural changes as well as changes in the frequency spectrum of the NAO may have a direct influence on the interaction with the ocean via the generation of sea surface temperature (SST) anomalies. Data from from the U.S. National Centers for Environmental Prediction/National Center for Atmospheric Research (NCEP/NCAR) reanalysis dataset (Kalnay et al., 1996; Kistler et al., 2001) were primarily used for the examinations in this thesis, but also other datasets reconstructed on the basis of observations were employed. The data sources are introduced and discussed in chapter 2. The leading coupled

mode of tropospheric and lower stratospheric variability is discussed in chapter 3. Regimes are defined for the strength of the stratospheric polar vortex, and forcing mechanisms acting on the time mean flow are examined by analyzing the Eliassen-Palm flux (Edmon et al. 1980) and single terms of the time mean streamfunction tendency equation (Cai and van den Dool, 1994; Feldstein, 1998). Chapter 4 illustrates the structural changes in the North Atlantic teleconnection patterns in the vicinity of the different polar vortex regimes. The lifecycles of geopotential height (or streamfunction) anomalies associated with the North Atlantic teleconnection patterns are examined and involved dynamical processes are discussed. Furthermore, impacts on storm tracks, precipitation, SST, and other (atmospheric) variables in the North Atlantic sector are investigated. In chapter 5, it is examined if the ocean-atmosphere connection in the North Atlantic region remained unchanged throughout the 20th century. Nonstationarity would be associated with changes in the relative importance of remote influences from outside the North Atlantic sector on the SST. For this purpose, concurrent variations of the wintertime NAO, geopotential height, and SST are discussed. An overview with a discussion of the results and an outlook are given in chapter 6.

Chapter 2

Data and methods

This thesis focuses on changes in the spatial patterns and the temporal variability structure atmospheric teleconnections in the North Atlantic region during the last four to five decades. The connection with stratosphere-troposphere coupling and with sea surface temperature is examined in reanalyses an observations. This chapter presents the datasets employed for this thesis as well as methods of data processing.

2.1 Datasets

Two datasets were employed for this thesis:

- reanalysis data from the National Centers for Environmental Prediction/National Center for Atmospheric Research (NCEP/NCAR; Kalnay et al., 1996; Kistler et al., 2001) and
- the sea surface temperature (SST) dataset by Kaplan et al. (1997; 1998).

The analyses presented in this thesis are mainly based on NCEP/NCAR reanalysis data (Kalnay et al., 1996; Kistler et al., 2001), covering the years 1948 to present. Several variables were used, which are stored on different grids: geopotential height, air temperature, vorticity, and wind (at various levels), as well as sea level pressure are stored on a $2.5° \times 2.5°$ grid. In contrast sea surface temperature (SST) and precipitation rates, are stored on a Gaussian 192×94 grid (approx. $1.875° \times 1.9°$).

The NCEP/NCAR reanalysis dataset is known to be affected by two major changes in the observing system (Kistler et al., 2001): The first was from 1948 to 1957, when the upper-air operational network was established. The second change took place in 1979 due to the introduction of satellite data. The changes in the observational data basis lead to the generation of jumps and spurious trends. Kistler et al. (2001) therefore recommended not to estimate trends with the reanalysis. Pawson and Fiorino (1999) showed that, in the tropics, reanalyzed stratospheric NCEP/NCAR temperatures near the tropopause underwent a large discontinuous increase near 1979, when satellite-based observations became available. This finding is supported by Perlwitz (2000) who compared 50 hPa and 500 hPa geopotential heights from NCEP/NCAR reanalyses with observational datasets: the observational long term dataset from the Freie Universität Berlin (FUB, Pawson et al., 1993) of stratospheric geopotential heights and temperatures and the National Center of Meteorology (NMC) dataset of 500 hPa geopotential height data. She concluded that data from the Southern Hemisphere (SH) and the low latitudes of the Northern Hemisphere (NH) before the incorporation of satellite data should not be used for studies on climate change. In contrast, reanalysis data after 1958 from NH mid- and high latitudes in boreal winter and NH high latitudes in boreal summer revealed to be quite reliable for analyzing trends: Perlwitz (2000) showed that the expansion coefficients of the first two coupled modes of NH mid- and high latitude 50- and 500 hPa geopotential heights for winter months show strong agreement between NCEP/NCAR reanalyses after 1958 and the observational datasets (FUB/NMC). Thus, stratospheric NCEP/NCAR reanalyses from the NH extratropics after 1958 can quite reliably be used for studying coupled interannual stratospheric-tropospheric variability in winter, whereas upper-level data before 1958 should be handled with caution. This agrees to the finding of Kistler et al. (2001), who detected that the reliability of especially the upper-level reanalyses in the Southern Hemisphere suffers from the lack of upper-air observations before the satellite era, and in particular before 1958. In contrast, they found that, in the Northern Hemisphere extratropics, the reanalysis provides fairly accurate initial conditions for forecasts in lower levels, even before 1958.

Reid et al. (2001) showed that the reliability of daily precipitation rates in NCEP/NCAR reanalyses is limited, especially in areas and periods of high convective precipitation (e.g. in summer). However, the reliability of precipitation rates is larger during winter. Only wintertime (monthly mean) precipitation rates were examined in this thesis. Moreover, this thesis does not attempt to discuss the amount of precipitation at single points. Only large scale anomalies are discussed if they correspond to the direction and strength of the storm tracks.

Another dataset used in chapter 5 is the sea surface temperature (SST) dataset by Kaplan et al. (1997; 1998). It is based on observations and covers also the

first half of the 20th century, which is not captured by the NCEP/NCAR reanalysis. For deriving the dataset, optimal smoothing on EOF (Empirical Orthogonal Function, see appendix B.4) basis has been applied to monthly anomalies from the UK Meteorological Office historical sea surface temperature dataset (version MOHSST5) of the Global Ocean Surface Temperature Atlas (GOSTA). The data record ranges from 1856 to 1991 with a spatial resolution of $5° \times 5°$. However, the observational data basis in the North Atlantic region is especially sparse until about 1900. Thus, only data from 1900 to 1991 was used here.

2.2 Data processing

Chapter 3 and 4 concentrate on coupled variability between the stratosphere and the troposphere in winter. Thus, only NCEP/NCAR reanalysis data covering the period 1958 to 1998 were used for the examinations presented in those chapters. The stratospheric data were restricted to the Northern Hemisphere north of 30°N. Daily mean as well as monthly mean data were employed for the analyses in those two chapters. In the case of the daily mean data, the annual cycle was removed by subtracting Fourier harmonics corresponding to periods of 1 and 0.5 years, whereas in the case of the monthly mean data this was accomplished by subtracting the long-term mean of the corresponding month from each monthly mean. After removing the annual cycles the data processing was restricted to the winter season (November to April). The long-term winter means were subtracted from the data, which was afterwards detrended by subtracting a 10-year running mean. This procedure also removes a part of the decadal to interdecadal fluctuations. However, the focus of chapters 3 and 4 is on monthly to interannual variability, and the influence of the running means on the results presented in the following chapters reveals to be rather weak, anyway. Since this study concentrates on high winter, only the months December to March were considered for most of the analyses.

Chapter 5 of this thesis focuses on the large-scale interannual and decadal variability near or at the surface and in the midtroposphere. Concurrent variations of tropospheric geopotential heights and SST and their relations to the North Atlantic Oscillation are examined by means of correlation and regression analysis. Hence, the variables discussed in that chapter are the SST and the 1000- and 500 hPa geopotential heights. Upper level data is not examined in this context so that it is justified to use NCEP/NCAR reanalysis data from the extended period 1949 to 1998. January-to-March (JFM) means are discussed throughout chapter 5 because the centers of action of the North Atlantic Oscillation (NAO) are most pronounced during that season. However, the main features remain the same for December-to-February (DJF) means. Every analysis was performed

with raw as well as with detrended data in order to assess possible influences from trends. It turned out that correlation and regression maps from raw data are to be very similar to the ones presented in chapter 5 and, thus, do not seem to be dependent on linear trends. When using 500 hPa geopotential height data, we only discuss the Northern Hemisphere extratropics in order to omit the uncertainties in tropical and Southern Hemispheric data. The results derived from analyses with sea surface temperature and 1000 hPa geopotential height data, however, reveal to be reliable in the regions of interest (in the Northern Hemisphere) because the features discussed in section 3 can be fairly well reproduced with a different sea surface temperature dataset (the Kaplan SST dataset) and mean sea level pressure datasets, e.g. updates of the dataset used by Jones (1987) and of the NCAR mean sea level pressure dataset described by Trenberth and Paolino (1980).

2.3 Stratospheric polar vortex and regimes

In the discussion of the coupled stratospheric-tropospheric circulation in chapters 3 and 4, the stratospheric part is represented by the variability at the 50 hPa level. This has two major reasons: The first, a purely technical one, is that the uppermost level in many models (and also in the NCEP/NCAR reanalysis model) is at about 10 hPa. This means that realistic results can only be expected up to the 30 hPa level. The second reason is more physical: Chen et al. (2002) showed that the tropospheric E-P flux divergence in NH mid- and high latitudes is strongly coupled to the E-P flux divergence in the lower stratosphere, whereas upper levels in the stratosphere seem to be more connected to the tropospheric low latitudes. Black (2002) studied the downward propagation of Potential Vorticity anomalies in the stratosphere and argued that only anomalies from the lower stratosphere (i.e. from below 30 hPa) contribute significantly to the observed west wind anomalies in the troposphere.

Christiansen (2003) and Perlwitz and Graf (2001b) presented evidence that the strength of the stratospheric polar vortex is characterized by two regimes in which the vortex is either strong of weak. Periods characterized by either a strong or a weak stratospheric polar vortex are therefore discussed separately in chapter 3 and 4. The zonal mean zonal wind at 50 hPa and 65°N proved to be a good indicator for the strength of the polar vortex. It is shown in chapter 3 that it is reasonable to add all those months to the strong vortex regime (SVR) in which the monthly and zonal mean zonal wind at 50hPa and 65°N is stronger than 20m/s and all those in which it is weaker than 10m/s to the weak vortex regime (WVR; see also Castanheira and Graf, 2003). These thresholds approximately correspond to the average wind plus/minus a half standard deviation of the extended winter

season from November to April. Since we examined the months December to March (DJFM) only, the strong polar vortex regime (SVR) comprises 71 months (2146 days), whereas 32 months (971 days) belong to the weak polar vortex regime (WVR). Castanheira and Graf (2003) excluded the months with easterly wind from the WVR in order to omit strong warming events. During the DJFM season, however, there were only three months with (weak) easterly wind. The results presented in this these are not affected much by them. The monthly and zonal mean zonal wind used for separating the polar vortex regimes was not detrended and the seasonal cycle was not removed. The use of monthly means for the definition of polar vortex regimes reflects the characteristic timescale of stratospheric variability of several weeks (Baldwin and Dunkerton, 2001). This is much longer than the typical timescales of e.g. the NAO, which is in the order of 10 days (Feldstein, 2000) to two weeks (Feldstein, 2003).

Chapter 3

Coupled stratospheric-tropospheric circulation

It has been shown in numerous studies that the atmospheric circulation in the stratosphere and the troposphere are strongly coupled in winter. As discussed in the introduction, the leading coupled mode of monthly or seasonal mean geopotential height variability in the winterly Northern Hemisphere (NH) shows that a large part of the variability in the troposphere is related to the strength of the stratospheric polar vortex (Baldwin et al., 1994; Perlwitz and Graf, 1995; Perlwitz, 2000) In this chapter, the leading coupled mode derived on the basis of Singular Value Decomposition (SVD) is discussed. Christiansen (2003) and Perlwitz and Graf (2001b) presented evidence for a regime-like behavior of the stratospheric polar vortex. Hence, regimes for the polar vortex are defined in this chapter. It is assumed in literature that the leading coupled mode of NH circulation in winter evolves from interactions between upward propagating planetary waves from the troposphere and the mean flow in the stratosphere described e.g. by Charney and Drazin (1961) and by Matsuno (1970). In the last subsection of this chapter, wave-mean-flow interactions and forcing mechanisms acting on both, the stratospheric and the tropospheric flow are examined.

3.1 The leading coupled mode

The leading coupled mode of monthly mean stratospheric-tropospheric variability in winter is shown in Fig. 3.1. It was derived with the Singular Value Decomposition (SVD) method (see appendix B.5) applied to monthly mean geopotential

height fields at 50 hPa and 500 hPa. NCEP/NCAR reanalysis data were used covering the Northern Hemisphere north of 30°N and the months November to April from 1958 to 1998. The annual cycle was removed by subtracting the long term mean of the respective month from each monthly mean. The leading SVD mode describes the relationship between the strength of the stratospheric polar vortex and a tropospheric geopotential height structure which is not only characterized by a large degree of zonal symmetry but also by a wave-train-like structure over the North Atlantic and Europe. This mode corresponds to the leading coupled modes derived by Baldwin et al. (1994), Perlwitz and Graf (1995), Perlwitz (2000), and others. Kodera et al. (1996) found a similar structural relationship by deriving Empirical Orthogonal Functions (EOF, see appendix B.4) of the 50 hPa geopotential height and regressing tropospheric geopotential heights onto the temporal expansion coefficient of the leading EOF mode, i.e. the leading Principal Component (PC). The leading SVD mode presented in Fig. 3.1 combines the leading modes of geopotential height variability at both levels: Both, the stratospheric and the tropospheric patterns shown in Fig. 3.1 are very similar to the leading EOF modes at the respective levels. The first EOF modes of the 50- and 500 hPa geopotential heights explain 51% and 17% of the variability in the winterly Northern Hemisphere, respectively. The temporal expansion coefficients of SVD and EOF modes are correlated by 0.99 in the stratosphere and by 0.95 in the troposphere.

The homogeneous regression pattern for the 50 hPa geopotential height (Fig. 3.1a) exhibits an almost zonally symmetric structure with anomalies of one sign in high latitudes and anomalies of opposite sign in midlatitudes and subtropics. This pattern describes changes in the strength of the stratospheric polar vortex. The latter is associated with strong westerly flow around the pole in stratospheric mid to subpolar latitudes, the so-called Polar Night Jet (PNJ, Fig. 3.2) whose strength is strongly fluctuating. The first EOF of monthly and zonal mean zonal wind at 50 hPa in the Northern Hemisphere north of 30°N is presented in Fig. 3.3. This leading EOF mode is associated with 79% of the variability of the zonal mean zonal wind and is mainly related to changes in the strength of the zonal mean wind maximum between 60°N and 70°N, i.e. in the core of the PNJ. The corresponding PC timeseries is closely correlated with the stratospheric timeseries of the first SVD mode (0.98). The zonal mean zonal wind in the core of the PNJ may thus be used as an index for the strength of the polar vortex.

The homogeneous SVD regression pattern for the 500 hPa geopotential height (Fig. 3.1b) is also characterized by a large degree of zonal symmetry with one center of action in the Arctic and others, with opposite polarity, in the midlatitudes to subtropics. This pattern resembles the tropospheric part of the Northern Annular Mode (NAM), an equivalent barotropic geopotential height structure with

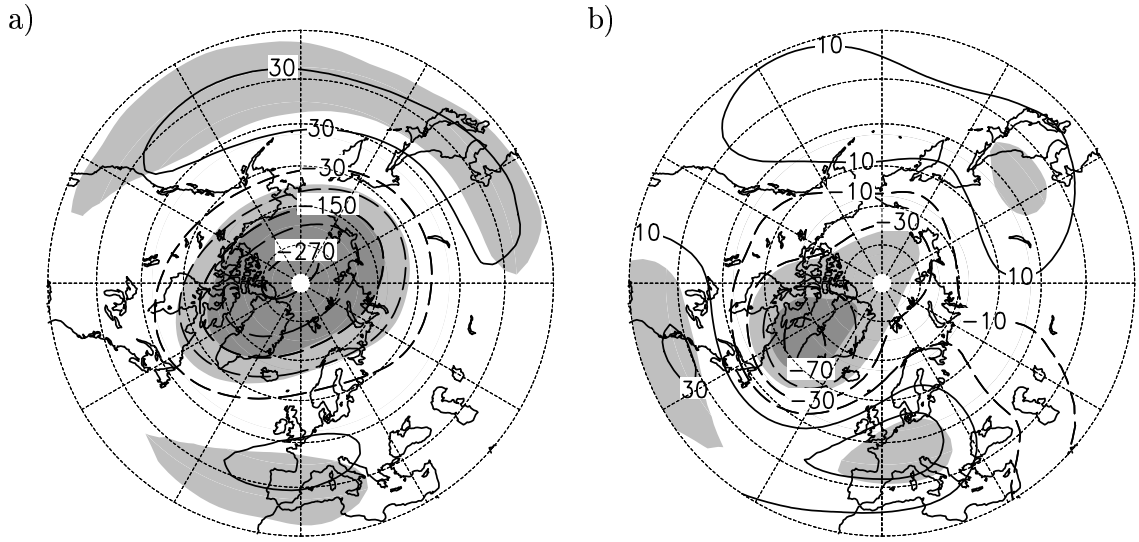

Figure 3.1: *Maps of homogeneous regression coefficients ([gpm], isolines) and correlation coefficients (shadings) for the first SVD mode of monthly mean 50- and 500 hPa geopotential heights in the Northern Hemisphere north of 30°N from November to April. Maps for (a) 50 hPa heights and (b) 500 hPa heights. The isoline intervals are 60 gpm for the 50 hPa level and 20 gpm for the 500 hPa level. The zero contour is omitted. Light and dark shadings indicate absolute correlation coefficients above 0.5 and 0.75, respectively.*

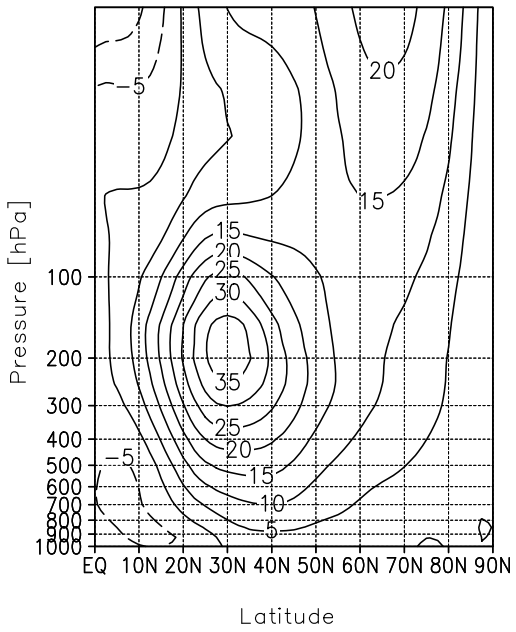

Figure 3.2: *Zonal mean zonal wind [m/s] in the Northern Hemisphere averaged over the winter season (November to April).*

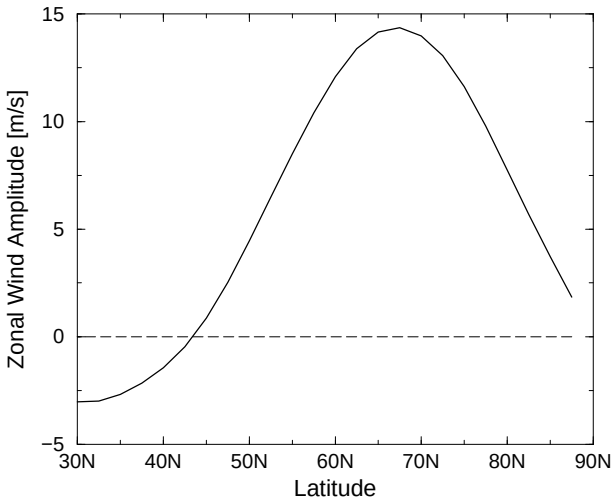

Figure 3.3: *First EOF of 50 hPa zonal mean mean zonal wind [m/s] in the Northern Hemisphere north of 30°N, determined from monthly means from November to April. The annular cycle was removed. The amplitude corresponds to one standard deviation of the PC timeseries.*

a large degree of zonal symmetry which amplifies from the surface up to the lower stratosphere. The surface imprint of this mode is commonly known as the Arctic Oscillation (AO; Thompson and Wallace, 1998). In the troposphere, both, the SVD mode presented in Fig. 3.1b and the NAM, are characterized by large anomalies in particular in the North Atlantic sector. The homogeneous regression pattern in Fig. 3.1b exhibits a tripole structure in this region with one center of action over Greenland/northeastern Canada, and two centers with opposite polarity over the subtropical western North Atlantic and over western Europe. The tropospheric part of the leading SVD mode is therefore related to changes in the north-south pressure gradient over the North Atlantic as is the North Atlantic Oscillation (NAO). The correlation between the temporal expansion coefficient of the tropospheric part of the leading SVD mode and a monthly mean NAO index (see appendix A) amounts to about 0.3 for the months December to March.

The strength of the polar vortex is not only coupled to a large part of the geopotential height variability in the troposphere but is also related to fluctuations in lower tropospheric temperature (Perlwitz and Graf, 1995) and precipitation in particular in the North Atlantic region. Fig. 3.4 shows the correlation coefficients of the stratospheric SVD timeseries with monthly means of the 850 hPa temperature (left panel) and precipitation (right panel) at each grid point. A strong (weak) vortex is related to lower-than-normal (above-normal) temperatures over the Labrador Sea/northeastern Canada, whereas there are above-normal (lower-than-normal) temperatures over western and northern Europe and Siberia as well as over the subtropical North Atlantic off the US east coast. Reduced (enhanced) temperatures can also be observed over North Africa, the eastern Mediterranean, and the Middle East. There is less-than-normal (enhanced) precipitation over the subtropical North Atlantic and southern Europe, whereas there is more (less) precipitation over the northern North Atlantic and northern Europe to Siberia. The correlations shown in Fig. 3.4 are significant above the 99%-level although they are not large (see appendix B.3). The latter implies that the NH troposphere is characterized by a large part of variability on monthly (and shorter) timescales, which cannot be attributed to the coupled stratospheric-tropospheric mode. On the basis of winter means, however, the correlations are larger (up to ± 0.6).

3.2 Regimes of the stratospheric polar vortex

The stratospheric circulation in Northern Hemisphere winter is characterized by strong westerly flow in subpolar latitudes (Fig. 3.2), whereas weaker easterly winds dominate during summer. The stratospheric polar vortex usually forms in early winter as a consequence of the cooling of the northern polar region due to

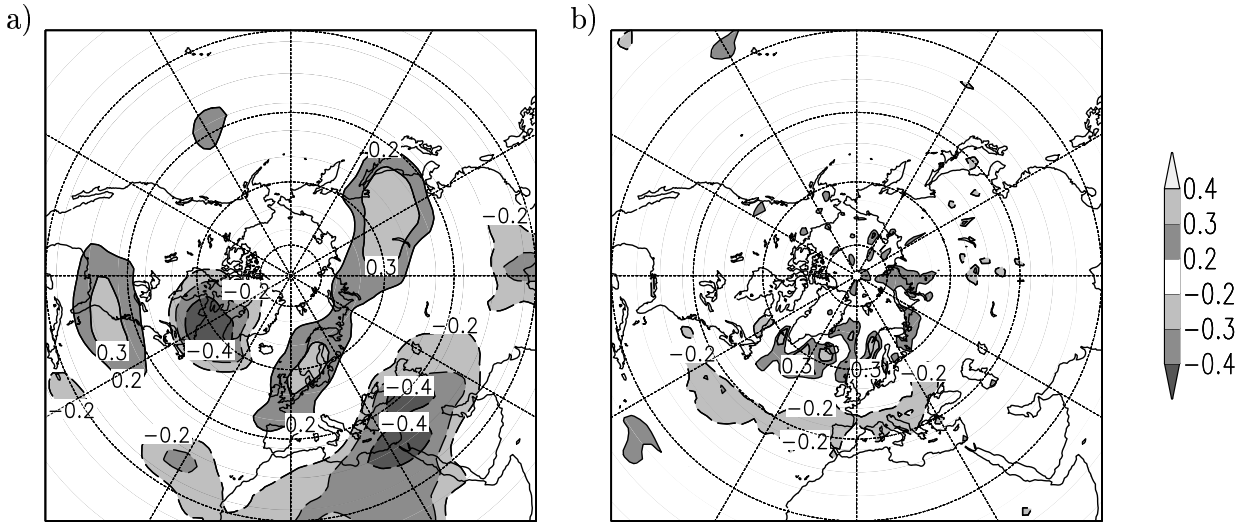

Figure 3.4: *Correlation coefficients between the stratospheric timeseries of the leading SVR mode presented in Fig. 3.1 and November to April monthly means of (a) the 850 hPa temperature and (b) the precipitation rate at each grid point. Only values exceeding ±0.2 are shown. These values are also significant above the 99% level.*

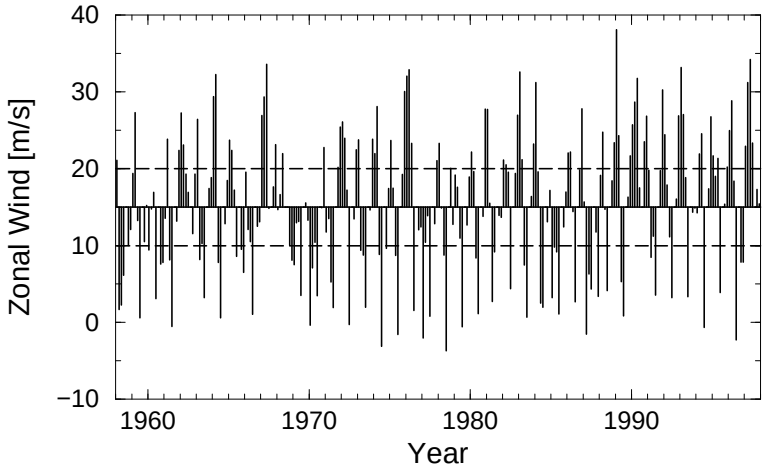

Figure 3.5: *Monthly mean zonal mean zonal wind [m/s] at 50 hPa and 65°N. Only the months November to April are shown. The dashed lines indicate the thresholds used for determining strong or weak stratospheric polar vortex episodes. They correspond to the average plus or minus a half standard deviation.*

the reduced incoming solar radiation. The final breakdown of the vortex normally takes place in late winter to early spring ('Final Warmings') when the circulation changes back to the summer situation. However, the vortex may also be subject to disturbances during high winter. They are assumed to be mainly caused by the interaction of planetary waves from the troposphere with the (zonal) mean flow in the stratosphere (Matsuno, 1970). However, several external factors may also influence the strength of the polar vortex and the probability for the development of a major warming event, such as volcanic eruptions, variations of the solar radiation, ozone depletion or the greenhouse effect.

Fig. 3.5 shows the strength of the monthly and zonal mean zonal wind at 50 hPa and 65°N for the months November to April. The data was not detrended and the annular cycle was not removed. Indicated are also thresholds at 20 m/s and 10 m/s which correspond to to the mean plus or minus a half standard deviation. In the following, the vortex is defined as strong, if the monthly and zonal mean zonal wind at 50 hPa and 65°N exceeds 20 m/s. In turn, the vortex is declared to be weak, if the zonal wind is weaker than 10 m/s. These thresholds seem to be somewhat arbitrary, but will be substantiated in the following.

In his examination of probability density Christiansen (2003) showed that the first PC timeseries of winter mean geopotential heights in the middle and lower stratosphere has a bimodal probability density distribution. The strength of the

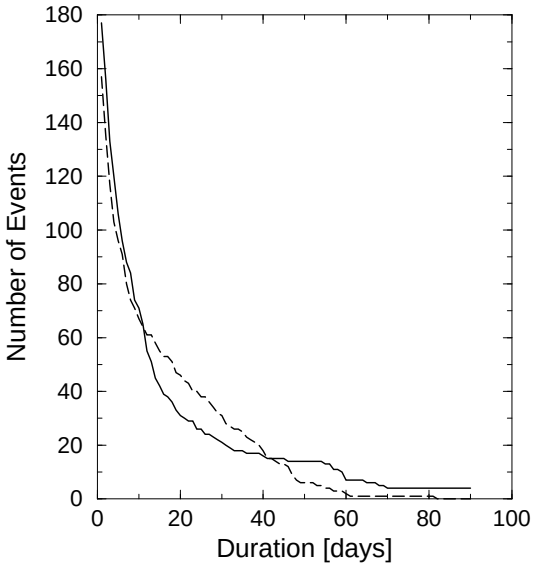

Figure 3.6: *Number of episodes with a persistent strong or weak polar vortex as a function of minimum duration, exceeded. Solid line: strong vortex, dashed line: weak vortex. The figure bases on daily means of the zonal mean zonal wind at 50 hPa and 65°N.*

winter mean stratospheric polar vortex is thus characterized by two regimes in which the vortex is either preferredly strong or weak. Christiansen (2003) admits that the results are not as clear for monthly means. Perlwitz and Graf (2001b), however, also reported bimodality in the distribution of anomaly correlations of the monthly mean zonal mean zonal wind at the 50 hPa level.

Even on a daily mean data basis, the zonal mean zonal wind at 50 hPa and 65°N and, thus, the strength stratospheric polar vortex, shows some persistence. Fig. 3.6 displays the number of periods during which the daily mean zonal mean zonal wind at 50 hPa and 65°N stays either stronger than 20 m/s or weaker than 10 m/s for at least the number of days indicated on the x-axis. There is a large number of periods in which the vortex stays strong or weak for only a couple of days. However, there are also indications for a persistent behavior: There are 31 (46) periods in which the vortex stays stronger than 20 m/s (weaker than 10 m/s) for at least 20 days. There are 21 strong vortex periods and 31 weak vortex periods with a minimum duration of 30 days. In the strong vortex case, there are still 7 periods with at least 60 days, and 2 such periods in the weak vortex case. This means i) that the polar vortex is to some degree characterized by a persistent behavior and ii) that it is justified to discuss monthly means of the zonal mean wind.

In the following, the two polar vortex regimes are discussed separately. The data were therefore subdivided into the two regimes characterized either by a strong or a weak stratospheric polar vortex: All months in which the monthly mean zonal mean zonal wind at 50 hPa and 65°N is stronger than 20 m/s were counted to the strong polar vortex regime (SVR) and those months in which it is weaker than 10 m/s were counted to the weak vortex regime (WVR).

Most of the SVR months occur during high winter, i.e. during December to February, whereas the WVR months are concentrated to late winter/early spring (see tables 3.1a and b). This thesis, however, focuses on the high winter season. Thus, only the months December to March (DJFM) were used for the analyses presented in the following. This means that 71 SVR months and 32 WVR months were considered instead of 75 SVR and 72 WVR months in the November-to-April season (NDJFMA). The regimes then comprise 2146 and 971 days, respectively. Even in the DJFM season, the WVR is dominated by the month March. Most of the analyses presented in this thesis were therefore repeated without the March data in order to check if the results are determined by this month. However, no evidence was found for such a behavior.

Castanheira and Graf (2003) used the same thresholds for SVR and WVR regimes as presented here, with the exception that they excluded the months with easterly wind from the WVR in order to dismiss stratospheric major warming events. Most of these months were already rejected here by excluding the month April. The remaining three months with negative zonal mean zonal wind do not have a strong influence the results presented in the following.

Christiansen (2003) presented evidence for a regime shift in the strength of the stratospheric polar vortex in the last half of the 1970s. He showed that both regimes were visited before and after this shift but that the frequency of the regime changed somewhen around 1978 in favor of the strong vortex regime. Tables 3.1a, b, and c show that a regime shift also manifests itself in the numbers of SVR and WVR months during the two subperiods 1958 – 1978 and 1979 – 1998. For both, the DJFM and the NDJFMA season, the number of SVR months is larger for the last decades than during the years before. The opposite is true for the number of WVR months. For the NDJFMA season, the ratio of the numbers of SVR and WVR months is almost reversed in favor of the SVR months during 1979 – 1998, while for the DJFM season the ratio SVR:WVR changes from almost 3:2 during the years 1958 – 1978 to 3:1 during 1979 –1998. The ratios reveal to be almost similar if the subperiods were separated between the years 1974 and 1975 (not shown). Thus, the regime shift must have happened somewhen during the late 1970s, possibly over several years.

a) **Number of SVR months**

Years	Nov	Dec	Jan	Feb	Mar	Apr	NDJFMA	DJFM
1958 – 1998	3	19	25	20	7	1	75	71
1958 – 1978	2	8	12	9	3	0	34	32
1979 – 1998	1	11	13	11	4	1	41	39

b) **Number of WVR months**

Years	Nov	Dec	Jan	Feb	Mar	Apr	NDJFMA	DJFM
1958 – 1998	4	5	5	7	15	36	72	32
1958 – 1978	3	3	4	4	8	18	40	19
1979 – 1998	1	2	1	3	7	18	32	13

c) **Ratio SVR : WVR**

Years	NDJFMA	DJFM
1958 – 1998	1.04	2.22
1958 – 1978	0.85	1.68
1979 – 1998	1.28	3.0

Table 3.1: *Number of SVR and WVR months counted for every single winter month and for the seasons November to April (NDJFMA) and December to March (DJFM). The lower table shows the ratio of SVR and WVR months in the seasons NDJFMA and DJFM.*

3.3 Changes in the tropospheric mean flow

The atmospheric variability in the troposphere is characterized by Rossby waves with a broad spectrum of wavenumbers and timescales, whereas the atmospheric flow in the stratosphere is dominated by ultra-long planetary waves. This can be explained with the strong filtering of upward propagating planetary waves throughout the troposphere and stratosphere. The filtering can be illustrated in a zonally symmetric framework by discussing the quasigeostrophic index of refraction (see e.g. Andrews et al., 1987). Depending on the zonal wavenumber, the latitude, and the static stability, this index predicts that a reduction of the westerly zonal mean wind as well as a larger (positive) vertical shear of the zonal mean zonal wind are associated with enhanced vertical propagation of planetary waves (Hu and Tung, 2002). The refractive index furthermore depends on the vertical curvature of the zonal mean zonal wind. If critical values for the latter parameters are exceeded so that the squared refractive index becomes negative, waves are reflected towards areas with higher (positive) values of the squared refraction index. For most (upward propagating) waves in midlatitudes, this means that they are reflected downwards and in meridional direction, mainly equatorwards. For short waves, the critical values are normally already exceeded well below the tropopause so that only very long waves have the possibility to reach the stratosphere (Charney and Drazin, 1961).

Limpasuvan and Hartmann (2000) and Hu and Tung (2002) showed that the vertical propagation of planetary waves with zonal wavenumber 1 is more effectively impeded at the tropopause in years with high phase of the Northern Annular Mode (NAM) than in years with low NAM. Hu and Tung (2002) found that the associated changes in the refractive index near the subpolar tropopause can mainly be attributed to changes in the strength of the zonal wind there: In the high (low) NAM phase, the westerly zonal wind is enhanced (reduced) near the subpolar tropopause. In the SVR, a larger fraction of even the ultra-long planetary waves is therefore reflected downwards or in meridional direction and, thus, does not disturb the stratospheric polar vortex. Limpasuvan and Hartmann (2000) argued that this might explain the predominantly strong (weak) stratospheric polar vortex during high (low) NAM phases.

Perlwitz and Harnik (2003) presented evidence for a reflecting surface for vertically propagating waves with zonal wavenumber 1 in the upper stratosphere. They found that this reflecting surface is related to the vertical curvature of the zonal mean zonal wind profile associated with a negative shear in the upper troposphere. Perlwitz and Harnik (2003) also found that this reflecting surface coincides with a clear meridional waveguide in the lower to middle stratosphere that channels the reflected wave activity to the high latitude troposphere and, thus, prevents it from getting absorbed in the stratosphere. Perlwitz and Harnik (2003)

argued that, on seasonal timescales, a strong vortex in the (lower) stratosphere is related to enhanced negative wind shear in the upper stratosphere and, thus, there is enhanced downward reflection in years when the vortex is strong. This might be an explanation for the significant feedback between stratosphere and troposphere which was detected by Perlwitz and Graf (2001a) for waves with zonal wavenumber 1 only in years with extraordinarily strong vortex.

This thesis does not attempt to decide which reflecting level is more important, the near-tropopause region or the upper stratosphere. It shall only be remarked that, according to the theory of the refractive index, a large fraction of the ultra-long planetary waves is reflected in the strong vortex case, whereas this is less so in the weak vortex case. These differences in the reflection/transmission properties lead to changes in the tropospheric planetary wave structure, which will be discussed in the following.

Forcing of the zonal mean flow

The zonal mean zonal wind structure in the winterly (DJFM) Northern Hemisphere is characterized by a maximum of westerly wind speed at the subtropical tropopause, the subtropical jet (Fig. 3.2). In the SVR, however, a second jet can be observed with a center in the subpolar stratosphere, the Polar Night Jet (Fig. 3.7, left panel). The enhancement of the subpolar westerly wind in the SVR is significant above the 99% level (t-test, see appendix B.3) in both, the stratosphere and the troposphere (Fig. 3.7, right panel). In the SVR, there is also a significant (above 99 %) reduction of zonal wind speed in the subtropical stratosphere and troposphere. However, Hu and Tung (2002) argue that subtropical latitudes are not an important gateway for upward propagating waves into the stratosphere. There is no significant reduction of the zonal wind speed in the core of the zonal mean subtropical jet, but from Fig. 3.8, it can be inferred that the North Atlantic subtropical jet is (significantly) displaced northwards in the SVR by about 5° and is slightly more tilted from the southwest to the northeast than in the WVR.

Interactions between eddy fluxes and the mean flow can be described with the Eliassen-Palm flux and its divergence (Eliassen and Palm 1961; Edmon et al. 1980; see appendix B.6). In order to enhance the clearness of the results, the definition of strong and weak vortex regimes is modified only for the discussion of E-P fluxes in this subsection. With a regime definition that is accurate to a day it is possible to describe the wave dynamics in terms of the E-P flux, its divergence, and their anomalies more precisely. This new definition bases on daily means of the zonal mean zonal wind at 50 hPa and 65°N from November to March. The SVR then consists of all days from periods in which the zonal mean zonal wind

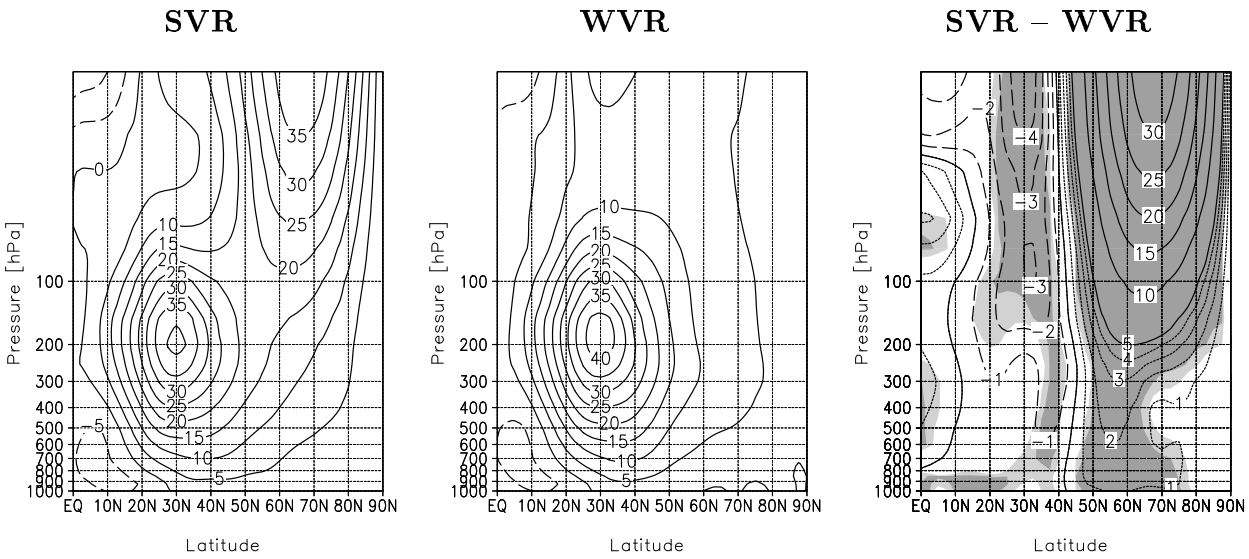

Figure 3.7: *Zonal mean zonal wind [m/s] in the Northern Hemisphere averaged over SVR and WVR, respectively, and mean difference between SVR and WVR. Light and dark shadings indicate t-test significance above the 95- or 99%-level based on monthly means.*

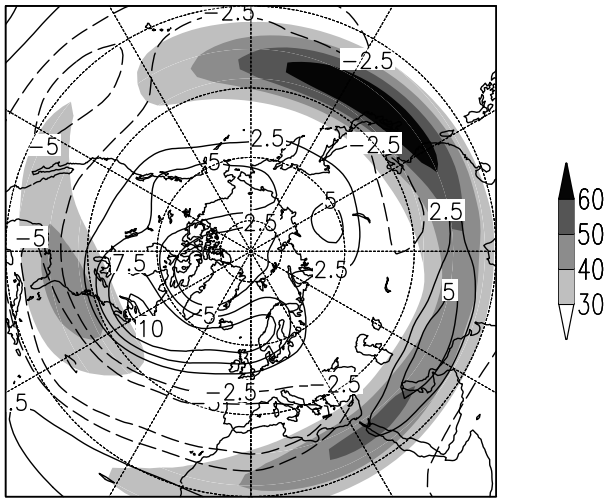

Figure 3.8: *Winter mean (DJFM) zonal wind [m/s] at 200 hPa (shadings) and mean difference between SVR and WVR (isolines).*

at 50 hPa and 65°N stays stronger than 20 m/s for at least 30 days. The WVR is made up of all periods in which the zonal wind remains weaker than 10 m/s (but stronger than 0 m/s) also for at least 30 days. The SVR then comprises 777 days and the WVR 473 days. This definition has been used by Castanheira and Graf (2003) for the discussion of stationary E-P fluxes. However, the main features discussed in the following remain the same if the monthly-mean-based definition of polar vortex regimes is applied.

The stationary E-P flux vectors point upward showing that the poleward heat flux dominates the winterly Northern Hemispheric E-P flux in the low and mid-troposphere (Fig. 3.9). Baroclinic energy conversions prevail in these regions. At upper tropospheric levels, the arrows tilt towards the equator indicating important momentum convergence near the subtropical jet stream region. The convergence reaches its maximum amplitude in the mid and upper troposphere, whereas there is divergence near the surface in mid and high latitudes (not shown). The stationary eddies thus tend to reduce the midlatitude westerly flow in the mid to upper troposphere and in the subtropical jet stream region below the tropopause. Only weak upward directed E-P fluxes can be observed in the lower stratosphere, where the eddy fluxes disturb the polar vortex. The latter can be inferred from the maximum of E-P flux convergence in the subpolar stratosphere. In the SVR, the upward directed E-P fluxes in the stratosphere are smaller than in the WVR. Such a behavior corresponds to the discussion of the refractive index by Hu and Tung (2002), implying that the strengthening of the westerly zonal wind in the SVR (Fig. 3.7) leads to enhanced reflection of upward propagating (ultra-long) planetary waves near the subpolar tropopause. Fig. 3.9 shows that the E-P flux difference between SVR and WVR is directed equatorwards at the tropopause level. However, the fact that the upward directed E-P fluxes in the (lower) stratosphere are smaller in the SVR than in the WVR is also in agreement with downward reflection at a reflecting surface in the upper troposphere described by Perlwitz and Harnik (2003). They argue that downward reflection of waves back to the troposphere results in a reduction of upward E-P fluxes in the lower stratosphere.

Fig. 3.9 shows that the stationary E-P flux convergence is stronger in the WVR than in the SVR. The disturbing influence of stationary eddy fluxes on the stratospheric polar vortex is therefore weaker in the SVR than in WVR. This means that a weak vortex is even more disturbed and, thus, does not become strong, whereas there is a large potential for a strong vortex to stay strong. In the upper troposphere, however, the difference of E-P flux divergences between SVR and WVR is negative in the midlatitudes and the subtropics. The stationary eddies thus act to reduce the anomalous westerly flow in the upper level midlatitudes as well as in the subtropical jet region (see Fig. 3.7). In contrast, the difference of E-P flux divergences between SVR and WVR is positive, in the

midtropospheric midlatitudes, indicating stationary eddy forcing of the anomalous westerly flow there. Limpasuvan and Hartmann (2000) showed that, in the vertical mean, the stationary eddies are responsible for the largest part of the zonal mean flow forcing.

The stationary E-P fluxes are almost entirely associated with planetary waves characterized by zonal wavenumbers 1 to 3 (lower row in Fig. 3.9). Due to the zonal averaging process, mixed terms with different zonal wavenumbers vanish so that the E-P flux contributions from single zonal wavenumbers add linearly (see Andrews et al., 1987). Fig. 3.10 shows separate E-P flux contributions from stationary eddies with zonal wavenumbers 1, 2, and 3. The reduced convergence in the SVR stratosphere is mainly related to eddies with zonal wavenumbers 1 and 2. Eddy fluxes associated with wavenumber 3 and larger an be neglected in the stratosphere. This corresponds to the theory that only very long waves can reach the stratosphere, whereas shorter waves are mainly reflected below. The disturbance of the subtropical jet and the westerly flow in the upper troposphere, however, is mainly associated with enhanced eddy fluxes from wavenumbers 1 and 3. While poleward heat- and equatorward momentum fluxes increase in the SVR for wavenumbers 1 and 3 in midlatitudes, the fluxes associated with wavenumber 2 reduce. The reduced fluxes are related to net E-P flux divergence and, thus, to anomalous forcing of the westerly wind in the midlatitude midtroposphere, i.e. the net westerly forcing by stationary eddy fluxes is mainly due to weaker wavenumber-2 E-P flux divergence in the SVR.

The unfiltered transient E-P fluxes are larger in magnitude than the corresponding stationary fluxes (Fig. 3.11). However, the transient and stationary E-P flux and divergence patterns look quite similar. In the stratosphere, the transient eddy fluxes counteract the westerly flow equatorward of 50°N in both regimes, the SVR and the WVR. The difference of the transient E-P flux divergences at these levels is positive equatorward of 50°N but negative poleward of 60°N. The transient eddy fluxes thus counteract the anomalous stationary eddy forcing north of 60°N. The stationary forcing, however, is stronger. Fig. 3.11 also shows the contributions from low pass and band pass filtered eddies. The Blackmon and Lau (1980) low and band pass filters (see appendix B.1) were used to isolate fluctuations with periods longer than 10 days and from 2.5 to 6 days, respectively. Fig. 3.11 illustrates that, in the stratosphere, the transient eddy forcing of the mean flow is mainly related to low frequency transients. Synoptic eddy fluxes are negligible there.

The westerly flow in the mid to upper troposphere is counteracted in midlatitudes as well as in the subtropical jet region in both stratospheric regimes. The transient E-P flux convergence is a bit larger in magnitude than for the stationary eddies and has a maximum at the core of the subtropical jet at 30°N,

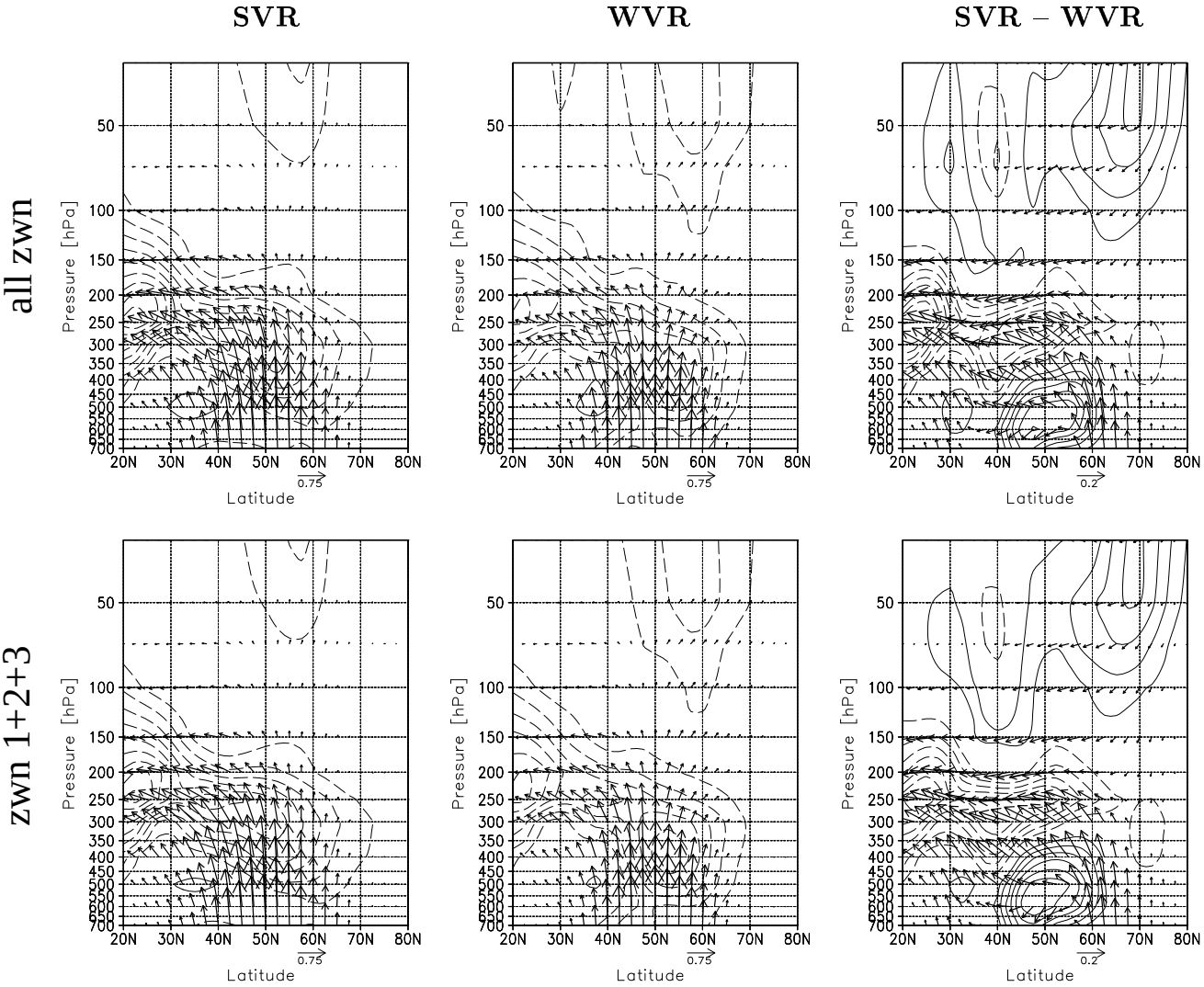

Figure 3.9: *Eliassen-Palm sections for the SVR (left column), the WVR (middle column), and the mean difference between SVR and WVR (right column), for stationary eddies. For the panels in the lower row, only stationary eddies with zonal wavenumbers 1 to 3 were considered. Vectors indicate the magnitude and direction of the E-P flux, the contours its divergence. The contour interval is* $0.5 \cdot 10^{15} m^3$ *for the SVR and WVR and* $0.2 \cdot 10^{15} m^3$ *for the SVR-WVR difference. The zero contour is omitted. The scaling factors are* $10^{15} m^3$ *for the meridional E-P flux component and* $10^{20} m^3 Pa$ *for the vertical component. The unit vector is indicated below each panel. Its length is 0.75 for SVR and WVR and 0.2 for SVR-WVR differences.*

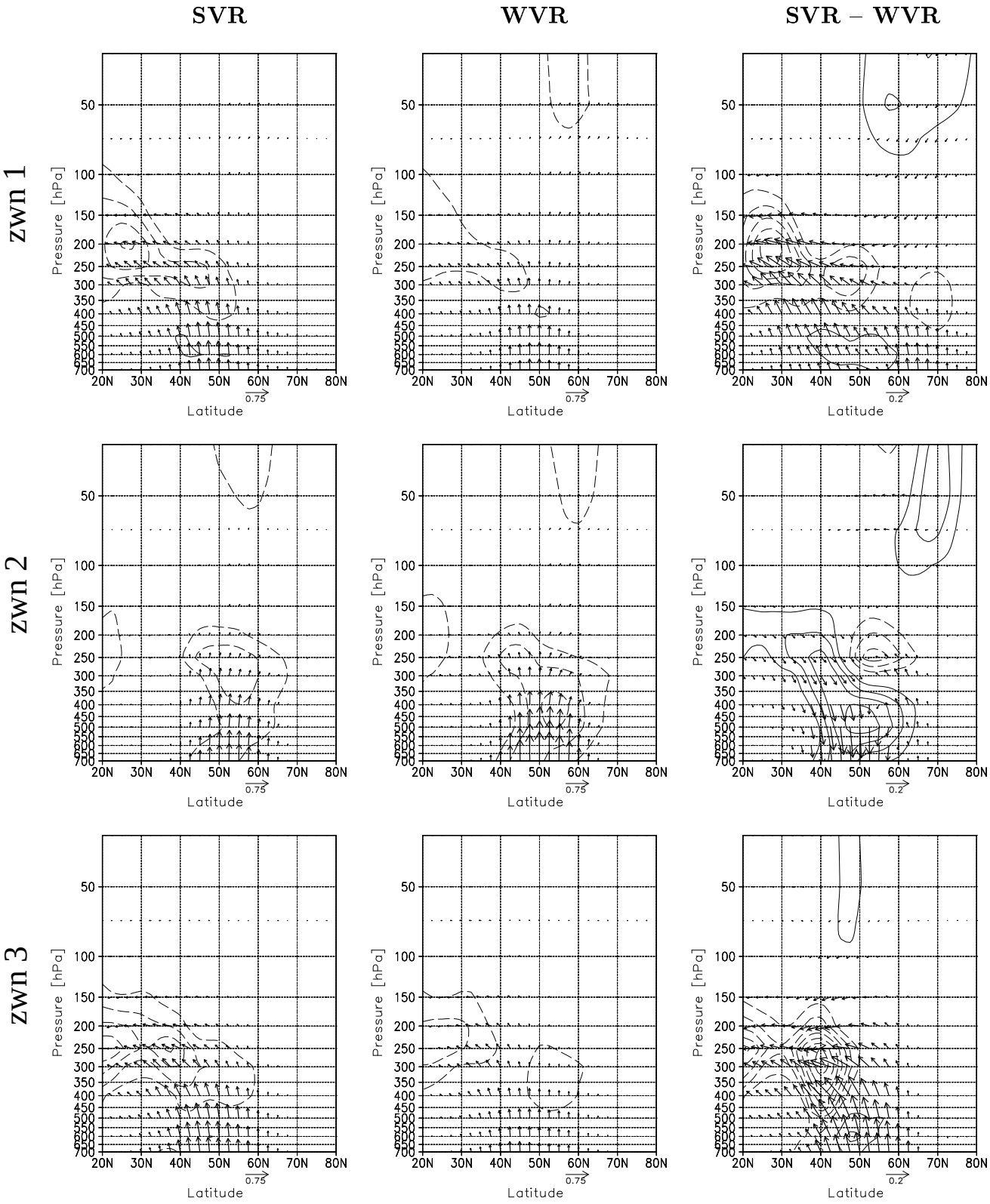

Figure 3.10: *As in Fig. 3.9 but for stationary eddies with zonal wavenumber 1 (upper row), zonal wavenumber 2 (medium row), and zonal wavenumber 3 (bottom row).*

between 200 and 250 hPa. The difference of E-P flux divergences between SVR and WVR reveals a net forcing contribution towards anomalous westerly flow at the upper-level troposphere in midlatitudes and a reducing contribution below. This is opposite to the stationary eddy contributions. The sum of anomalous E-P flux divergences from stationary and transient eddies, however, is positive in the mid to upper troposphere (not shown). The anomalous low frequency forcing of the upper tropospheric westerlies is positive, whereas band pass filtered (synoptic) eddies act to reduce the mean westerly flow in the midtroposphere in midlatitudes and below the subtropical jet. The anomalous forcing of the subtropical jet by all transient eddies is mainly towards an upward and equatorward displacement in the SVR. The low pass filtered poleward heat flux is reduced in the SVR between 40°N and 65°N, whereas the corresponding band pass filtered flux is enhanced between 45°N and 70°N. This corresponds to stronger transient heat fluxes poleward of 55°N and reduced transient heat fluxes between 40°N and 50°N.

In summary, the analysis of the E-P flux reveals that the anomalous zonal mean westerly flow troposphere and stratosphere of the Northern Hemisphere is driven by both, stationary and transient eddy fluxes of heat and momentum. It has been shown that only very long waves (zonal wavenumber 1 and 2) are associated with noteworthy E-P fluxes in the stratosphere and that the persistent behavior of the polar vortex strength is supported by anomalous stationary eddy fluxes. In midlatitudes, the anomalous westerly flow in the upper troposphere is supported by anomalous transient eddy fluxes and counteracted by anomalous stationary eddy fluxes. This is vice versa in the midtroposphere. It is therefore necessary to examine the influence of the different types of eddies on the tropospheric flow in more detail.

Forcing of tropospheric mean flow patterns

The different reflection/transmission properties for upward propagating planetary waves in the two regimes of the stratospheric polar vortex strength lead to changes in the structure of tropospheric planetary wave patterns. The polar vortex regimes applied in the remainder of this thesis are defined as described in section 3.2 and chapter 2 using monthly mean zonal wind data. Fig. 3.12 shows the mean 300 hPa geopotential height difference between SVR and WVR. The pattern clearly resembles the tropospheric variability pattern associated with the leading coupled stratospheric-troposphere mode (Fig. 3.1b). It exhibits strong anomalies in particular in the North Atlantic sector showing the typical tripole pattern with a negative anomaly over Greenland/northeastern Canada and positive anomalies over western Europe and over the subtropical western North At-

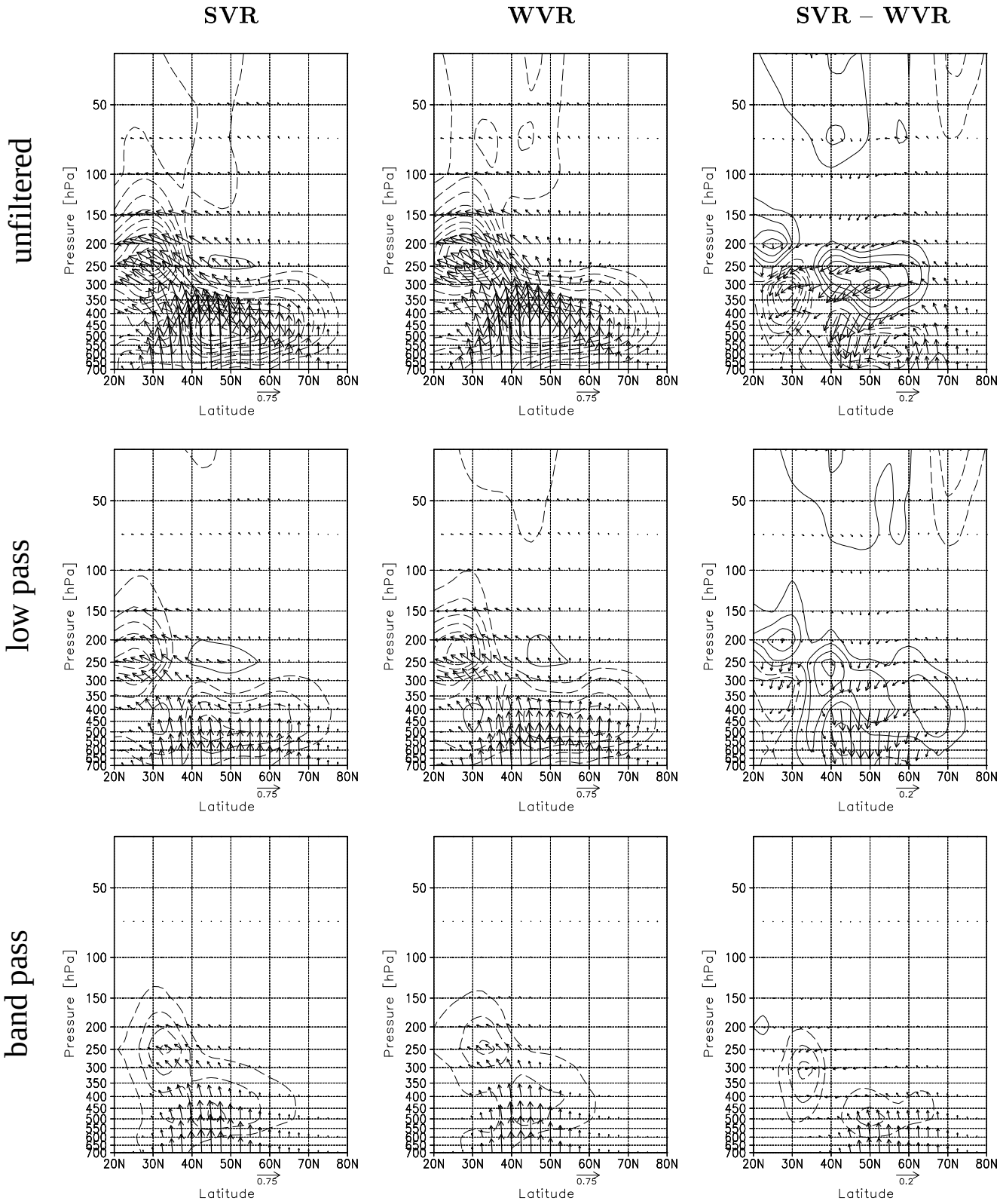

Figure 3.11: *As in Fig. 3.9 but for unfiltered transient eddies (upper row), low pass filtered transient eddies (medium row), and band pass filtered transient eddies (bottom row).*

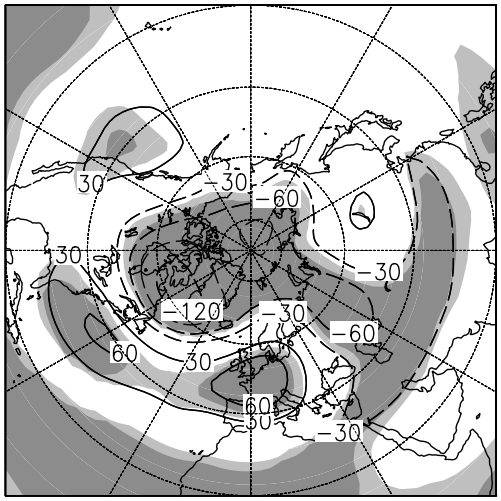

Figure 3.12: *Mean difference of the geopotential height of the 300 hPa level [gpm] between SVR and WVR. The zero contour is omitted. Light and dark shadings indicate t-test significance above the 95- or 99%-level based on monthly means.*

lantic. A comparison of the deviations from the zonal mean (Fig. 3.13) yields that the mean geopotential height anomaly in the SVR (WVR) mainly represent an enhancement (reduction) of the 1958–1998 mean stationary wave structure in particular in the North Atlantic sector.

Not only the stationary wave structure but also the transient eddies are affected by changes of the polar vortex regime. Fig. 3.14 shows the root mean square (rms) of the 10 day-low pass filtered 300 hPa geopotential height. The filtering has been accomplished with the low pass filter introduced by Blackmon and Lau (1980; see appendix B.1). In the WVR, the rms (Fig. 3.14b) is maximum in middle and subpolar latitudes, especially over the North Atlantic and the North Pacific. One outstandingly strong maximum is located over northeastern Canada and the Labrador Sea, where the mean geopotential height difference between SVR and WVR is largest (Fig. 3.12). In the SVR (Fig. 3.14a), a totally different picture arises: The North Pacific maximum is slightly stronger and the North Atlantic maximum is located over the central to eastern North Atlantic. It is also located further south than in the WVR, i.e. between 55° and 60°N, south of Iceland. The North Atlantic maximum is also much broader than in the WVR.

The rms of 2.5-to-6 day-band pass filtered 500 hPa geopotential height is a good indicator for the strength and direction of the storm tracks. The filter applied for this task is the band pass filter introduced by Blackmon and Lau (1980;

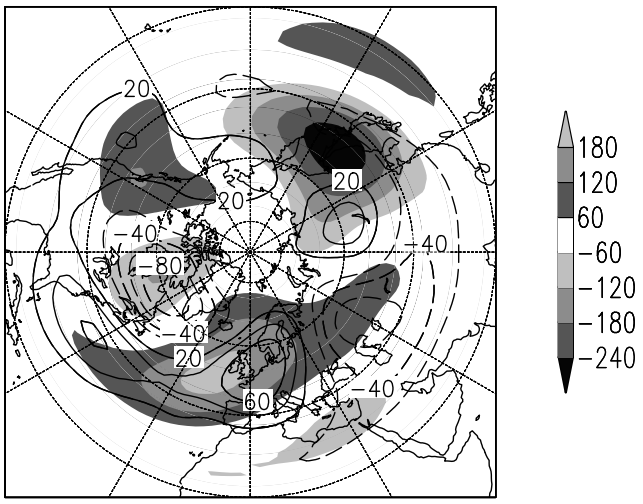

Figure 3.13: *Deviations from the zonal mean of the 300 hPa geopotential height [gpm], i.e. the stationary waves with a zonal wavenumber larger than 0. Shown are the the winter mean (DJFM, shadings) and the mean difference between SVR and WVR (isolines) based on monthly means. The zero contour is omitted.*

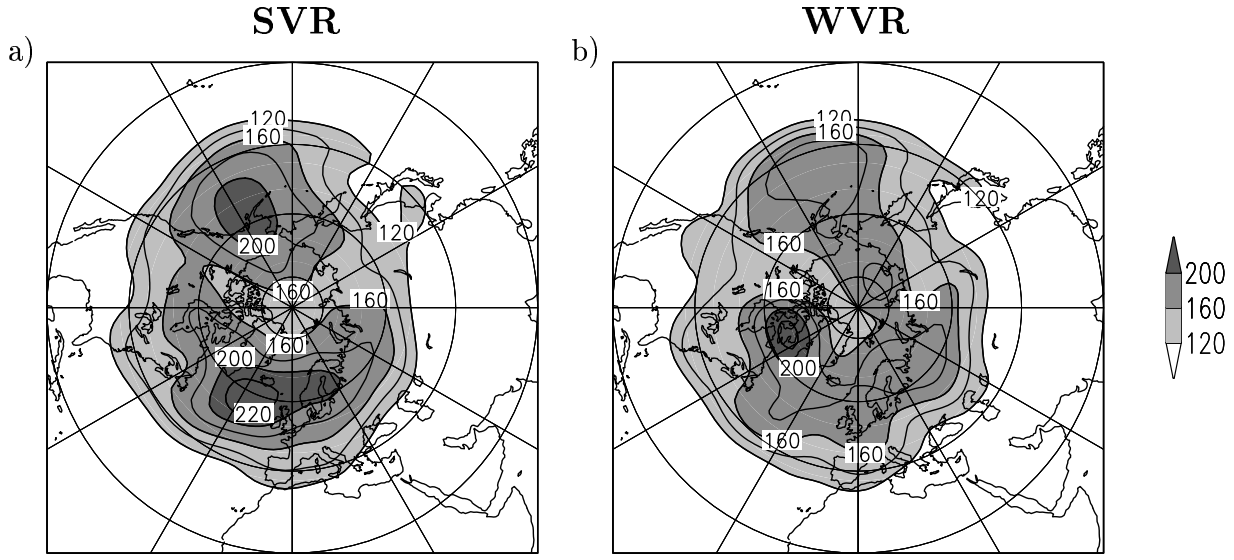

Figure 3.14: *Root mean square of the low pass filtered 300 hPa geopotential height [gpm] in (a) SVR and (b) WVR. For simplicity, only values above 120 gpm are shown.*

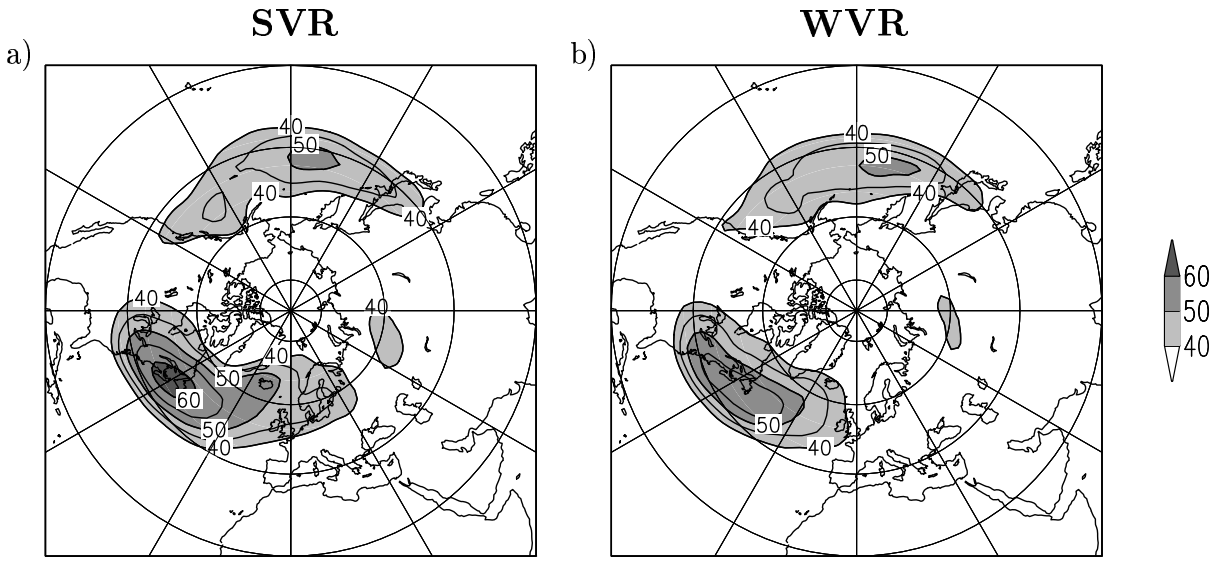

Figure 3.15: *Root mean square of the band pass filtered 500 hPa geopotential height [gpm] in (a) SVR and (b) WVR. For simplicity, only values above 40 gpm are shown.*

see appendix B.1). Fig. 3.15 shows that mainly the North Atlantic storm track is affected by changes in the polar vortex regime: It is more intense in the SVR than in the WVR. The core of the storm track in the SVR is also located slightly north of the core in the WVR. The storm track exit is strongly tilted from the southwest to the northeast in the SVR, whereas the storm track is more zonally oriented in the WVR. There are only small and non-significant changes in the North Pacific storm track. In summary, the changes in both, the stationary wave pattern and the transient variability structure, reveal to be most pronounced in the North Atlantic sector.

Time mean streamfunction tendency equation

As discussed in the previous section, both, stationary and transient eddies influence the zonal mean flow in the troposphere. In the following, the consequences for the stationary wave patterns in the troposphere are examined. Contributions from different forcing mechanisms acting on the time mean flow can be assessed by analyzing single terms of the streamfunction tendency equation (Cai and van den Dool, 1994; Feldstein, 1998; Orlanski, 1998). In the quasigeostrophic framework, the streamfunction is directly associated with the geopotential height z,

by $\psi = gf^{-1}z$, with the gravitational acceleration g and the Coriolis parameter f. Thus, positive streamfunction tendency is related to increasing geopotential height. The streamfunction ψ is defined as the inverse Laplacian of vorticity. Hence, by applying the inverse Laplacian to the vorticity equation, an equation for the streamfunction tendency can be derived (Cai and van den Dool, 1994):

$$\frac{\partial \psi}{\partial t} = \nabla^{-2}\left(\frac{\partial \zeta}{\partial t}\right) = -\nabla^{-2}\left(\nabla \cdot \left(\left(\zeta + f\right)\vec{v}\right)\right) - \nabla^{-2}\left(\vec{k} \cdot \nabla \times \left(\omega \frac{\partial \vec{v}}{\partial p}\right)\right) + R \quad (3.1)$$

with the relative vorticity ζ, the horizontal wind vector $\vec{v} = (u, v)$, the vertical unit vector $\vec{k}$, and the vertical velocity ω. The term R corresponds to a residual and includes diabatic processes and dissipation.

In the time mean, it is $\frac{\partial \overline{\psi}}{\partial t} = 0$ and equation 3.1 reduces to

$$\begin{aligned} 0 \;=\; & -\nabla^{-2}\left(\nabla \cdot \left(\left(\bar{\zeta} + f\right)\bar{\vec{v}}\right)\right) - \nabla^{-2}\left(\nabla \cdot \left(\overline{\zeta' \vec{v}'}\right)\right) \\ & -\nabla^{-2}\left(\vec{k} \cdot \nabla \times \left(\bar{\omega}\frac{\partial \bar{\vec{v}}}{\partial p}\right)\right) - \nabla^{-2}\left(\vec{k} \cdot \nabla \times \left(\overline{\omega' \frac{\partial \vec{v}'}{\partial p}}\right)\right) + \bar{R}, \end{aligned} \quad (3.2)$$

where the overbar denotes the time mean and the primes deviations therefrom. The first term on the right hand side represents the forcing of the time mean streamfunction pattern by the time mean flow, i.e. by stationary eddy vorticity fluxes, whereas the second term represents the contribution from transient eddy vorticity fluxes. The combined third and fourth term is the forcing by vertical vorticity advection and tilting. The forcing contributions were calculated for the 300 hPa as well as for the 500 hPa level. For the 300 hPa (500 hPa) tendencies, the vertical derivatives were approximated by centered differences between the 200 hPa (400 hPa) and the 400 hPa (600 hPa) level.

The forcing term related to stationary eddy vorticity fluxes can be splitted up into contributions from stationary eddy vorticity advection and stationary eddy divergence:

$$-\nabla^{-2}\left(\nabla \cdot \left(\left(\bar{\zeta} + f\right)\bar{\vec{v}}\right)\right) = -\nabla^{-2}\left(\bar{\vec{v}} \cdot \nabla\left(\bar{\zeta} + f\right)\right) - \nabla^{-2}\left(\left(\bar{\zeta} + f\right)\nabla \cdot \bar{\vec{v}}\right). \quad (3.3)$$

The contributions from transient eddies with different timescales can be analyzed by applying filters. As before, the low pass and band pass filters introduced by Blackmon and Lau (1980) were used (see appendix B.1). The streamfunction tendency forcing by low frequency eddy vorticity fluxes is then

$$-\nabla^{-2}\left(\nabla \cdot \left(\overline{\zeta^L \vec{v}^L}\right)\right), \quad (3.4)$$

the contribution from band pass filtered (synoptic) eddy fluxes

$$-\nabla^{-2}\left(\nabla\cdot\left(\overline{\zeta^B\vec{v}^B}\right)\right), \tag{3.5}$$

and the forcing by interaction between low pass and band pass filtered eddies is

$$-\nabla^{-2}\left(\nabla\cdot\left(\overline{\zeta^L\vec{v}^B}\right)\right)-\nabla^{-2}\left(\nabla\cdot\left(\overline{\zeta^B\vec{v}^L}\right)\right). \tag{3.6}$$

The superscripts 'L' and 'B' indicate low pass and band pass filtered quantities, respectively.

In order to examine the forcing mechanisms responsible for the differences in the mean streamfunction (or geopotential height) between the two polar vortex regimes, the contributions to the time mean streamfunction tendency in the SVR minus the corresponding contributions in the WVR are discussed here (Fig. 3.16). The tendency differences from stationary and low pass filtered transient eddies almost cancel each other. The anomalous low over Greenland in the geopotential height difference pattern (Fig. 3.16) is mainly forced by stationary eddy vorticity fluxes, but is counteracted by low frequency eddy vorticity fluxes. Together with the positive forcing anomaly over the subtropical North Atlantic this means that stationary wave interactions act to enhance the westerly flow over the midlatitude North Atlantic. This corresponds to the positive anomaly of stationary E-P flux divergences in the midlatitudes. The stationary forcing can be split up into contributions from stationary vorticity advection and from stationary divergence (Fig. 3.17). The geopotential height anomalies over Greenland (low) and the subtropical North Atlantic (high) reveal to be mainly forced by stationary vorticity advection at the 300 hPa and the 500 hPa level with an additional forcing contribution from stationary divergence towards maintaining the anomalous low near Greenland at the 500 hPa level.

The anomalous low over the Arctic is in turn forced by low frequency transients, as well as are the anomalous highs over the North Pacific and over western Europe. They are counteracted by stationary eddy vorticity fluxes. The counteraction can be mainly attributed to stationary divergence (Fig. 3.17). The difference patterns of streamfunction tendency related to low frequency eddy forcing are mainly similar at the 300 hPa and the 500 hPa level. In the Arctic region, in the subtropics, and over western Europe they are a bit larger in magnitude at 300 hPa than at 500 hPa, whereas the opposite is true for the anomaly over Greenland and over the subtropical North Atlantic. This means that the forcing of the anomalous zonal mean westerly flow by the low frequency transients is stronger in the upper than in the middle troposphere, whereas, in the midtroposphere, the forcing of the anomalous westerly wind over the North Atlantic by the stationary eddies is stronger. This corresponds to the E-P flux divergences discussed previously in this section.

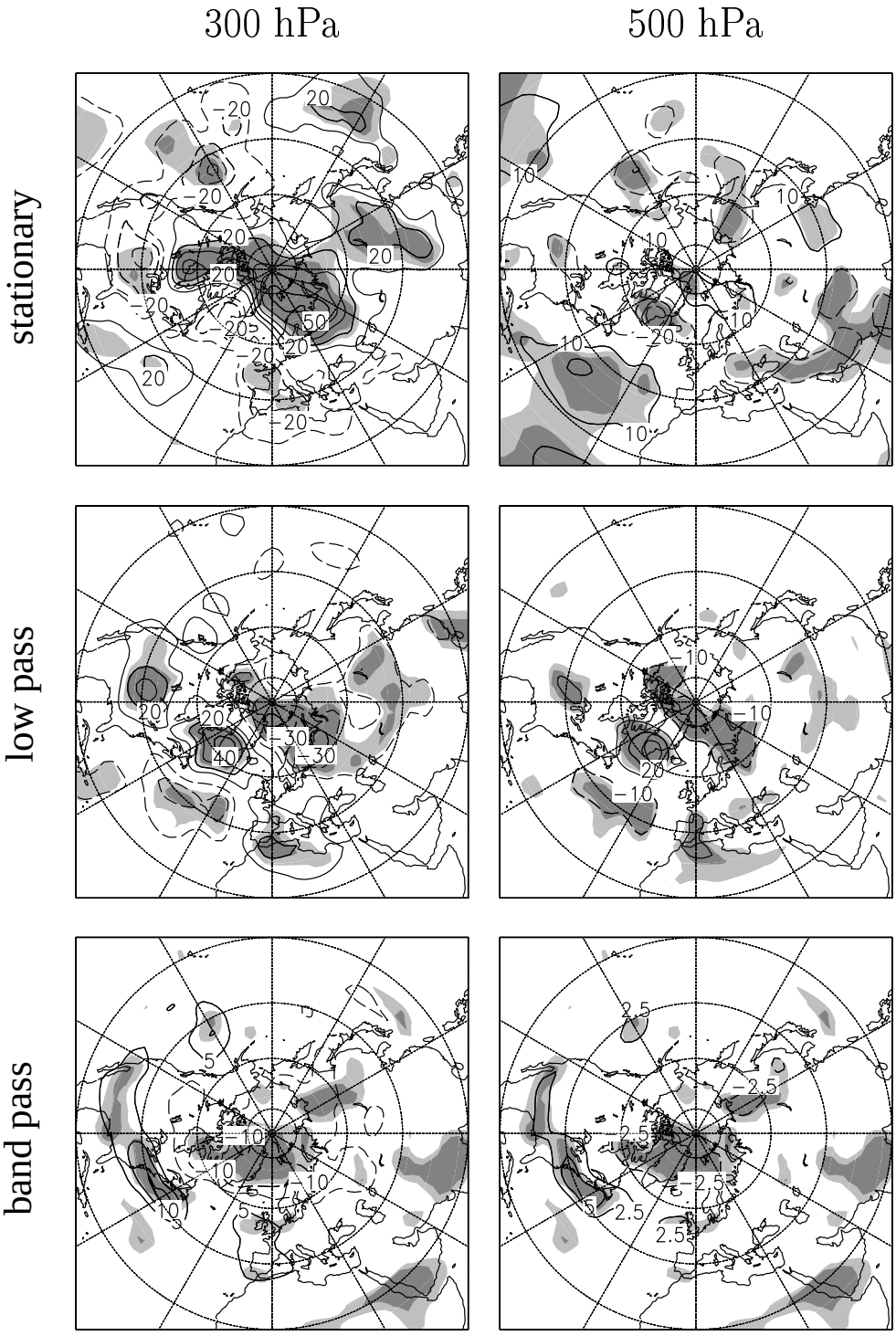

Figure 3.16: *Differences of the forcing terms of the time mean streamfunction tendency equation 3.3 between SVR and WVR [m^2s^{-2}] on the 300 hPa level (left column) and on the 500 hPa level (right column). Shown is the anomalous forcing by stationary (upper row), low pass filtered (medium row), and band pass filtered eddy vorticity fluxes (bottom row). The isoline intervals are 10 m^2s^{-2} in the upper two rows, 5 m^2s^{-2} in the lower left panel and 2.5 m^2s^{-2} in the lower right panel. The zero contour is omitted. Light and dark shadings indicate t-test significance above the 95- and 99%-level.*

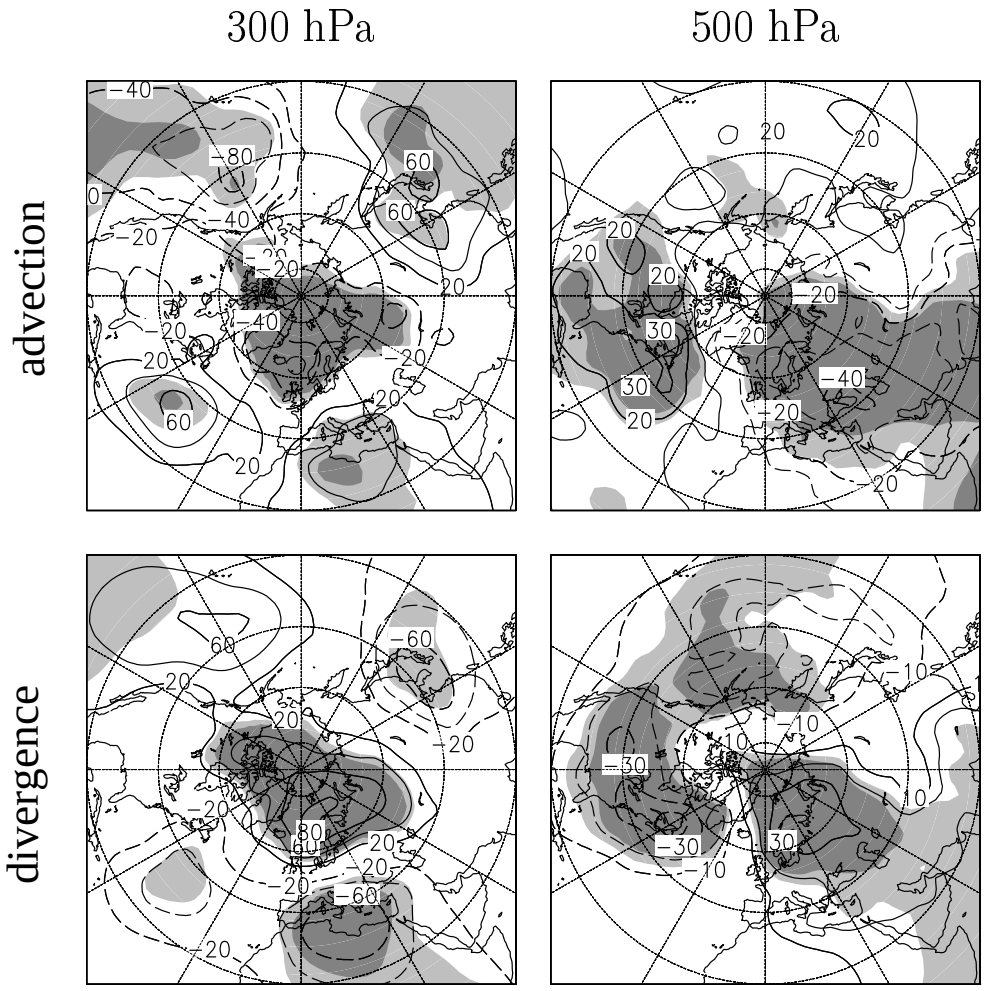

Figure 3.17: *As in Fig. 3.16, but for stationary vorticity advection (upper row) and divergence (lower row). The isoline intervals are 20 m^2s^{-2} for the 300 hPa patterns and 10 m^2s^{-2} for the 500 hPa patterns. The zero contour is omitted.*

The band pass filtered eddy vorticity fluxes force the negative height anomaly near Greenland as well as over the Arctic, but the tendencies are smaller than those originating from stationary or low frequency eddies. The anomalous synoptic eddy forcing is positive over the midlatitude western North Atlantic. Thus, it supports westerly winds in the North Atlantic sector. This is even stronger at 500 hPa than at 300 hPa. Hoskins et al. (1983) showed that high frequency eddies increase the mean barotropic westerly wind at the storm track entrance. The dipole structures in Fig. 3.16, bottom row, thus correspond to the enhancement (and northward displacement) of the North Atlantic storm track in the SVR case (Fig. 3.15). The forcing resulting from the interaction between low frequency and synoptic eddies (not shown) is small and, thus, negligible as well as is the forcing by vertical vorticity advection and tilting. The difference of the residual terms R (not shown) is characterized by only small anomalies in the North Atlantic and North Pacific sector and is therefore not discussed either.

3.4 Summary

A large part of the tropospheric variability in the winterly Northern Hemisphere is linearly related to the strength of the polar vortex in the (lower) stratosphere (e.g. Baldwin et al., 1994; Perlwitz and Graf, 1995; Perlwitz, 2000). Two regimes can be isolated for the latter, characterized by either strong or weak zonal mean westerly wind the subpolar lower stratosphere (Christiansen, 2003; Perlwitz and Graf, 2001b). Analyses presented in this thesis were therefore conducted separately for the two polar vortex regimes. It has furthermore been shown that the number of months with a strong stratospheric polar vortex is increased since the 1970s in comparison to the number of months with a weak vortex.

Changes in the strength of the stratospheric polar vortex are associated with different reflection/transmission properties in particular for ultra-long upward propagating planetary waves (Charney and Drazin, 1961; Limpasuvan and Hartmann, 2000; Hu and Tung, 2002; Perlwitz and Harnik, 2003). By analyzing the Eliassen-Palm flux (E-P flux; see Edmon et al., 1980) and its divergence it has been shown in this chapter that i) only very long waves (zonal wavenumbers 1 and 2) are associated with noteworthy stationary momentum and heat fluxes in the stratosphere and that ii) the zonal mean westerly wind in the lower stratosphere is less counteracted by stationary eddy fluxes in the strong vortex regime (SVR) than in the weak vortex regime (WVR). The latter implies that a vortex which is already strong has an enhanced potential to stay strong, whereas a weak vortex is more subject to disturbances and, thus, does not become strong very easily. This forcing towards a persistent strong or weak polar vortex is counteracted by transient eddy fluxes, in particular from the low frequency domain

(periods $\geq$ 10 days). The stationary eddy forcing, however, is dominant.

The different reflection/transmission properties in the SVR and the WVR do not only induce changes in the stationary wave structure in the troposphere but are also accompanied by a reorganization of transient eddies. The mean geopotential height difference between the SVR and the WVR is characterized by a negative anomaly over the Arctic with a pronounced extension over Greenland, the Labrador Sea and northeastern Canada. Large positive anomalies can be found over the subtropical North Atlantic and western Europe. An examination of the forcing terms involved in the time mean streamfunction equation at 300 hPa and 500 hPa confirms the findings gained from the analysis of E-P fluxes that both, stationary and transient eddy forcing, are responsible for maintaining the geopotential height (or streamfunction) difference between SVR and WVR in the troposphere. Both forcing contributions drive the difference pattern in some aspects and act to destroy it in others. At the same time, stationary and low frequency eddy forcing mainly counteract each other. The negative anomaly over the Arctic is maintained mainly by low frequency eddy vorticity fluxes, with a small contribution from synoptic (periods 2.5–6 days) eddy vorticity fluxes. The forcing increases from the middle to the upper troposphere. The low frequency transients also act to maintain the positive anomaly over western Europe. The forcing by stationary eddy vorticity fluxes, however, supports the negative anomaly maximum near Greenland, which is also maintained by synoptic eddy forcing.

The largest differences in both, the tropospheric mean flow and the transient variability between the two polar vortex regimes can be observed in the North Atlantic sector. It may therefore be anticipated that this region is most sensitive to external influences affecting the strength of the polar vortex, such as changes in the solar radiation, volcanic eruptions or injection of greenhouse gases. Such influences, however, have to be examined with modeling studies because observational data records are not long enough to draw robust conclusions. The results presented in this chapter suggest that, when applying models in order to study the coupled stratospheric-tropospheric circulation, it is of crucial importance that the strength of the polar vortex and the related reflection/transmission properties are properly represented. Unfortunately, many general circulation model (GCM) experiments are characterized by a too strong polar vortex ('cold bias'; Perlwitz, 2000) so that the mean modeled circulation in the troposphere mainly corresponds to SVR conditions. The strength of the polar vortex reveals to be better represented in GCMs with a high resolution of the upper stratosphere or even higher levels (Shindell, 1999). This point will be further discussed in chapter 6.

Chapter 4

North Atlantic teleconnections under weak and strong polar vortex conditions

This chapter concentrates on the tropospheric low frequency variability in the North Atlantic region and on the teleconnections associated with it. The dominant tropospheric teleconnection pattern in the North Atlantic sector is the North Atlantic Oscillation (NAO). It exerts a strong influence on wintertime surface air and sea surface temperature over wide regions of the North Atlantic ocean, Eurasia and the Mediterranean, the Arctic, and North America. Fluctuations of the NAO are also associated with changes in the strength and direction of the North Atlantic storm tracks and, thus, with changes in precipitation over Europe and the Mediterranean. Structural changes in the North Atlantic Oscillation might therefore have a strong impact on the atmospheric variability in a large part of the Northern Hemisphere.

It has been shown in the previous section that not only the stationary wave pattern but also the low frequency variability structure is different in the two polar vortex regimes. This chapter focuses on changes in the low frequency variability, in particular with respect to teleconnection patterns in the North Atlantic sector. NCEP/NCAR reanalyses for the winter months December to March during 1958 – 1998 were employed for the analyses presented in this chapter in order to examine structural changes in the teleconnection patterns as well as their lifecycles and involved dynamical processes. Moreover, impacts on atmospheric variables in the North Atlantic sector are discussed.

4.1 Patterns

Teleconnection is defined as a large scale correlation or anticorrelation between variables at remote locations. Fluctuations associated with teleconnections are characterized by low frequency timescales. Teleconnection patterns take the form of standing waves with fixed nodes and antinodes, called 'centers of action'. Wallace and Gutzler (1981) examined the atmospheric teleconnection patterns in the Northern Hemisphere by applying correlation analysis to observations. Their methods will be adopted in the following. For each gridpoint i the correlation r_{ij} of a variable Q with the values at another gridpoint j is

$$r_{ij} = \frac{\frac{1}{N}\sum_{t=1}^{N}(Q'_i(t) \cdot Q'_j(t))}{\sqrt{\frac{1}{N}\sum_{t=1}^{N}(Q'_i(t))^2} \cdot \sqrt{\frac{1}{N}\sum_{t=1}^{N}(Q'_j(t))^2}}. \tag{4.1}$$

r_{ij} is called correlation coefficient, $Q'_i(t)$ and $Q'_j(t)$ are the timeseries of a variable Q at the gridpoints i and j, respectively. The prime indicates the deviation from the time mean. N is the length of the timeseries. If r_{ij} is calculated for every gridpoint j, then i is named the 'base point'. The matrix of correlation coefficients constitutes the 'correlation matrix'. r_{ij} will be large in the neighborhood of the base point, converging to 1 as j approaches i, and will drop to zero if the distance of point j from the base point is larger than the typical radius of coherent circulation systems. Large positive or negative values of r_{ij} outside this area indicate some kind of teleconnection.

Wallace and Gutzler (1981) introduced the variable 'teleconnectivity' in order to detect teleconnections without a priory information about the location of possible centers of action. For a grid point i, the correlation with the timeseries at every other gridpoint is computed. The teleconnectivity at this grid point i is then defined as the amount of the largest negative correlation:

$$T_i = |(r_{ij})\ minimum\ for\ all\ j\ | \tag{4.2}$$

Fig. 4.1 shows the teleconnectivity of the 15 day-low pass filtered 300 hPa geopotential height for the winter months December to March (DJFM) during the period 1958 to 1998. The filtering was accomplished with a Fourier filter (see appendix B.1). There are two large diffuse maxima extending zonally over almost the entire North Atlantic: one in subpolar and middle latitudes and the other, south of the first, in the subtropics. The geopotential heights in these areas are anticorrelated at -0.5 to -0.55. The maximum anticorrelation in these broad areas can be found over the western subtropical North Atlantic and northeastern

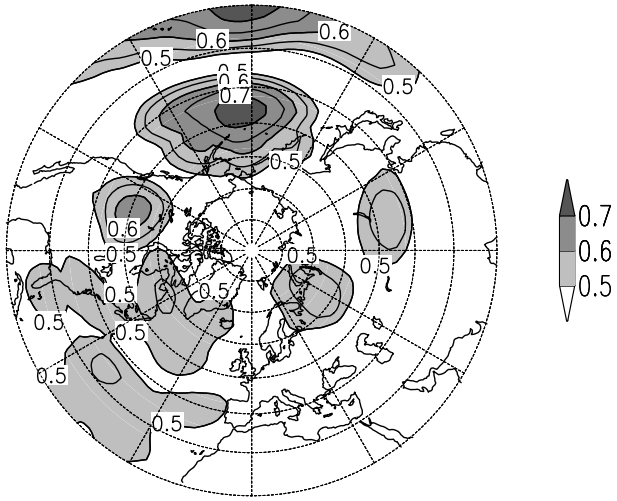

Figure 4.1: *Teleconnectivity of the 15 day-low pass filtered geopotential height of the 300 hPa level in December to March from 1958 to 1998. The isoline interval is 0.05. Only values larger than 0.5 are shown.*

Canada, respectively. There are also several maxima of teleconnectivity over the Pacific and North America. They constitute a wavetrain-like teleconnection pattern reaching from the (sub)tropical Pacific to the southeastern US coast.

A somewhat different picture arises if the strong (SVR) and the weak (WVR) polar vortex regime are treated separately (for the definitions see chapter 2). In the SVR, there are two zonally elongated areas of strong teleconnectivity over much of the North Atlantic (Fig. 4.2a). Their centers are located southeast of Greenland (55°–60°N, 30°–45°W) and in the subtropical North Atlantic (30°–35°N, 35°–45°W), respectively. An inspection of the correlations of geopotential heights area averaged over these two centers (Fig. 4.3) exhibits that the teleconnection maxima indeed constitute a teleconnection pattern of geopotential height with a dominant north-south dipole structure. The two major centers of action are anticorrelated at a value of more than -0.6. The center near Greenland also reveals to be (negatively) correlated with the geopotential height over central Europe. The anticorrelation is, however, somewhat weaker than that between the two major centers over the central North Atlantic. Hence, the teleconnection pattern may be regarded as mainly characterized by a dipole structure. In the following, we will refer to this teleconnection pattern as the NA-SVR pattern, where the NA stands for 'North Atlantic' and the SVR for the strong vortex regime. The NA-SVR pattern is reminiscent of a southwestward displaced North Atlantic Oscillation pattern or of the combined 'western Atlantic' and 'eastern Atlantic' patterns described by Wallace and Gutzler (1981). They deduced the

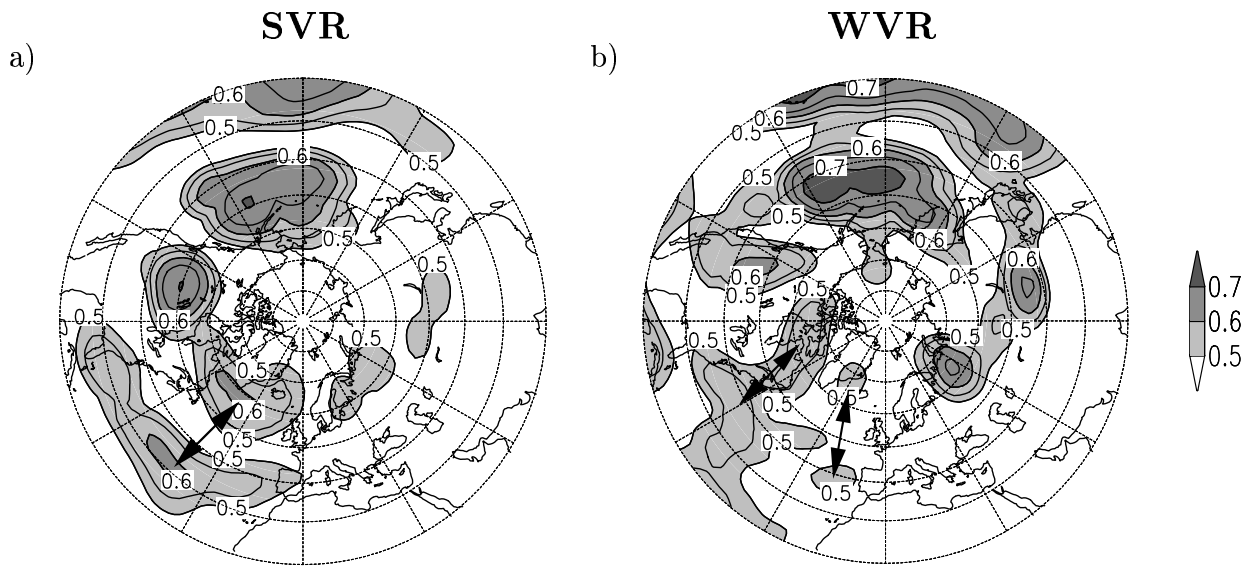

Figure 4.2: *Teleconnectivity of the 15 day-low pass filtered geopotential height of the 300 hPa level for (a) SVR and (b) WVR. The isoline interval is 0.05. Only values above 0.5 are shown. The arrows mark the dominant centers of action of the teleconnection patterns discussed in this chapter.*

latter patterns from observed monthly mean 500 hPa geopotential heights. The centers of the 'eastern Atlantic' pattern, however, are located about 5° south of the corresponding NA-SVR pattern centers (see also Barnston and Livezey, 1987). In Fig. 4.3, the geopotential height in the northern center of action is furthermore weakly anticorrelated with the height in the North Pacific/Aleutian region. The anticorrelation is rather weak on the discussed timescale (-0.3) but it increases to almost -0.45 on the basis of monthly means (not shown). Castanheira and Graf (2003) found that such an anticorrelation between the subpolar North Atlantic and North Pacific is only present in months where the stratospheric polar vortex is strong, whereas there is almost no (anti-)correlation if the vortex is weak.

While the SVR is thus characterized by a single teleconnection pattern over the central North Atlantic, there are two north-south dipole patterns in the weak vortex regime (WVR; Fig. 4.2b). The western pattern comprises centers of action over northeastern Canada and over the western part of the subtropical North Atlantic. The geopotential heights in these centers are anticorrelated at almost -0.6. The second teleconnection pattern is located over the eastern North Atlantic. Its northern center of action is situated northwest of Iceland/east of

Greenland, whereas the southern center is located west of the Iberian peninsula. The geopotential height (anti)correlation between these two centers is about -0.53. In the following, the two patterns will be referred to as the western and the eastern NA-WVR pattern, respectively. The eastern NA-WVR pattern (Fig. 4.4a,b) resembles very much the NAO, which is the dominant North Atlantic teleconnection pattern at the surface (see e.g. Wallace and Gutzler, 1981, their Fig. 9b). Geopotential height fluctuations in the centers of action of the western NA-WVR pattern are not only stronger anticorrelated than those of the eastern NA-WVR pattern, but are also related to a larger fraction of variability. This can be inferred from the root mean square of the 10 day-low pass filtered 300 hPa geopotential height (chapter 3, Fig. 3.14b), which is maximum close to the northern center of the western NA-WVR pattern. Neither of the two NA-WVR patterns shows significant correlations with geopotential height over the North Pacific. This agrees to Castanheira and Graf (2003), who found that such a connection is only eminent in the SVR regime. The weak vortex regime is characterized by a large number of March events due to the decay of the vortex in late winter/early spring. However, the two NA-WVR patterns can also be identified in teleconnection maps for the months December, January, and February, discarding the month March. This means, that the differences between the teleconnectivity structures in the two stratospheric regimes are not simply due to the change from winter to spring conditions.

Outside the North Atlantic sector, wavetrain-like teleconnection patterns emerge which reach from the tropical Pacific region over the North Pacific and North America to the southeastern US (Fig. 4.2). These patterns resemble the Pacific/North American (PNA) pattern (e.g. Wallace and Gutzler, 1981; Barnston and Livezey, 1987). The centers of action, however, are displaced about 10° of longitude further to the east than the original PNA pattern. The teleconnection patterns in Fig. 4.2 may thus rather be interpreted as a combination between the PNA and the Tropical/Northern Hemisphere (TNH) pattern (Barnston and Livezey, 1987). The centers of the latter are shifted eastward with respect to those of the PNA, so that they are located on the node lines of the PNA pattern, i.e. the two patterns are out of phase. The correlation between the North American and the North Pacific center of action is stronger in the SVR case than in the WVR, in which the North Pacific center is more strongly correlated with the tropical Pacific (Fig. 4.5). Hence, the center over the southeastern US is weaker and more obscure in the WVR than in the SVR. In both regimes, there is only weak correlation with the North Atlantic region. Moreover, the centers of action are more or less located on the node lines of the North Atlantic patterns, i.e. the wavetrains are out of phase with the North Atlantic patterns. This thesis concentrates on the North Atlantic sector. The remainder of this chapter thus only addresses the North Atlantic teleconnection patterns. The effect of stratospheric regime changes on the North Pacific/North American sector (see Castanheira and

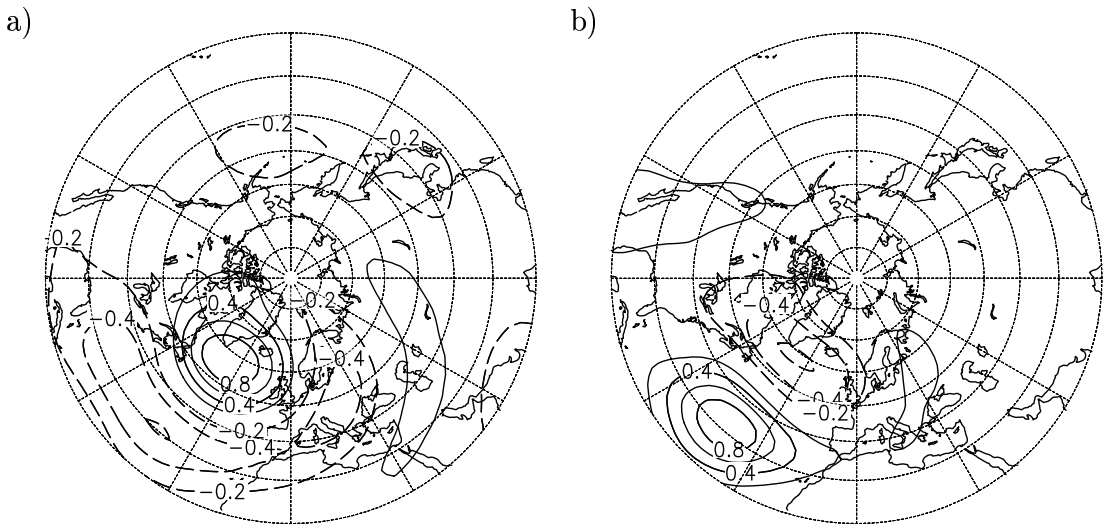

Figure 4.3: *Correlation between the 15 day-low pass filtered 300 hPa geopotential height at every grid point and area averages over the centers of action of the NA-SVR pattern. Area average over (a) the northern center of action (55°–60° N, 32.5°–42.5° W) and over (b) the southern center of action (30°–32.5° N, 37.5°–45° W). The data basis is the SVR. The zero contour is omitted.*

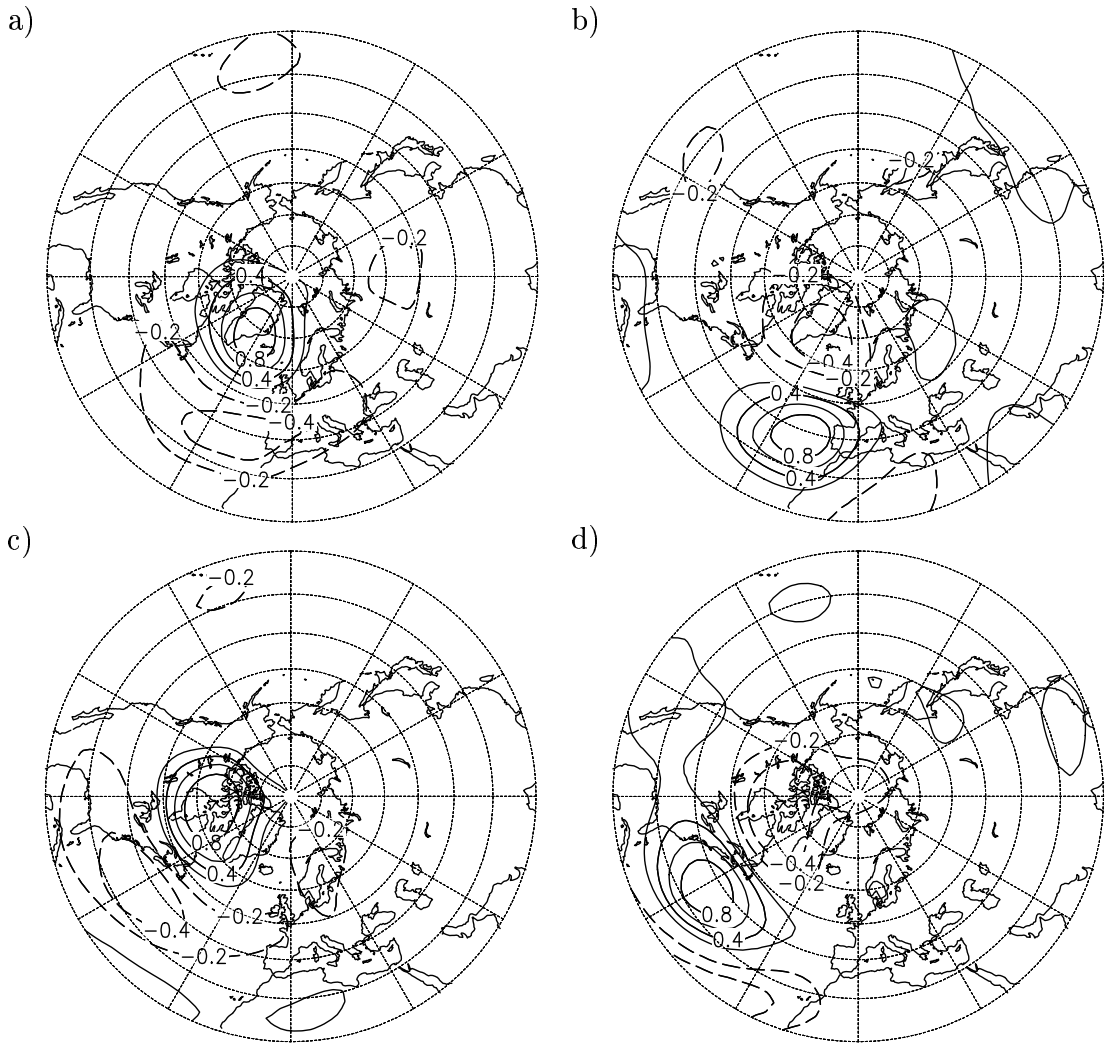

Figure 4.4: *Correlation between the 15 day-low pass filtered 300 hPa geopotential height at every grid point and area averages over the centers of action of the two NA-WVR patterns. Area average over (a) the northern center of the eastern NA-WVR pattern (65°–70°N, 27.5°–35° W), over (b) the southern center of the eastern NA-WVR pattern (37.5°–40°N, 15°–22.5° W), (c) the northern center of the western NA-WVR pattern (62.5°–65°N, 77.5°–82.5° W), and over (d) the southern center of the western NA-WVR pattern (35°–37.5°N, 55°–62.5° W). The data basis is the WVR. The zero contour is omitted.*

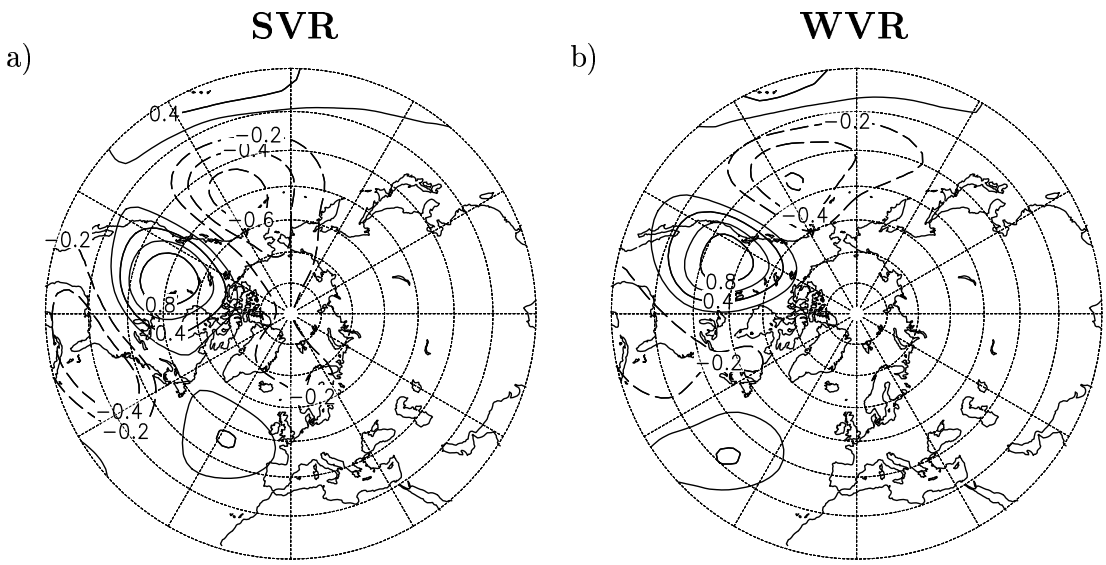

Figure 4.5: *Correlation between the 15 day-low pass filtered 300 hPa geopotential height at every grid point and area averages over the North American teleconnectivity maximum. (a) SVR: area average over 47.5°–52.5°N, 102.5°–110° W, and (b) WVR: area average over 45°–47.5°N, 110°–115° W. The zero contour is omitted.*

Graf, 2003) should, however, be more explicitly examined in future studies.

The structures of the teleconnection patterns do not depend much on the time filter. They can also be identified in teleconnectivity maps with geopotential height data filtered with the Blackmon and Lau (1980) low pass filter (appendix B.1), which leaves periods longer than 10 days (Fig. 4.6). However, the WVR patterns do not emerge as clearly because of the high frequency background noise in particular in the WVR. The western NA-WVR pattern is concealed by other teleconnection maxima that vanish if higher frequencies are removed from the data (see Fig. 4.2b). However, the eastern NA-WVR pattern can still be identified. The anticorrelation between its two centers of action amounts to -0.45. On a monthly mean basis (Fig. 4.7), all three patterns emerge very clearly with maximum anticorrelations between -0.7 and -0.8. The NA-SVR pattern is moved about 10° eastward and the eastern NA-WVR pattern is moved about 5° northward in comparison with the 15 day-low pass filtered data. The patterns are furthermore highly reproducible in subsets of the NCEP/NCAR reanalysis dataset (not shown).

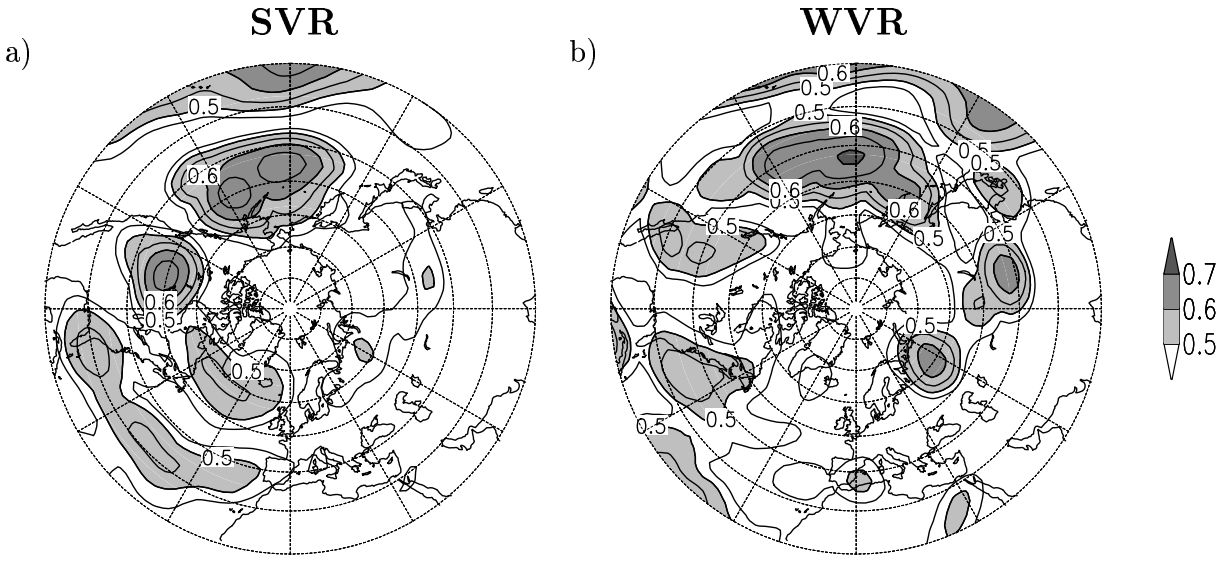

Figure 4.6: *As in Fig. 4.2, but for 10 day-low pass filtered data (Blackmon and Lau, 1980; see appendix B.1). The isoline interval is 0.05. Only values larger than 0.45 are shown.*

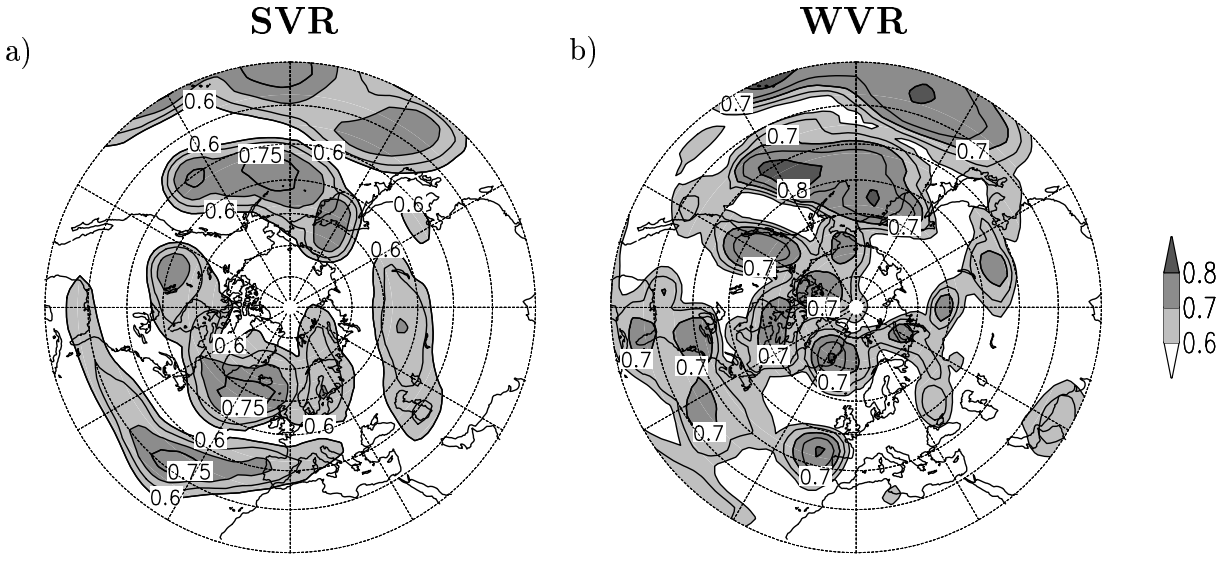

Figure 4.7: *As in Fig. 4.2, but for monthly mean data. The isoline interval is 0.05. Only values larger than 0.6 are shown. Please note the modified shading conventions.*

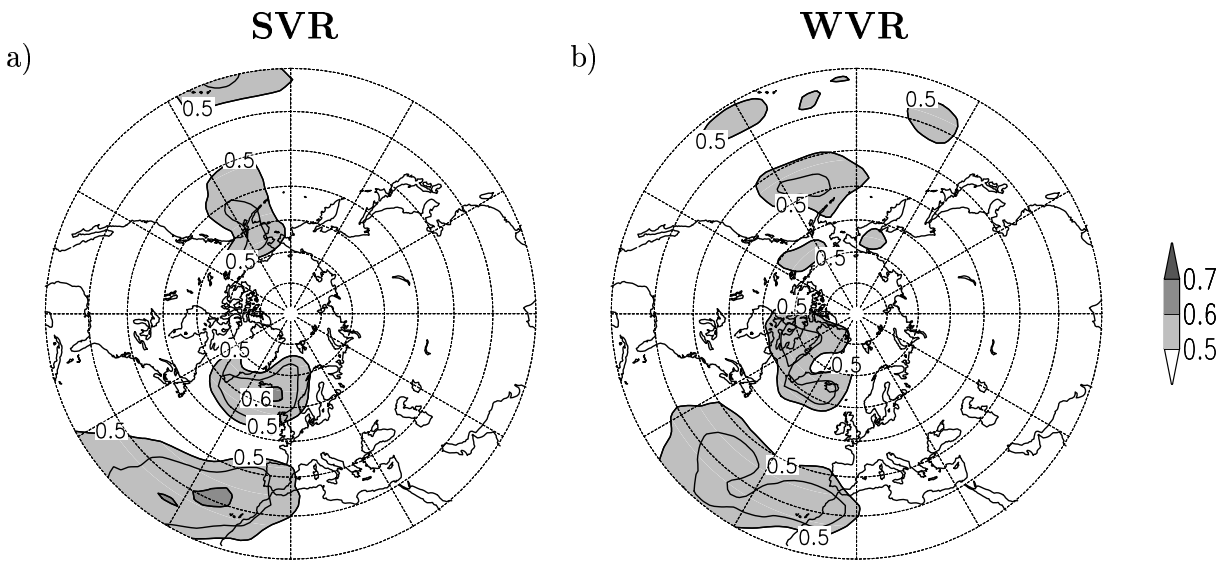

Figure 4.8: *As in Fig. 4.2, but for 15 day-low pass filtered data at the 1000 hPa level. The isoline interval is 0.05. Only values larger than 0.5 are shown.*

While the teleconnection maps for the 500 hPa geopotential height (not shown) are almost identical to the 300 hPa maps, the situation is somewhat different near the surface. Fig. 4.8 shows teleconnectivity maps for the 15 day-low pass filtered geopotential height at the 1000 hPa level. All centers of action are located further east than at upper pressure levels, i.e. there is a slight westward shift with height. In the WVR, there are imprints of the western NA-WVR pattern with centers over the Baffin Bay/northeastern Canada and over the central subtropical North Atlantic. The imprints of the eastern NA-WVR pattern and the NA-SVR pattern are difficult to distinguish. Although the subtropical center of the NA-SVR pattern is located about 10° west of the corresponding center of the eastern NA-WVR pattern, the northern centers of action overlap. This is due to the fact that the eastern NA-WVR pattern is located more south than in the upper troposphere. If it is intended to examine the stratospheric influence on low frequency teleconnection patterns, the focus should therefore be on the middle to upper troposphere.

Temporal relationships

In order to examine the temporal behavior of low frequency anomalies, index timeseries were defined for each teleconnection pattern according to the definitions given in appendix A. The indices display the difference of normalized anomalous 300 hPa geopotential heights between the centers of action of the respective teleconnection pattern.

It turns out that the western and eastern NA-WVR pattern indices are only weakly correlated with each other. If the 15 day-low pass filter is applied the concurrent correlation amounts to 0.18. The maximum correlation of (only) 0.37 is reached if the eastern NA-WVR index leads the western NA-WVR index by about 4 days. Therefore, the two NA-WVR patterns can approximately be considered as two different patterns. For monthly mean index timeseries, however, this correlation increases to 0.41 due to the averaging process.

The monthly mean index for the eastern NA-WVR pattern is very closely correlated with a 'classic style' NAO index (defined as the difference of normalized monthly 1000 hPa geopotential height anomalies between the Azores and Iceland, see appendix A). The correlation amounts to 0.91, whereas the correlations between this classic style NAO index on the one hand and the western NA-WVR and NA-SVR pattern indices on the other hand are 0.62 and 0.74, respectively.

The monthly mean teleconnection index of the western NA-WVR pattern is correlated at a value of 0.68 with the zonal mean zonal wind at 50 hPa and 65°N. Lagged correlations with 10 day and 15 day low pass filtered index timeseries reveal that the connection between the western NA-WVR pattern index and the strength of the zonal mean zonal wind is strongest if the polar vortex leads by one to two days. In particular the northern center of action of the western NA-WVR pattern (Fig. 4.2) coincides with a major anomaly in the mean geopotential height difference field between SVR and WVR (Fig. 3.12). The western NA-WVR pattern therefore seems to be associated with changes in the polar night jet strength and possibly also with breakdowns of the latter. The NA-SVR and eastern NA-WVR patterns indices are not significantly correlated with the strength of the zonal mean zonal wind at 50 hPa and 65°N (0.22 and 0.28 for monthly means, respectively).

4.2 Dynamics of persistent episodes

It has been shown that the structures of North Atlantic teleconnection patterns are strikingly different in the two polar vortex regimes. In this section, lifecycles

of high and low teleconnection index events will be discussed. The purpose is to identify the dynamical mechanisms involved in the growth and decay of such low frequency anomalies. This is achieved by analyzing the streamfunction tendency in the upper troposphere and the contributions from single forcing terms.

Index timeseries calculated from low pass filtered 300 hPa geopotential height were used for the following examinations. In contrast to the previous section, the Blackmon and Lau (1980) 10 day-low pass filter was applied instead of a 15 day-low pass Fourier filter (appendix B.1). Although the patterns of teleconnectivity emerge more clearly in the 15 day-low pass filtered height fields (Fig. 4.2) an objective investigation of lifecycles requires the incorporation of timescales shorter than 15 days, which, however, still belong to the low frequency range.

The streamfunction is defined as the inverse Laplacian of relative vorticity. In the quasigeostophic framework, streamfunction ψ and geopotential height z are related by $\psi = gf^{-1}z$, where g is the gravitational acceleration and f the Coriolis parameter. The patterns of the 10 day-low pass filtered 300 hPa streamfunction linearly regressed onto the index time series of the three North Atlantic teleconnection patterns are presented in Fig. 4.9. The figure clearly shows the basically dipolar structures of the teleconnection patterns. The correlation with the index timeseries exceeds +/- 0.8 in both centers of action. However, the NA-SVR pattern has also an additional weak maximum over eastern Europe. This maximum has the same sign as the anomaly at the southern center of action, but the amplitude is only half as large and the correlation with the NA-SVR teleconnection index is below 0.4. This corresponds to the fact that the correlation with the geopotential height at the northern center of action is stronger than with the geopotential height at the southern center (Fig. 4.3). A secondary maximum over Europe can also be observed for the western NA-WVR pattern (Fig. 4.9c), but it is even weaker than for the NA-SVR pattern: The streamfunction anomaly does not exceed $5 \cdot 10^6$ m^2/s^2.

For the following examination of lifecycles, persistent episodes with either extraordinarily high or low teleconnection index values have to be categorized. In this study, an episode with positive index values is defined as persistent if the index stays larger than 0.75 times the standard deviation σ for at least 5 days. The examination of the lifecycles focuses on the growth phase of the anomalies. Thus, episodes had to be selected in which the anomalies really grow and are not already large. We therefore introduced the following constraint: The index values must be lower than 0.5 σ for at least 5 days before the onset day, i.e. the day before the index becomes larger than 0.75 σ. For episodes with negative index values the procedure is analogous but with the limits -0.75 σ and -0.5 σ. If there are two such episodes within 20 days the incident with the stronger increase or decrease of index values on the onset day is chosen. The thresholds were selected

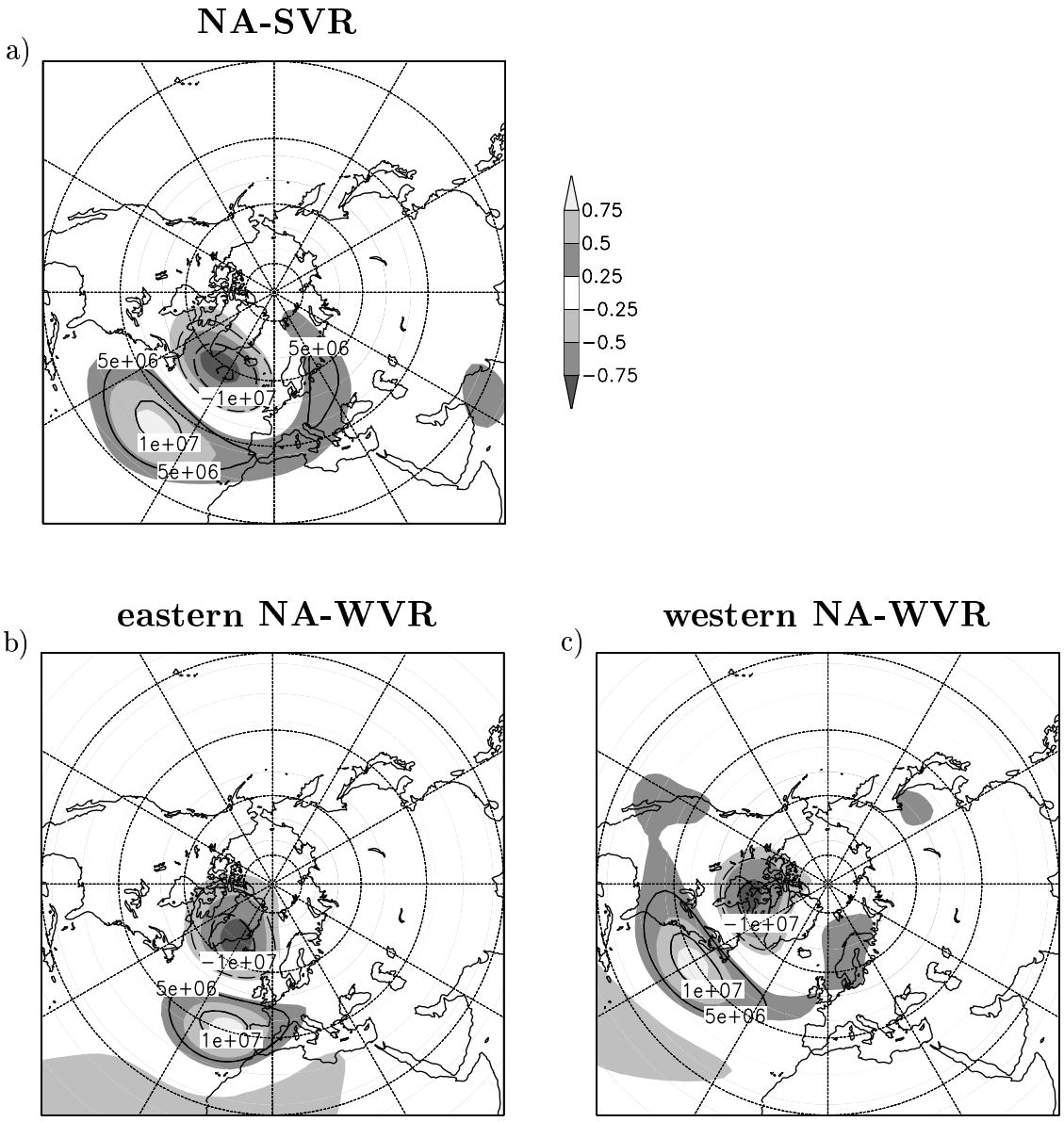

Figure 4.9: *Linear regression coefficient [m^2/s, isolines] of the 10 day-low pass filtered 300 hPa streamfunction at each grid point regressed onto the index timeseries of the (a) NA-SVR pattern, (b) the eastern NA-WVR pattern, and (c) the western NA-WVR pattern. The shadings display the correlation coefficients. The regression coefficients correspond to one standard deviation of respective the index timeseries and are calculated only with data from the vortex regime in which the teleconnection index is defined.*

in such a way that only very large persistent episodes are captured and that the number of the selected episodes is not too small.

In order to display the growth or decay of the teleconnection patterns, the low pass filtered 300 hPa streamfunction field was projected onto the regression patterns in Fig. 4.9. Prior to this, the regression patterns were standardized by division with the (spatial) root mean square value over all gid points. Fig. 4.10 shows composites of such projections. The projections range from 10 days before to 10 days after the onset day. The thick lines represent the average over all persistent episodes, i.e. over 30 positive or 23 negative NA-SVR index episodes and over 9 (10) positive or 12 (12) negative eastern (western) NA-WVR index episodes. The gray lines display the average plus or minus a half standard deviation. In all cases, the average projections start with values of opposite sign and reach their largest values 3–5 days after the onset day. It takes 6–8 days from crossing the zero line to reach the maximum values. The interpolated average duration of such persistent episodes thus amounts to about two weeks. The amplitudes of the NA-SVR fluctuations have almost equal amounts for both polarities, whereas for the NA-WVR patterns, the composite amounts during the negative phases are larger than during the positive phases. However, an inspection of the corresponding composite streamfunction fields (not shown) revealed that these differences are only gradual. The spatial structures are almost identical for both polarities of the respective teleconnection pattern and similar to the regression patterns in Fig. 4.9. The decay of the averaged anomalies seems to be less rapid than their growth. This is a consequence of compositing based on the onset day which favors rapid growth on that day (Feldstein and Lee, 1996). Another consequence of this procedure is that the standard deviation of the projections is smaller close to the onset day than for longer time lags. The focus of the following examinations will be on the growth phase, when the standard deviations are smallest.

Fig. 4.11 shows composites of the low pass filtered 300 hPa streamfunction anomaly for positive and negative NA-SVR pattern index events at different time lags. Only weak anomalies can be identified in the North Atlantic sector 4 days before the onset day (Fig. 4.11, upper row). The structure of the teleconnection pattern does not emerge at that time. Instead, there are weak positive (negative) streamfunction anomalies over the subpolar North Atlantic and negative (positive) ones over the subtropics for the positive (negative) index events. This reflects the previous finding that the composite projection onto the standardized regression pattern (Fig. 4.10, upper row) is weak but of opposite sign several days before the onset day. The sign of the anomalies is changed on the onset day (Fig. 4.11, medium row). The anomaly structures over the North Atlantic are then similar to the regression patterns. The anomalies grow until they reach their maximum values 4 days after the onset day (Fig. 4.11, lower row).

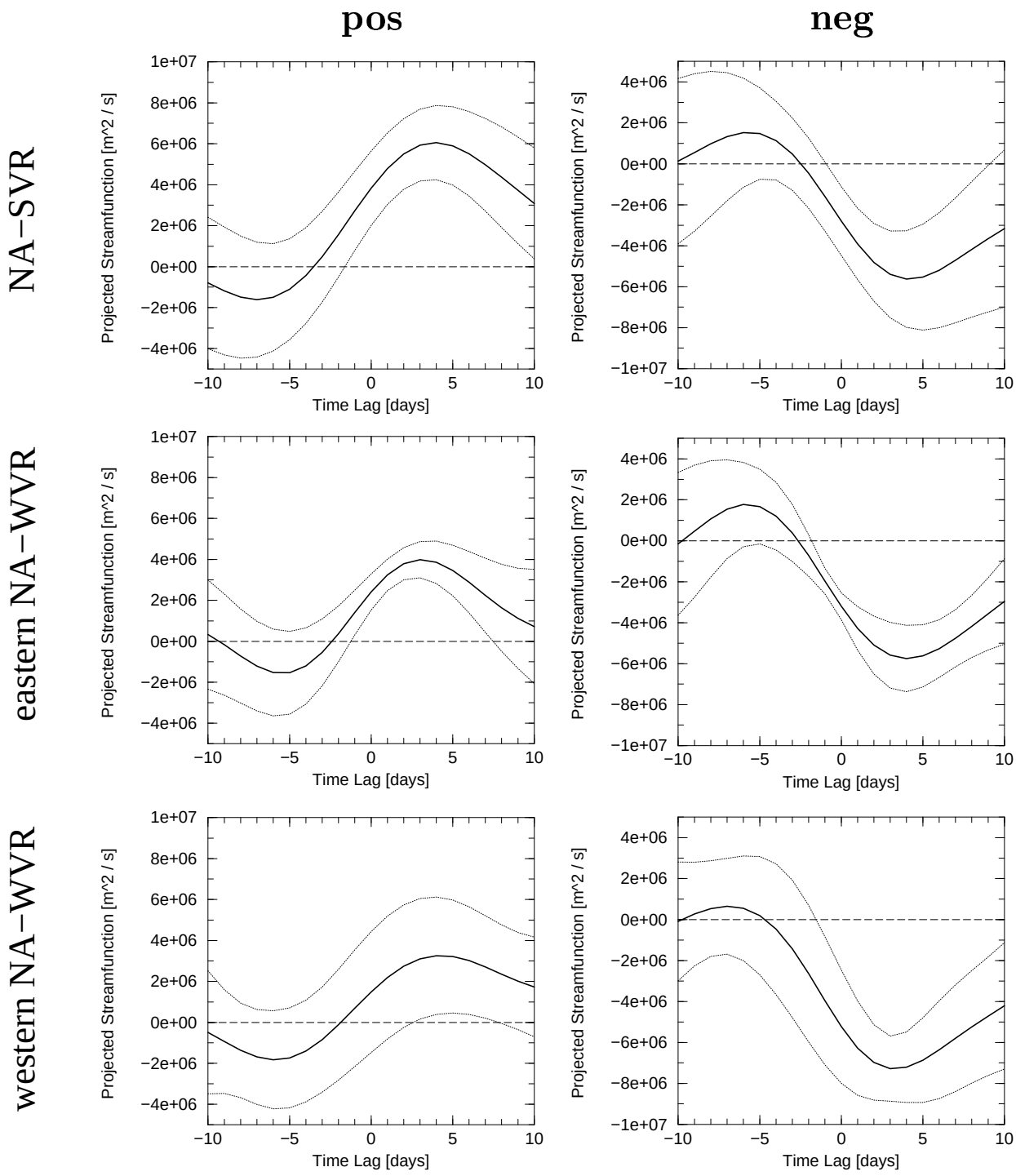

Figure 4.10: *Projection of the 10 day-low pass filtered 300 hPa streamfunction anomaly field onto the standardized regression patterns in Fig. 4.9 [m^2/s]. The solid lines display the composite projection for the persistent anomalies defined in the text, the gray lines the composite plus/minus one standard deviation. Shown are composites for positive (left column) and negative (right column) events of the NA-SVR (upper row), the eastern NA-WVR (medium row), and the western NA-WVR pattern index (lower row).*

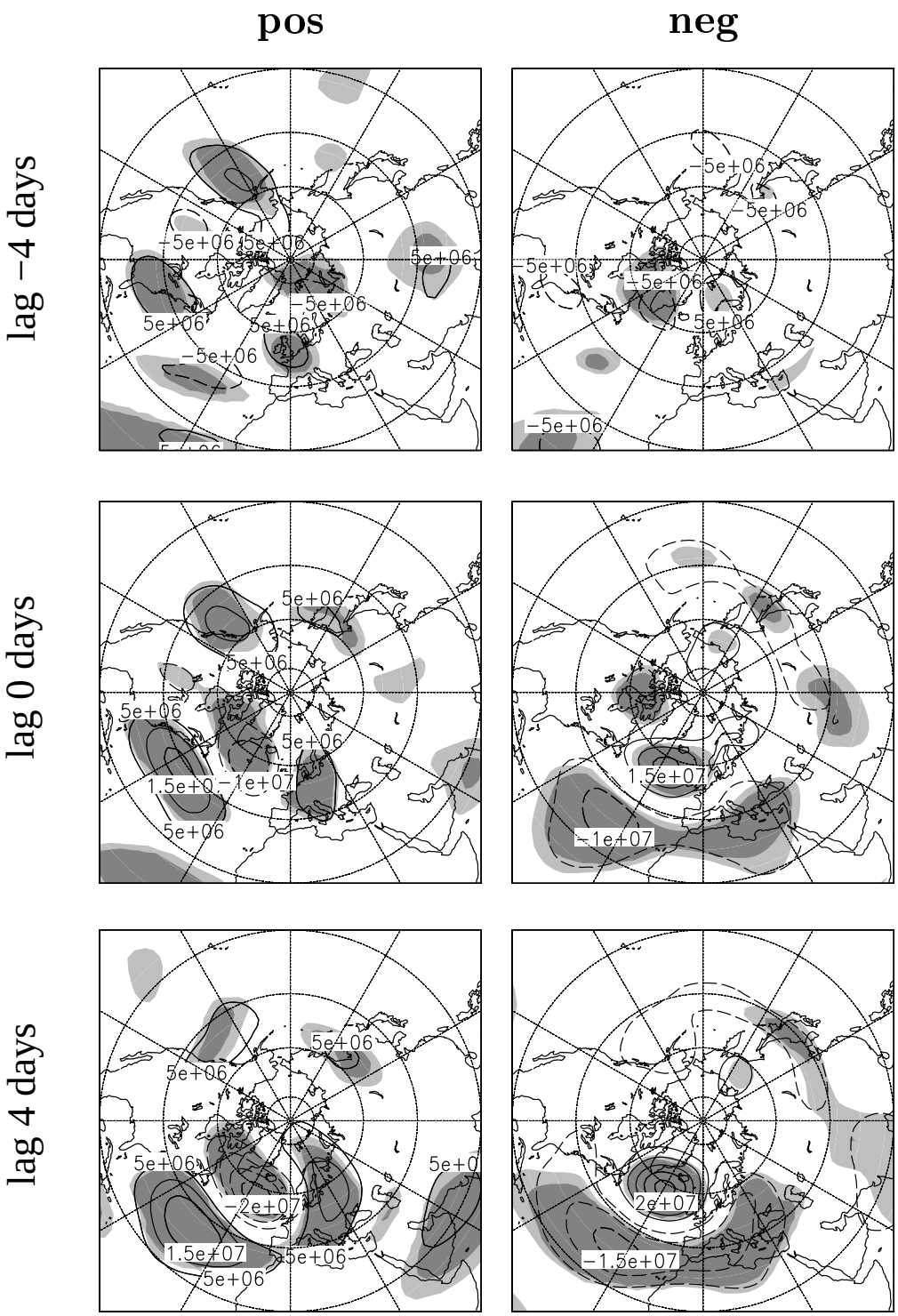

Figure 4.11: *Composite low pass filtered 300 hPa streamfunction [m^2/s] at different time lags for the positive (left panels) and negative (right panels) persistent NA-SVR pattern index episodes. Upper row: lag -4 days; medium row: lag 0 days; lower row: lag 4 days. The shadings indicate that the t-test significance of the anomalies is above 95% (light shading) or 99% (dark shading).*

The positive phase of the NA-SVR pattern seems to be connected with a wavetrain across North America, but there is no such link neither in the negative phase of the NA-SVR pattern nor for both polarities of the eastern NA-WVR pattern (not shown). In his examination of NAO lifecycles Feldstein (2003) also described a connection with such a wavetrain only for the positive phase of the NAO, but he found nothing like this in the negative NAO phase. It seems from the left panels of Fig. 4.11 that the subtropical high at the positive NA-SVR pattern events additionally moves eastward from the North American east coast. This, however, is not the case for the negative index events, in which the anomalies grow in almost fixed positions. Moreover, there is no indication for such distinctly moving anomalies in the NA-WVR pattern composites. For all patterns and polarities, however, the maximum growth phase is characterized by almost fixed structures identical to the regression patterns in Fig. 4.9. Therefore, the differences in the initial streamfunction patterns at the very beginning of the growth phase will not be discussed.

Low frequency streamfunction tendency equation

Forcing mechanisms involved in the growth and decay of the teleconnection anomalies are examined by analyzing the low frequency streamfunction tendency equation term by term in a similar manner as in chapter 3, section 3.3 for the time mean. Following the procedure applied by Cai and van den Dool (1994) and Feldstein (1998), the low frequency streamfunction tendency equation can be written as

$$\frac{\partial \psi}{\partial t} = \sum_{i=1}^{8} \chi_i + R, \tag{4.3}$$

with the residual R and the single terms χ_i representing the forcing by advection of planetary vorticity

$$\chi_1 = \nabla^{-2}\left(-\vec{v}^L \cdot \nabla f\right), \tag{4.4}$$

by advection of (relative) vorticity due to the interaction of low frequency eddies with the zonal mean part of the time mean flow

$$\chi_2 = \nabla^{-2}\left(-\left[\bar{\vec{v}}\right] \cdot \nabla \xi^L - \vec{v}^L \cdot \nabla \left[\bar{\xi}\right]\right), \tag{4.5}$$

by advection of (relative) vorticity due to the interaction of low frequency eddies with the zonally asymmetric part of the time mean flow, i.e. with the stationary eddies

$$\chi_3 = \nabla^{-2}\left(-\bar{\vec{v}}^* \cdot \nabla \xi^L - \vec{v}^L \cdot \nabla \bar{\xi}^*\right), \tag{4.6}$$

by the low frequency contribution to the divergence term

$$\chi_4 = \nabla^{-2}\left(-\left(f+\bar{\xi}\right)\nabla\cdot\vec{v}^L - \xi^L\nabla\cdot\bar{\vec{v}}\right), \tag{4.7}$$

by transient eddy vorticity fluxes

$$\chi_{tr} = \nabla^{-2}\left(-\nabla\cdot\left(\vec{v}'\xi'\right)\right)^L, \tag{4.8}$$

and by vertical vorticity advection and tilting terms

$$\chi_8 = \nabla^{-2}\left(-\vec{k}\cdot\left(\nabla\times\left(\omega^L\frac{\partial\bar{\vec{v}}}{\partial p} + \bar{\omega}\frac{\partial\vec{v}^L}{\partial p} + \omega'\frac{\partial\vec{v}'}{\partial p}\right)\right)\right)^L. \tag{4.9}$$

ψ represents the streamfunction, ξ the relative vorticity, and $\vec{v}$ the horizontal wind vector (u, v), where u is the zonal and v the meridional component. ω is the vertical wind component, a the Earth's radius, and f the Coriolis parameter. An overbar denotes a time mean, a prime a deviation from the time mean, square brackets indicate a zonal mean, and an asterisk a deviation therefrom. The superscript 'L' represents low pass filtered quantities. As before, the 10 day-low pass filter introduced by Blackmon and Lau (1980) was applied (see appendix B.1).

In order to separately determine the influence of synoptic and low frequency fluctuations, the unfiltered variables $\vec{v}'$ and ξ' in term χ_{tr} (Eq. 4.8) were filtered in time. For this task, both, the Blackmon and Lau (1980) band pass and low pass filters were applied (see appendix B.1). This means that, in the band pass case, fluctuations with periods between 2.5 and 6 days are captured, and in the low pass case fluctuations with periods longer than 10 days. Synoptic and low frequency fluctuations are therefore well separated. Hence, term χ_{tr} can be splitted up into forcing contributions from low frequency eddy vorticity fluxes

$$\chi_5 = \nabla^{-2}\left(-\nabla\cdot\left(\vec{v}^L\xi^L\right)\right)^L, \tag{4.10}$$

from band pass filtered (synoptic) eddy vorticity fluxes

$$\chi_6 = \nabla^{-2}\left(-\nabla\cdot\left(\vec{v}^B\xi^B\right)\right)^L, \tag{4.11}$$

and from mixed terms describing the interaction between the low frequency and the synoptic eddies

$$\chi_7 = \nabla^{-2}\left(-\nabla\cdot\left(\vec{v}^L\xi^B\right) - \nabla\cdot\left(\vec{v}^B\xi^L\right)\right)^L, \tag{4.12}$$

plus a residual originating from fluctuations which were not captured with the filters. The superscripts 'L' and 'B' represent low pass and band pass filtered quantities, respectively.

Even without splitting up term χ_{tr}, the budget in equation 4.3 is never perfectly balanced without incorporating the residual R. On the one hand, this term includes physical processes that have been neglected such as external forcing and dissipation. On the other hand, R also contains errors in the balance e.g. arising from the use of daily mean data. Additional errors result from the computation of the total streamfunction tendency with centered differences in time:

$$\frac{\partial\psi(t)}{\partial t} = \frac{\psi(t+\delta t) - \psi(t-\delta t)}{2\delta t}, \tag{4.13}$$

where the streamfunction ψ was calculated from the relative vorticity ξ as $\psi = \nabla^{-2}\xi$, and the time interval δt is one day.

Lifecycles

In the following, projections of the streamfunction tendency and of single terms in equation 4.3 onto the standardized regression patterns (Fig. 4.9) are discussed. Fig. 4.12 shows the projections for positive and negative NA-SVR index events. The maximum streamfunction tendency and, thus, the most rapid growth of the low frequency anomaly can be observed 1 – 2 days before the onset day. Fig. 4.12 shows that the forcing contribution from term χ_8, i.e. from the sum of the vertical vorticity advection and tilting terms, is very small throughout the whole lifecycle and can therefore be neglected. Most of the streamfunction tendency is explained by the terms χ_1 to χ_4 and χ_{tr}. This implies that the error in the imperfectly balanced budget in equation 4.3, the residual R, is substantially smaller than the sum of the other terms. The projections for the two NA-WVR patterns reveal to be qualitatively similar to those for the NA-SVR pattern in Fig. 4.12 and are therefore not shown.

Figs. 4.12c,d show that term χ_4, the low frequency contribution to the divergence term, is mainly responsible for the decay of the low frequency streamfunction anomalies. The projection reaches its largest value several days after the onset day, i.e. when the streamfunction anomaly is also large. This is not only true for the NA-SVR but also for the NA-WVR projections (Fig. 4.13). Feldstein (2003) argued that the low frequency divergence term χ_4 is associated with Ekman Pumping. Figs. 4.12c,d and 4.13 furthermore show that, in each case, the projection of term χ_4 starts with values of the opposite sign before the low frequency streamfunction anomaly develops. The reason is that, before

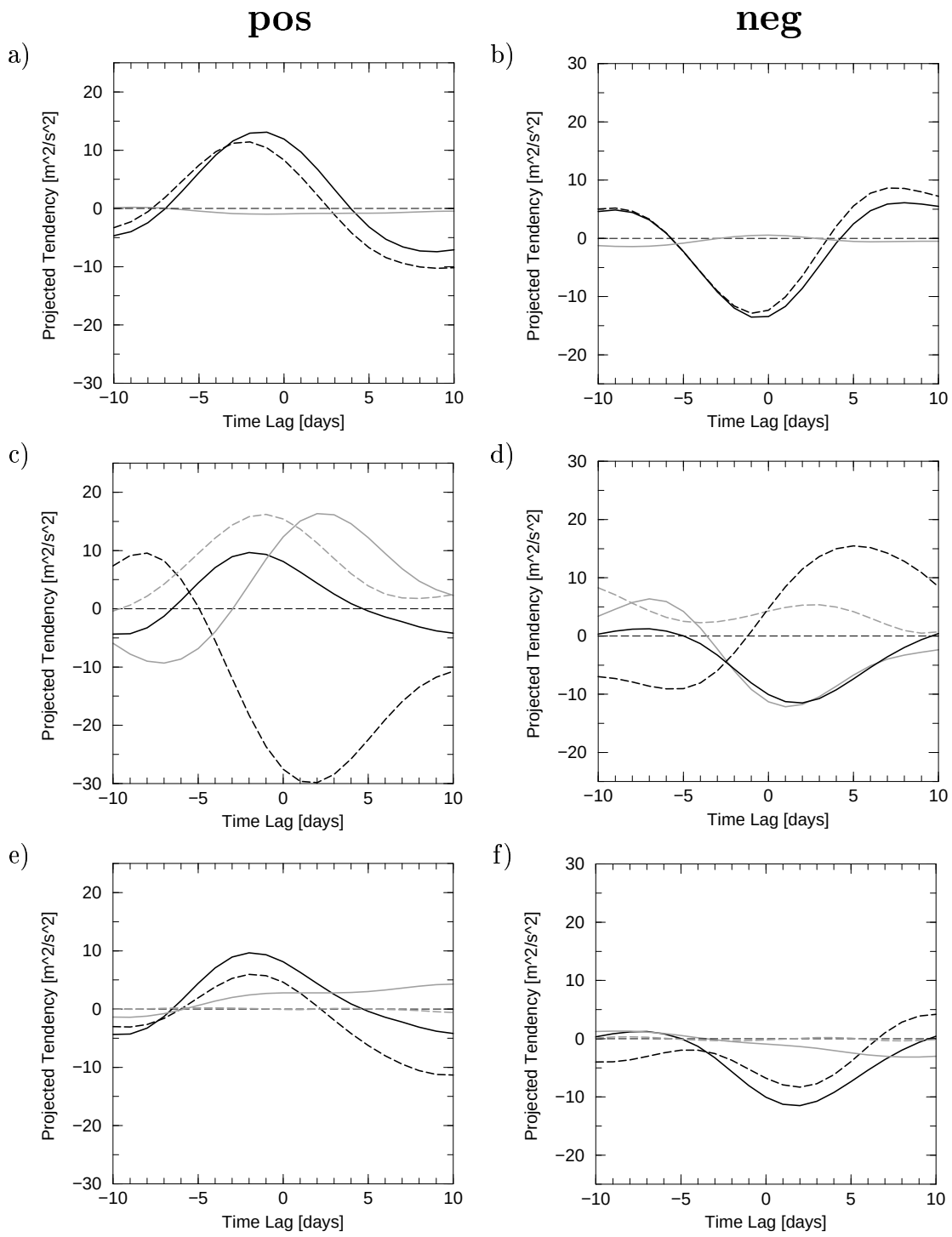

Figure 4.12: *Projection of the 10 day-low pass filtered 300 hPa streamfunction tendency and single terms of equation 4.3 [m^2/s^2] onto the standardized regression patterns (Fig. 4.9) for the positive (left panels) and negative (right panels) persistent NA-SVR pattern index episodes. Upper row: projection of the streamfunction tendency (black solid line), the sum of terms χ_1 to χ_4 and χ_{tr} (black dashed line), and term χ_8 (gray line). Medium row: projection of term χ_{tr} (black solid line), χ_4 (black dashed line), χ_3 (gray solid line), and the sum of terms χ_1 and χ_2 (gray dashed line). Lower row: projection of term χ_{tr} (black solid line), χ_5 (black dashed line), χ_6 (gray solid line), and χ_7 (gray dashed line).*

the actual anomaly develops, the streamfunction tendency field is characterized by (small) anomalies of opposite sign (Fig. 4.10). The divergence term acts to destroy them.

Transient eddy vorticity fluxes (term χ_{tr}) contribute much towards the growth of the streamfunction anomaly (Figs. 4.12c,d and 4.13). The largest projections can be observed during the growth phase, whereas they become small after the anomaly maximum. In most cases, they weakly contribute to its decay then. The contributions from transient eddies with different timescales are presented in Fig. 4.12e,f for the NA-SVR cases. (The projections for the two NA-WVR patterns reveal to be qualitatively similar and are therefore not shown.) During the anomaly growth, the forcing by low frequency eddy vorticity fluxes, χ_5, is the dominant contributor to the total transient eddy forcing χ_{tr} and is always in phase with the latter. The interaction among the synoptic eddies, χ_6, also contributes to the anomaly growth but is less important than the low frequency eddy forcing during times when the anomaly growth is most rapid. However, the synoptic eddy forcing is still acting towards amplification of the streamfunction anomaly, when the low frequency eddy forcing has already reduced and changed its sign. This means that forcing by synoptic eddy vorticity fluxes acts towards maintaining the anomaly after its maximum, whereas it plays a minor role during the anomaly growth. In his examination of the NAO lifecycle, Feldstein (2003) also found high-frequency eddy forcing after the anomaly maximum. Figs. 4.12e,f furthermore show that the contribution from the interaction of low frequency and synoptic eddies, χ_7, is negligible: The gray dashed lines in Fig. 4.12e,f are almost indistinguishable from the zero lines. The sum of the projections of the terms χ_5, χ_6, and χ_7 is almost equal to the projection of the total transient eddy forcing χ_{tr} (not shown). Thus, the contribution from eddies which were not captured with the filters is small. The only exception is the positive western NA-WVR case, in which the contribution from eddies with periods between 6 and 10 days is somewhat larger and in phase with the low frequency eddy contribution (not shown).

Three terms have not been discussed yet: χ_1, χ_2, and χ_3. The sum of terms χ_1 and χ_2 describes the low frequency advection of absolute vorticity due to the interaction of low frequency eddies with the zonally symmetric part of the time mean flow. The terms χ_1 and χ_2 force a westward (χ_1) or an eastward (χ_2) displacement of the streamfunction anomaly pattern (not shown). The terms have large amplitudes but cancel each other to a large degree. It is therefore reasonable to discuss the sum of χ_1 and χ_2 rather than the single terms. From Figs. 4.12c,d and 4.13 it can be inferred that the net forcing contribution from terms χ_1 and χ_2 is towards enhancing the streamfunction anomaly, except in the negative NA-SVR index case where there is a weak damping contribution.

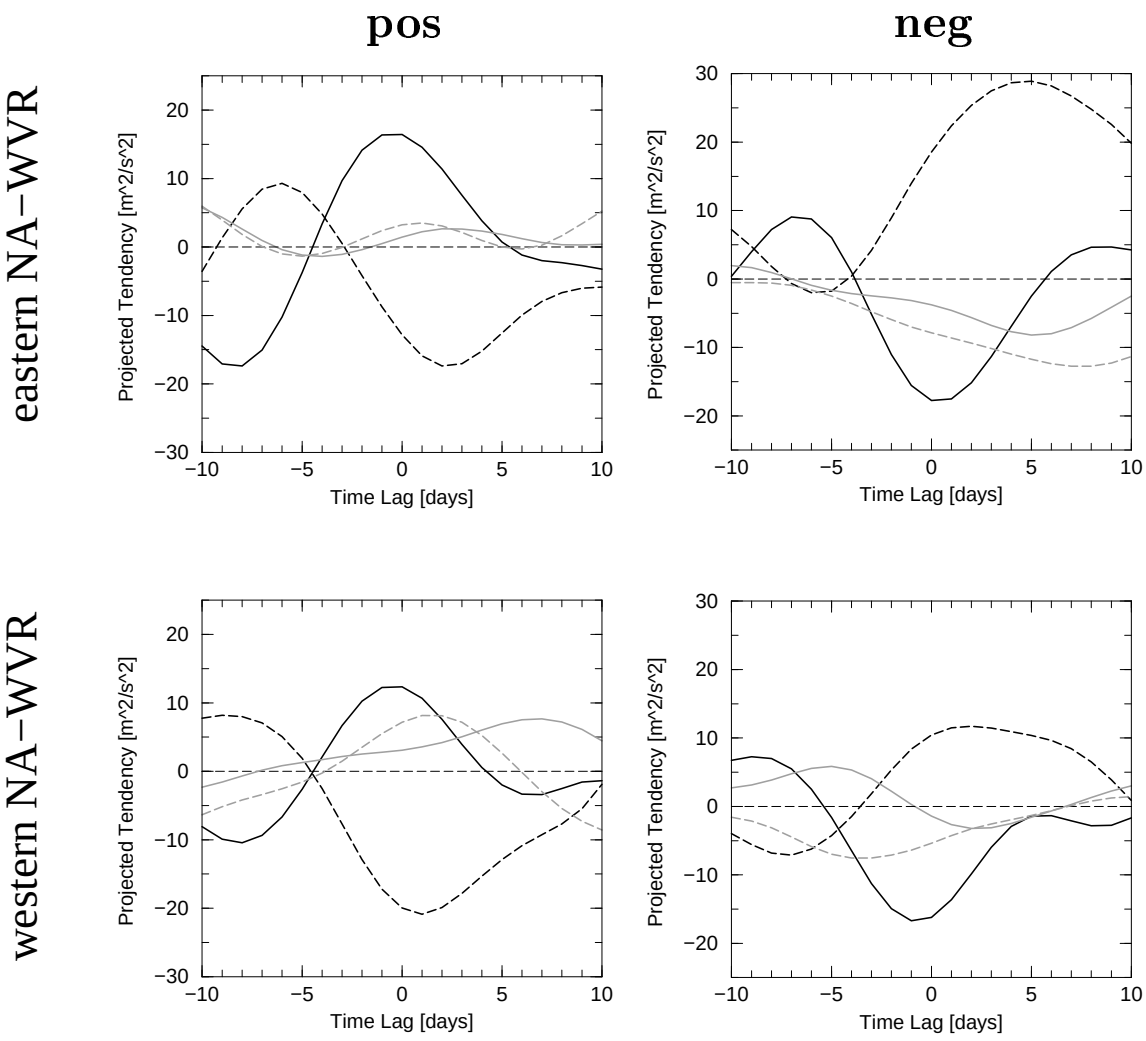

Figure 4.13: *As in Fig. 4.12c,d but for persistent positive (left column) and negative (right column) episodes of the eastern NA-WVR pattern index (upper row) and the western NA-WVR pattern index (lower row).*

The term χ_3 describes the forcing by low frequency advection of relative vorticity resulting from the interaction of low frequency eddies with the zonally asymmetric part of the time mean flow, i.e. with the stationary eddies. It acts towards the growth of the streamfunction anomaly. Its contribution is largest a few days after the most rapid growth, as if to maintain the anomaly. If one compares the magnitudes of this forcing term and of the forcing by transient eddy vorticity fluxes χ_{tr}, a considerable difference between the NA-SVR and the NA-WVR cases can be noticed: For the two NA-WVR patterns, the transient eddy vorticity fluxes χ_{tr} are the main contributor towards the growth of the streamfunction anomaly. In the NA-SVR cases, however, the contributions from the two forcing terms χ_3 and χ_{tr} have almost equal magnitudes when the anomaly growth is most rapid ($\sim$ lag -1 day). In the positive NA-SVR index case, term χ_3 becomes even larger afterwards.

The preceeding examinations revealed that the growth of the teleconnection patterns identified in section 4.1 is characterized by different physical mechanisms in the SVR and WVR. While the anomaly growth in the WVR is dominated by transient eddy vorticity fluxes, in particular from the low frequency domain, another forcing term is at least as important in the SVR: streamfunction tendency forcing by low frequency vorticity advection due to the interaction of low frequency eddies with the zonally asymmetric part of the time mean flow, i.e. with the stationary eddies. This means that the different tropospheric teleconnection structures in the North Atlantic region are not just related to a spatial reorganization of the transient eddies in the different stratospheric regimes but also to a modified interaction of (low frequency) eddies with the changed background flow. The anomaly decay, however, is related to mainly the same forcing mechanisms in the two polar vortex regimes: The decay is dominated by forcing by the divergence term, whereas synoptic eddy vorticity fluxes act towards maintaining the anomaly against decay.

Feldstein (2003) examined the lifecycle of the NAO and found that it is mainly driven by forcing resulting from both low and high frequency eddy vorticity fluxes, whereas the decay is due to the influence of the divergence term and a (small) contribution from low frequency eddy fluxes. These characteristics correspond to the lifecycles of the two NA-WVR patterns derived here. A possible explanation for the difference to the lifecycle of the NA-SVR pattern may be that, if the the two regimes are not analyzed separately, the differences between the mean flows in the two polar vortex regimes are interpreted as low frequency fluctuations. A part of the forcing which is related to the interaction between transient eddies and the time mean flow within the polar vortex regimes is then interpreted as related to interactions among transient eddies.

Transitions between the two stratospheric polar vortex regimes have not been examined in this thesis. They should, however, be subject of further studies because they may have a strong direct impact on the NAO (Baldwin and Dunkerton, 2001; Perlwitz, 2000)

Spatial patterns of forcing

In the following, spatial characteristics of the forcing terms in equation 4.3 are discussed. Two exemplary cases are illustrated for lag -1 day, when the streamfunction tendency is maximum: Fig. 4.14 displays composites for positive NA-SVR index events and Fig. 4.15 composites for positive eastern NA-WVR index events. Features described in the following are correspondingly true for all other teleconnection patterns and polarities.

Figs. 4.14a and 4.15a show the total streamfunction tendency. The structures are mainly similar to the streamfunction anomaly during its mature stage (Fig. 4.11) and to the regression patterns in Figs. 4.9. The divergence term has already been identified as the main contributor to the anomaly decay, whereas transient eddy vorticity fluxes appear to be important for the anomaly growth. This corresponds to the lifecycle of the NAO (Feldstein, 2003), whereas the growth of the Pacific/North American pattern revealed to be mainly associated with forcing by interaction of low frequency eddies with the time mean flow (Feldstein, 2002). Figs. 4.14d and 4.15d show that the divergence term, χ_4, is clearly counteracting the total streamfunction tendency in both centers of action of each teleconnection pattern. The damping by divergence is opposed in both centers of action by forcing due to transient eddy vorticity fluxes, in particular from the low frequency domain (Figs. 4.14e and 4.15e). The forcing by synoptic eddy vorticity fluxes also acts to enhance the streamfunction anomaly (Figs. 4.14f and 4.15f). It is rather weak during the phase of the most rapid growth, i.e. for the time lag -1 day displayed in Figs. 4.14 and 4.15. However, as discussed previously, the magnitude of this forcing contribution increases as the streamfunction anomaly grows. The forcing by synoptic eddies vorticity fluxes then acts towards maintaining the streamfunction anomaly against decay in both centers of action (not shown).

Turning back to the forcing resulting from the low frequency eddy vorticity fluxes (Figs. 4.14e and 4.15e), it can be observed that it is more emphasized at the northern center of action in the WVR than in the SVR. In the WVR, the growth of the northern center of action is thus mainly driven by low frequency eddy vorticity fluxes. In contrast, the deepening of the northern center of action in the SVR is strongly driven by forcing induced by vorticity advection due to the interaction of low frequency eddies with stationary eddies (Fig. 4.14c).

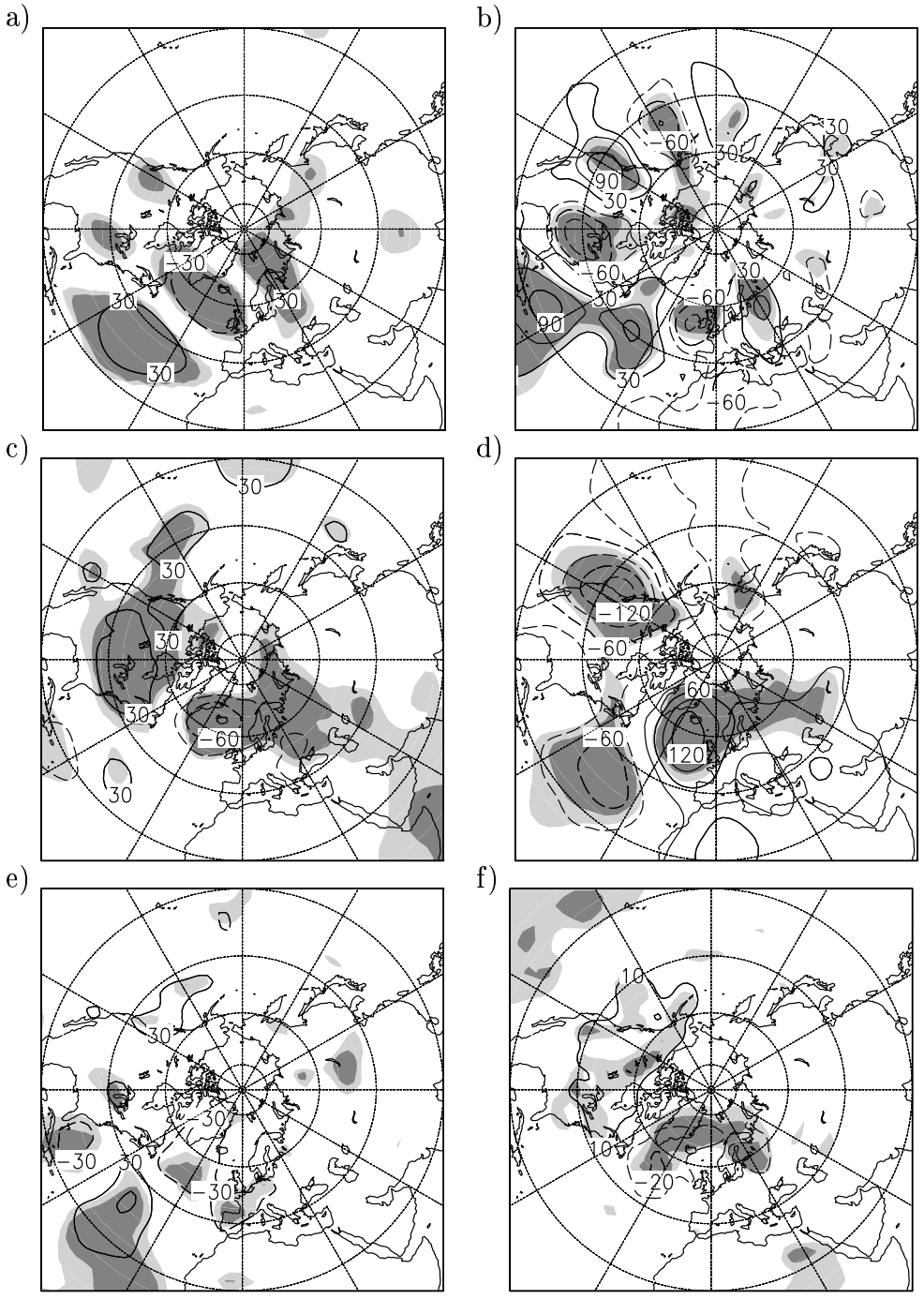

Figure 4.14: *Composite low pass filtered 300 hPa streamfunction tendency and single terms in equation 4.3 [m^2/s^2] at lag -1 day for the positive persistent NA-SVR pattern index episodes. Composites of (a) the total streamfunction tendency, (b) the sum of terms χ_1 and χ_2, (c) term χ_3, (d) term χ_4, (e) term χ_5, and (f) term χ_6. The isoline interval is 30 m^2/s^2 in all panels except (f), where it is 10 m^2/s^2. The zero contour is omitted. The shadings indicate t-test significance above 95% (light shading) or 99% (dark shading).*

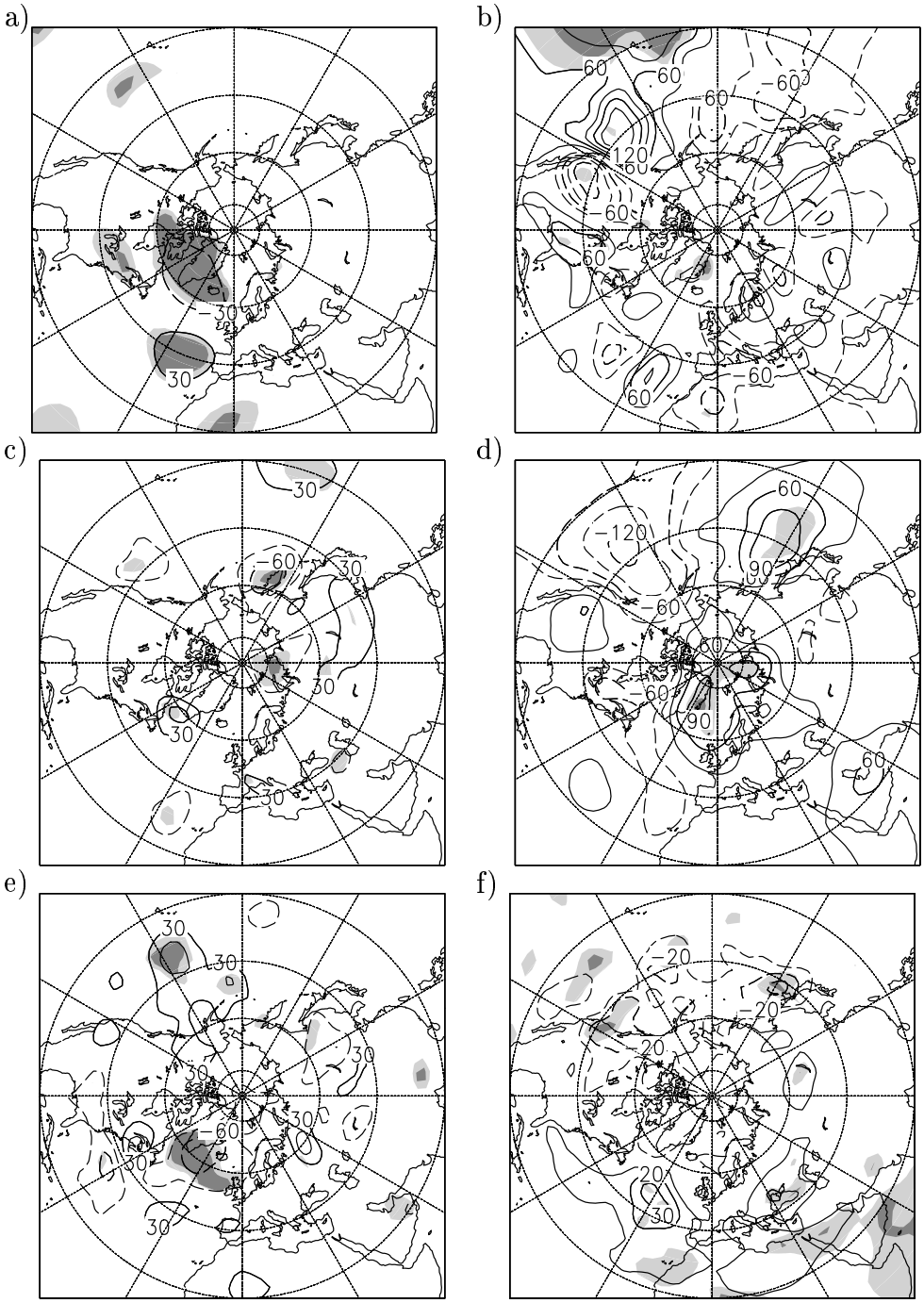

Figure 4.15: *As in Fig. 4.14 but for the persistent positive eastern NA-WVR pattern index episodes.*

The strength of the latter forcing contribution in the northern center of action (of the NA-SVR pattern) is associated with the intensified time mean low near Greenland in the SVR which is in turn maintained by stationary eddy vorticity fluxes (chapter 3, section 3.3). The intensified time mean low is related to strong time mean vorticity gradients and wind anomalies leading to enhanced forcing due to vorticity advection near Iceland. While this forcing mechanism is strong for both polarities of the NA-SVR pattern, its contribution hardly reaches the 95% significance level in the NA-WVR cases (Fig. 4.15c).

The terms χ_1 and χ_2 describe low frequency advection of absolute vorticity by interaction between low frequency eddies and the zonally symmetric part of the time mean flow, respectively. Together, they mainly force the growth of the subtropical centers of action (Figs. 4.14b and 4.15b). The forcing in the positive eastern NA-WVR pattern case, however, is not significant above the 95% level and is much weaker than in the NA-SVR cases. Comparison with the composite streamfunction anomalies for time lags -4 and 0 days (Fig. 4.11) exhibits that, in the positive NA-SVR index case, there is also a contribution towards an eastward displacement of the subtropical high. This eastward movement has already been mentioned in the discussion of the development of the streamfunction anomalies. From Fig. 4.14b, it becomes clear that the net influence from terms χ_1 and χ_2 (more precisely, from term χ_2) is responsible for that. Such a movement is not eminent neither in the negative NA-SVR nor in the NA-WVR cases.

In summary, it has been shown that the structural differences between the North Atlantic teleconnection patterns in the two regimes of the stratospheric polar vortex strength cannot only be associated with a reorganization of transient eddies but also with different dynamical mechanisms. The latter is mainly related to the different stationary eddy structures in the two regimes. Changes in the stationary eddy structure have consequences for the interaction with transient eddies, and, thus, for the forcing in particular at the northern center of action.

4.3 Impacts on storm tracks, precipitation, and temperature

It has been shown in the preceeding sections that teleconnections in the North Atlantic sector are subject to structural changes related to the two stratospheric polar vortex regimes. Without considering the polar vortex regimes the North Atlantic Oscillation (NAO) is the dominant mode of tropospheric variability in the North Atlantic region. Several studies suggest that the NAO is closely associated with the strength and direction of the North Atlantic storm tracks, with the precipitation and the temperature over Europe (Rogers, 1990; Hurrell, 1995; Hurrell

and van Loon, 1997). It is therefore most likely that the structural changes in the North Atlantic teleconnection patterns discussed in section 4.1 have an impact on these variables. In the following, some of these impacts are documented for monthly means.

For this section, the index definitions in appendix A were applied to monthly mean 300 hPa geopotential heights. Additionally, an index for the North Atlantic Oscillation is derived in a similar manner from the 1000 hPa geopotential height (see appendix A). This 'classic style' NAO index is defined for the entire period from 1958 to 1998, i.e. it is not restricted to a certain polar vortex regime. The definition of this index corresponds to the Hurrell (1995) NAO index, which incorporates sea level pressure data observed at stations on Iceland and on either the Azores or Lisbon.

Regression and correlation analyses were applied as well as composite analysis. In contrast to correlation or regression analysis, the latter method does not require that the changes in the variables are linear with respect to the sign of the teleconnection indices. The composites were averaged over all months in which the monthly mean timeseries of the respective teleconnection index exceeds a positive or a negative half standard deviation, respectively. This corresponds to averages over 26 (24) monthly values in the positive (negative) NA-SVR pattern index case and 11 (10) in the positive (negative) eastern NA-WVR as well as in the positive (negative) western NA-WVR pattern index case.

Time mean geopotential height

The NA-SVR and the eastern NA-WVR patterns mainly influence the geopotential height over the central to eastern North Atlantic, whereas fluctuations of the western NA-WVR pattern index are associated with variations in the strength of the time mean low pressure system over northeastern Canada (Fig. 4.16). It describes changes in the strength of the north-south geopotential height gradient over US east coast, i.e. in a region characterized by strong baroclinicity. As discussed in section 4.2, the monthly mean teleconnection index of this pattern is related to the strength of the zonal mean zonal wind at 50 hPa and 65°N.

The NA-SVR and eastern NA-WVR pattern indices are not significantly correlated with the strength of the zonal mean zonal wind at 50 hPa and 65°N. These patterns mainly describe changes in the tilt of the isohypses over the central North Atlantic. If the sign of the indices is positive, the isohypses are more zonally oriented and the north-south geopotential height gradient is enhanced. This is associated with a stronger westerly flow over the North Atlantic. In the negative index case, the isohypses are more meridionally oriented than in the pos-

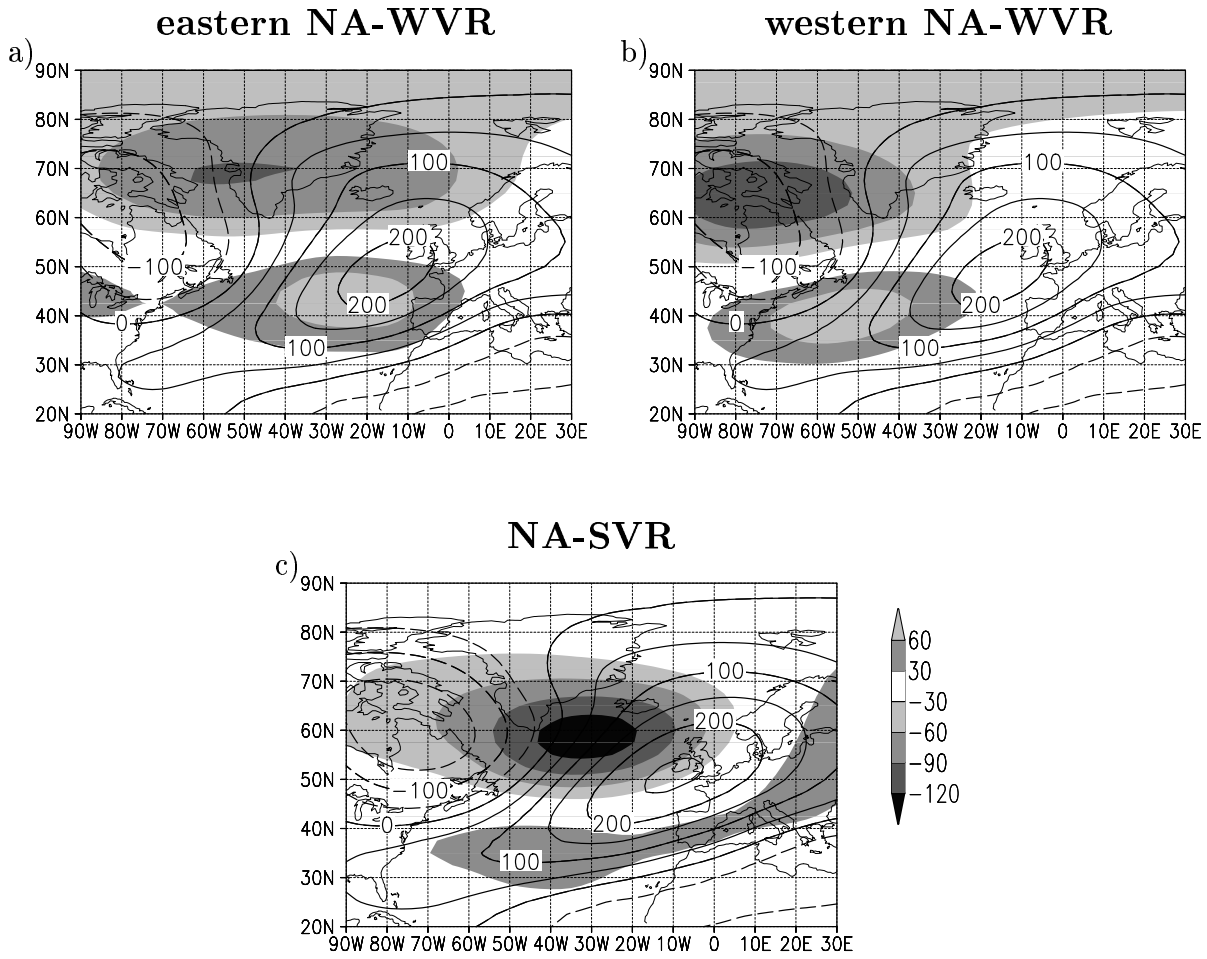

Figure 4.16: *Linear regression coefficient ([gpm]; shadings) of the monthly mean 300 hPa geopotential height in the North Atlantic sector regressed onto the monthly mean (a) eastern NA-WVR index, (b) western NA-WVR index, and (c) NA-SVR index. The isolines represent the deviation of the geopotential height averaged over the corresponding regime from its zonal mean [gpm]. The values of the regression coefficients correspond to one standard deviation of the respective teleconnection index.*

itive index case. The north-south pressure gradient is weakened corresponding to a reduction of the westerly flow.

The northern center of the eastern NA-WVR pattern seems to be displaced westwards in comparison to the regression pattern for the 300 hPa streamfunction in Fig. 4.9 which is based on 10-day low pass filtered data. The displacement can be explained explained with the variance of the 300 hPa geopotential height. Fig. 3.14 in chapter 3 shows that, in the WVR, the maximum of the root mean square (rms) of the 10-day low pass filtered 300 hPa geopotential height is located over the Labrador sea. For monthly means, the rms maximum reveals to be even more emphasized in this area (not shown). This means that although the correlation between the two centers of action of the eastern NA-WVR pattern is strongest over the eastern North Atlantic, the larger geopotential height anomalies associated with the northern center of action occur further west.

The NA-SVR pattern is characterized by a strong anomaly south of Greenland. In the positive phase of the NA-SVR pattern, this anomaly is negative and, thus weakens the northwestern edge of the time mean anticyclone west of Europe. Together with the positive geopotential height anomaly south and southeast of the anticyclone, this means that the positive phase of the NA-SVR pattern is associated with a southeast displacement of the time mean anticyclone east of Europe. Accordingly, the negative SVR pattern phase is associated with a northwest displacement of the anticyclone and is therefore related to a blocking situation.

Storm tracks and precipitation

In the following, some effects on the monthly mean North Atlantic circulation will be discussed in more detail by applying composite analysis. The variables considered in this context are i) the monthly root mean square (rms) value of band pass filtered 500 hPa geopotential height as a measure for the strength and direction of the storm tracks, and ii) monthly mean precipitation rates. The band pass filter applied here is once more the Blackmon and Lau (1980) band pass filter (appendix B.1), which captures fluctuations with periods between 2.5 and 6 days. In order to get an impression of the strength and direction of the storm track, the absolute rms values are displayed, whereas the precipitation rates are discussed as anomalies from the average over the entire period from 1958 to 1998. For explaining the storm track behavior, two more variables are considered: i) the monthly mean zonal wind in the upper troposphere at 200 hPa and ii) the (maximum) Eady growth rate (see appendix B.7) as a measure for the baroclinic production of transient eddies. It turns out that in all cases discussed in the following, the anomalies of the Eady growth rate are structurally similar

to the anomalies of the upper tropospheric zonal wind. This may be explained by the strong association of the Eady growth rate with the vertical wind shear.

Fig. 4.17 shows composites for the eastern NA-WVR pattern index, which consist of 11 (10) months in the positive (negative) index case. In the positive index phase, the North Atlantic storm track is more zonally elongated (Fig. 4.17a) in comparison to the negative index case (Fig. 4.17b) and has a stronger southwest-to-northeast tilt. The area with standard deviations (rms values) above 40 gpm reaches the zero meridian, whereas it reaches only to 30°W in the negative index case. In the positive index case, cyclones are lead to northwestern Europe bringing more precipitation to this area, whereas there is less precipitation over the Iberian Peninsula (Fig. 4.17c). The situation is vice versa when the index is negative. In this case, the cyclones reach Europe further south, resulting in enhanced precipitation over southwestern Europe and reduced precipitation over northwestern Europe (Fig. 4.17d).

The elongation of the storm track in the positive index case can be explained by the stronger upper level westerly wind south of the anomalous low near Iceland. The latter is connected to a larger Eady growth rate and, hence, stronger baroclinicity in this area. Positive (negative) wind anomalies are located north of the jet core and negative (positive) anomalies can be observed south of it, so that the area of strongest baroclinicity over the North American east coast (see appendix B.7, Fig. B.1a) is displaced northwards (southwards) in the positive (negative) index case. This is associated with a northward (southward) shift of the storm track axis.

The anomalies of precipitation rate, wind, and Eady growth rate are larger in the negative index phase than in the positive phase. The zonal wind anomalies, e.g., are almost twice as large as in the positive index phase. This can be explained by the fact that deviations from the whole-time-mean from 1958 to 1998 are discussed instead of deviations from the mean over the WVR. In the negative index phase, the negative wind anomaly over the North Atlantic adds to the mean reduction of the wind in the WVR (Fig. 3.8), whereas the positive wind anomaly in the positive index phase and the mean reduction cancel each other to some degree. This is analogously true for precipitation and Eady growth rate.

The composites for the western NA-WVR pattern also consist of 11 and 10 months, respectively. The storm tracks show a qualitatively similar dependence on the polarity of the teleconnection index (Fig. 4.18a,b) as in the eastern NA-WVR pattern case. In the positive phase, the storm track is longer and stronger than in the negative phase. The difference in the intensity is much more obvious than for the eastern NA-WVR pattern. This can be explained by the strong anomalies of the upper tropospheric westerly wind over the western North Atlantic and America. As a consequence, fluctuations in the strength of

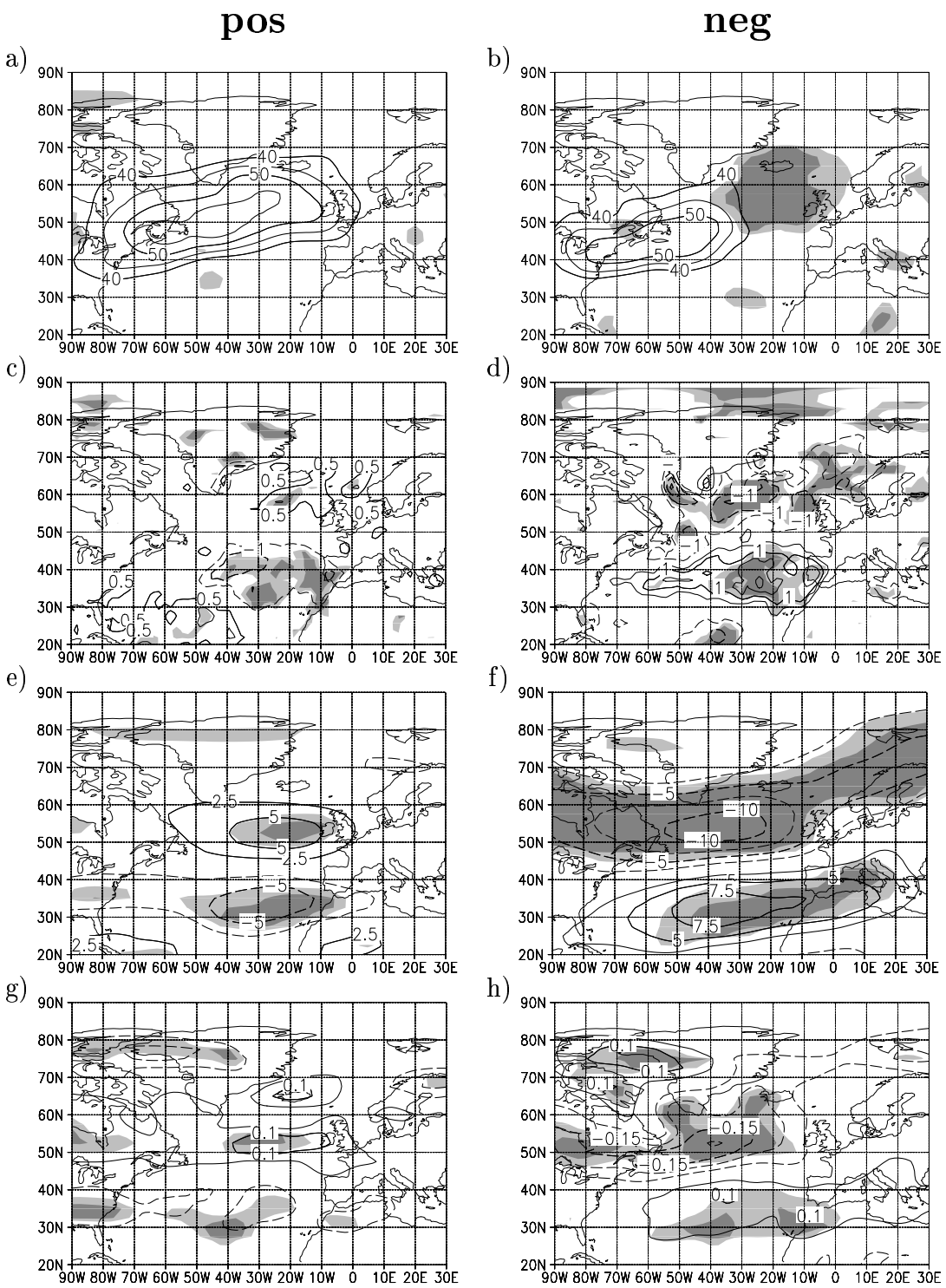

Figure 4.17: *Composites for the positive (left panels) and the negative phase (right panels) of the eastern NA-WVR pattern: (a,b) composite monthly rms of band pass filtered 500 hPa geopotential height [gpm] and composite monthly mean anomalies of (c,d) the precipitation rate [mm/d], (e,f) the zonal wind at 200 hPa [m/s], and (g,h) the Eady growth rate at 700 hPa [d^{-1}]. The anomalies are deviations from the 1958-to-1998 time mean. The shadings indicate deviations from the time mean above the 95% (light) and the 99% (dark) significance level according to a t-test.*

the western NA-WVR pattern strongly modify the baroclinicity over the North American east coast, i.e. in a region which is already characterized by synoptic eddy growth due to baroclinic instability. In the positive index phase, the position of the strongest baroclinicity is additionally displaced northward leading to a northward displacement of the storm track axis. The storm track tilt in the positive phase, however, is not as strong as for the eastern NA-WVR pattern, because of the weak influence of the western NA-WVR pattern over the eastern North Atlantic. The area of (weakly) enhanced precipitation is therefore located further south than in the positive eastern NA-WVR index case, i.e. over western to southern Europe, while the precipitation at the Norwegian coast is weakly but significantly reduced (Fig. 4.18c). The anomaly pattern of precipitation rates in the negative index case (Fig. 4.18d), however, resembles the negative eastern NA-WVR index case — apart from the fact that the maxima and minima are shifted to the west and that the effects over the continents are smaller.

Fig. 4.19 shows the composites for the NA-SVR pattern in the strong vortex regime, which consist of 26 (24) monthly values in the positive (negative) index case. For both polarities of the teleconnection index, the storm tracks span the entire North Atlantic Ocean. This corresponds to the fact that the time mean westerly flow in the midlatitude North Atlantic region is stronger in the SVR than in the WVR (chapter 3, Fig. 3.8). The storm track is extremely tilted in the negative index case (Fig. 4.19b), when a (blocking) anticyclone southeast of Iceland is associated with enhancement of the westerly flow to its north and with reduction south of it: The storm track axis runs from the southwest to the northeast over the Denmark Strait and north of Iceland. Cyclones move along this path to the Norwegian coast and are responsible for enhanced precipitation in this region (Fig. 4.19d). The spatially small precipitation rate anomalies at the Norwegian coast in Fig. 4.19d are significant above the 99.9% level according to a t-test (appendix B.3). The precipitation over the British Isles and western continental Europe is reduced corresponding to the blocking situation. When the NA-SVR index is in its positive phase, the westerly wind south of the anomalous low near Iceland is enhanced. Therefore, the storm track is zonally oriented (Fig. 4.19a). Cyclones reach northwestern Europe, more southerly than in the negative index case. This results in more precipitation over (north)western and less over southwestern Europe (Fig. 4.19c).

Temperature

As discussed in the preceding paragraphs, the tropospheric teleconnection patterns in the North Atlantic sector are associated with fluctuations in the strength of the westerly flow. This is not only true for the upper troposphere but also at

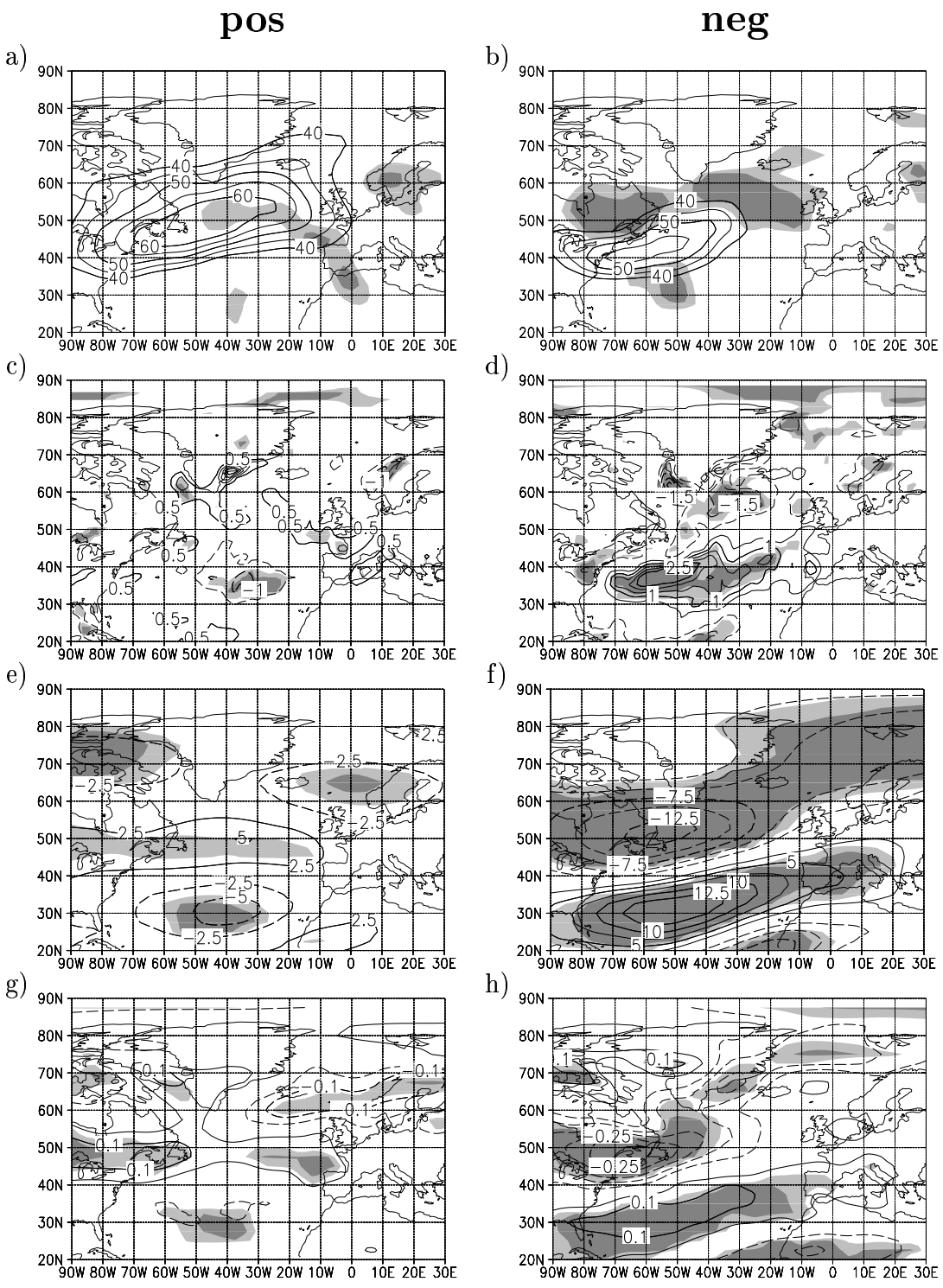

Figure 4.18: *As in Fig. 4.17 but for the western NA-WVR pattern.*

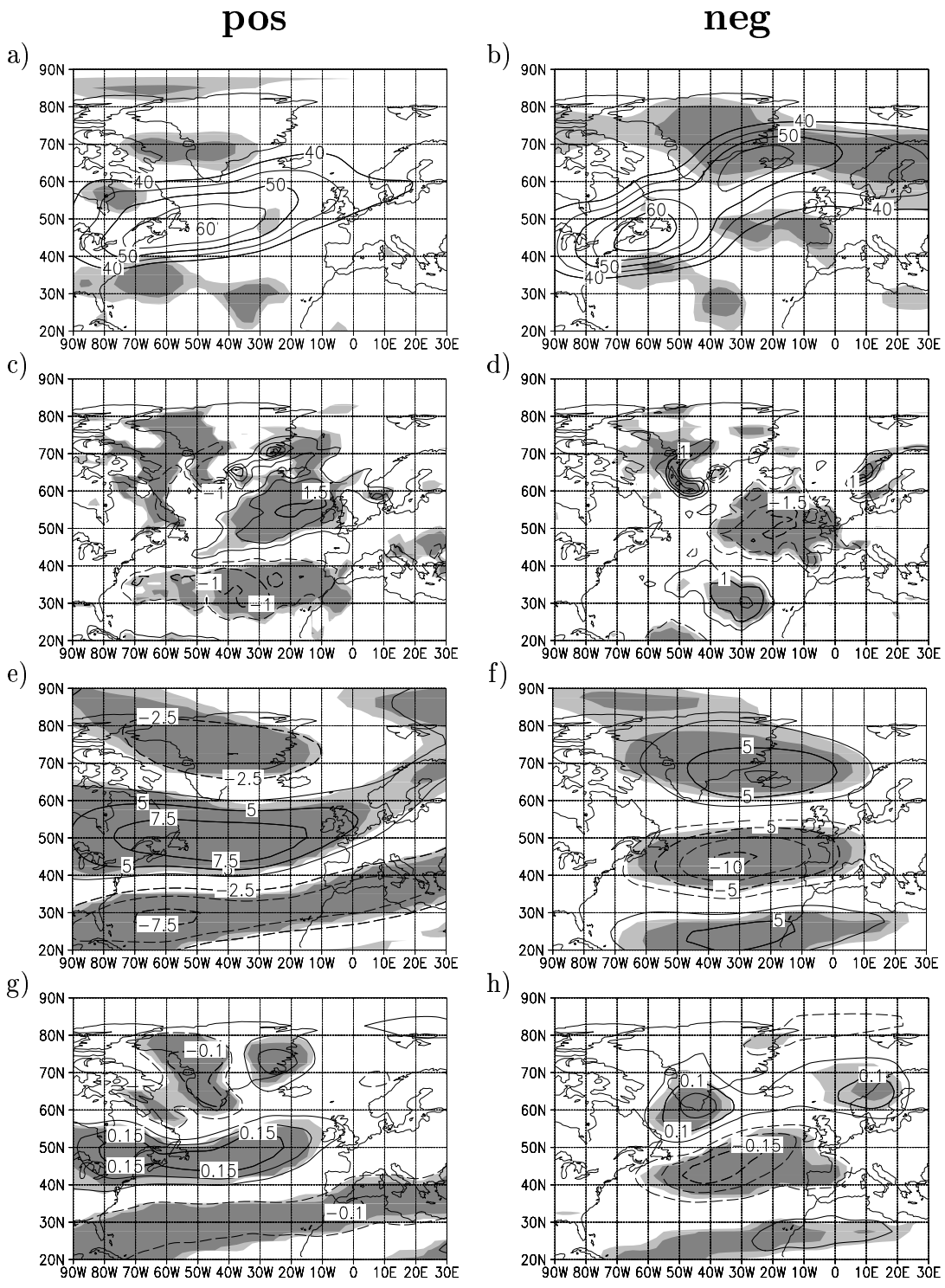

Figure 4.19: *As in Fig. 4.17 but for the NA-SVR pattern.*

lower levels and near the surface. The near-surface air temperature is influenced by (sensible and latent) heat fluxes from or to the surface. Changes in wind speed and direction close to the surface are therefore accompanied by anomalous advection of warm or cold air masses. Trigo et al. (2002) showed that NAO-related temperature patterns are mainly controlled by advection of heat by the anomalous mean flow. In the following, composites of monthly mean 850 hPa temperature anomalies will therefore be discussed together with composites of the anomalous monthly mean wind at 850 hPa.

Fig. 4.20 shows temperature and wind composites for the eastern NA-WVR pattern. In the positive (negative) index phase, the westerly flow over northeastern Canada is enhanced (reduced) associated with stronger (reduced) advection of cold continental air. As a consequence, the temperature over the Labrador Sea, northeastern Canada, and Greenland is lower (higher) than in the long term mean. The westerly flow over the midlatitude North Atlantic is strengthened (weakened) in the positive (negative) index case. In the negative index case, this is associated with negative temperature anomalies over northern Europe. In the positive index case, there is no such strong (positive) anomaly. This inhomogeneity between the two polarities of the eastern NA-WVR pattern is analogous to the anomalies of precipitation and zonal wind discussed previously. As supposed there, this is possibly due to the computation of anomalies relative to the whole-time-mean instead of deviations from the WVR mean. South of the subtropical high, the anomalous wind direction is opposite to that over the midlatitude North Atlantic, leading to enhanced (reduced) advection of warm air from the ocean to the US east coast, when the index is positive (negative).

The anomalies associated with the western NA-WVR pattern (Fig. 4.21) can be explained in a similar manner as in the eastern NA-WVR pattern case. The most striking difference is that the temperature anomalies over North America and the western North Atlantic are stronger than for the eastern NA-WVR pattern. This corresponds to the more westerly position of the centers of action. In contrast to the positive index case, the influence on temperature and wind reaches far across the North Atlantic in the negative index case.

The westerly flow over the midlatitude North Atlantic is enhanced (reduced) in the positive (negative) NA-SVR index phase (Fig. 4.22c,d). Together with the anomalous southwesterly (northerly) flow over northwestern Europe, this leads to in higher(lower)-than-normal temperatures in that region (Fig. 4.22a,b). In the negative NA-SVR index case, the wind anomalies over the North Atlantic correspond to the anticyclonic circulation around the anomalous (blocking) high south of Iceland. Thus, while the westerly flow over the midlatitude North Atlantic is reduced, it is enhanced between 60° and 70°N, from Greenland over Iceland to Scandinavia, bringing cold Arctic air to northern Europe. In the

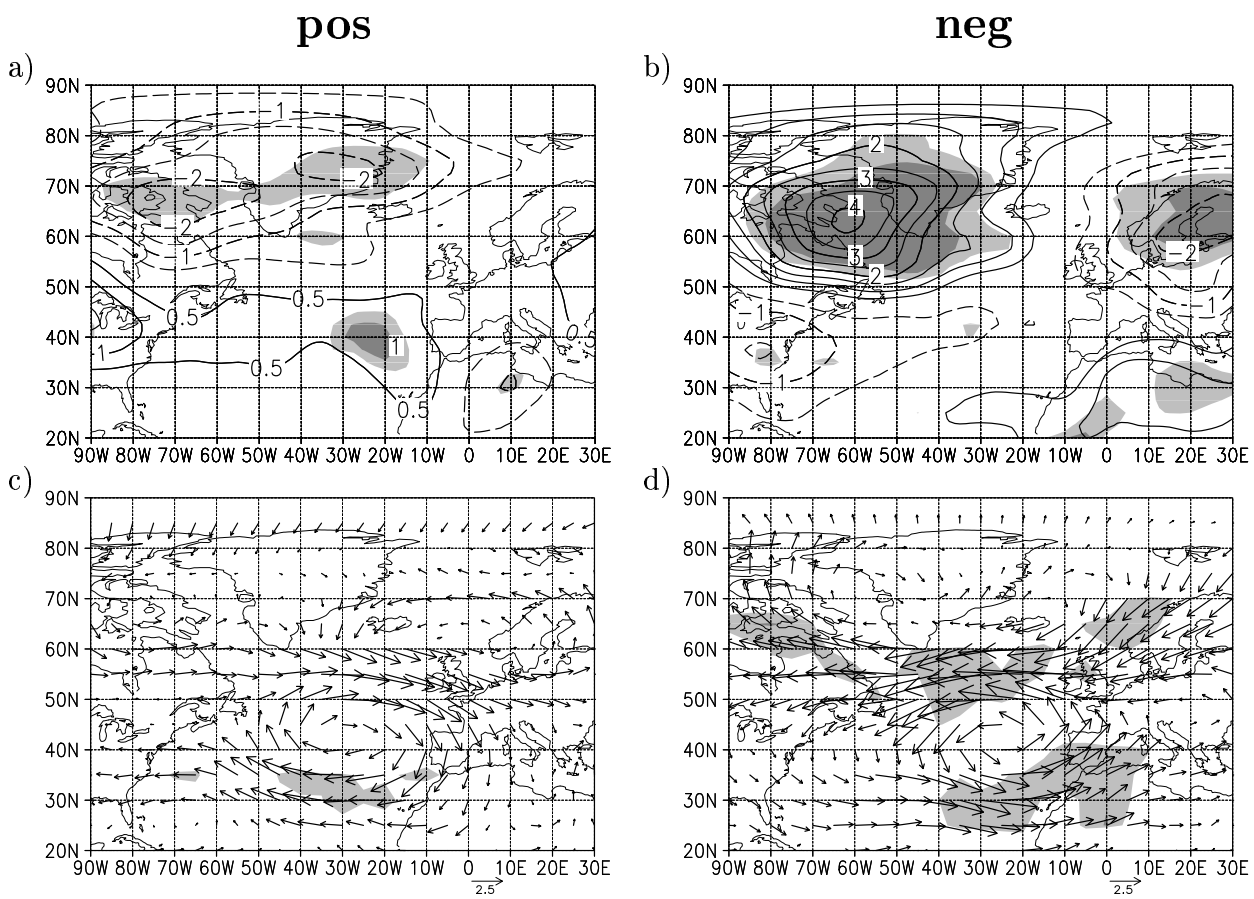

Figure 4.20: *Composite anomalies of (a,b) the 850 hPa temperature [K] and (c,d) the wind at 850 hPa [m/s] for the positive (left panels) and the negative (right panels) phase of the eastern NA-WVR pattern. The shadings indicate anomalies (from the 1958-to-1998 mean) above the 95% (light) and 99% (dark) significance level according to a t-test. For the wind vectors, the significance of the single components is weighted by the amounts of the components.*

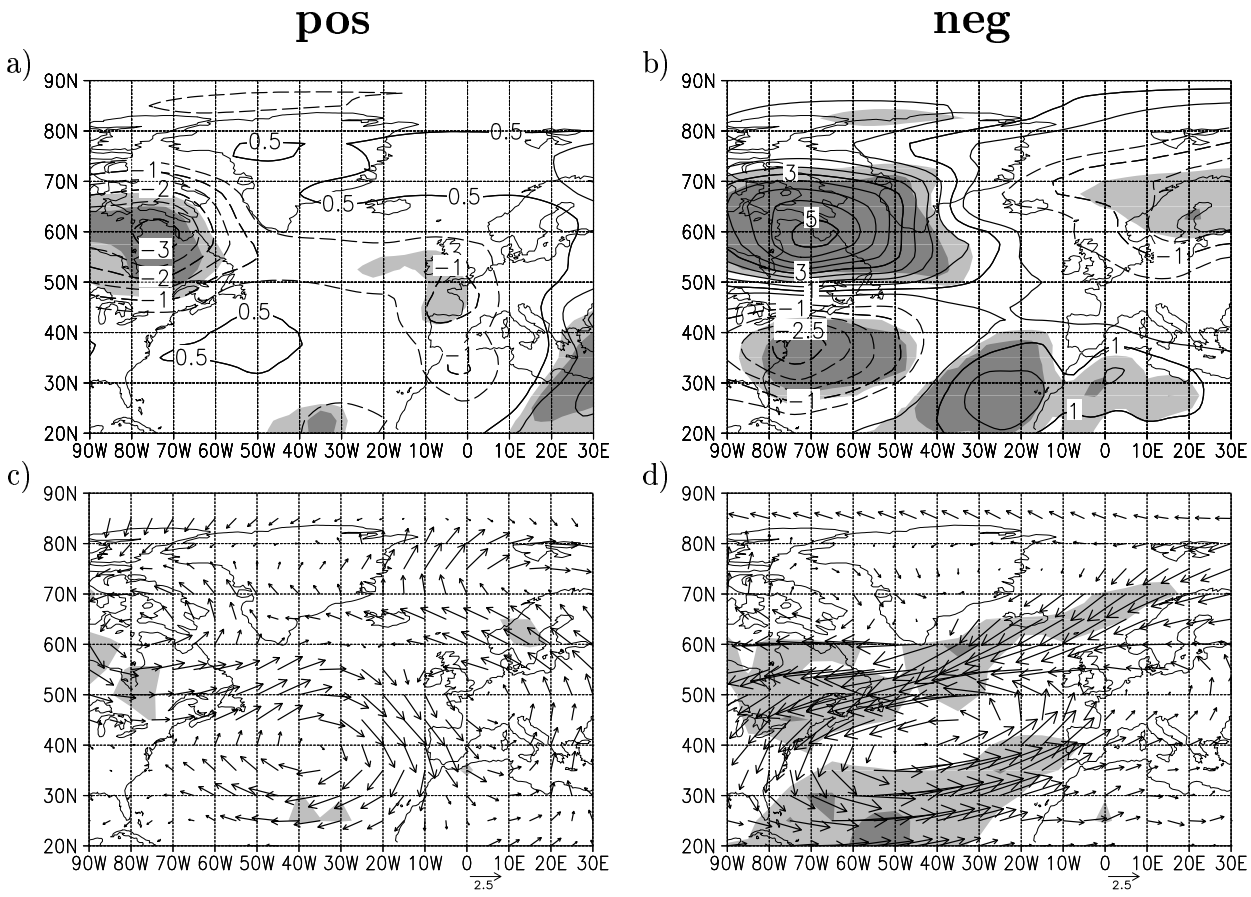

Figure 4.21: *As in Fig. 4.20 but for the western NA-WVR pattern.*

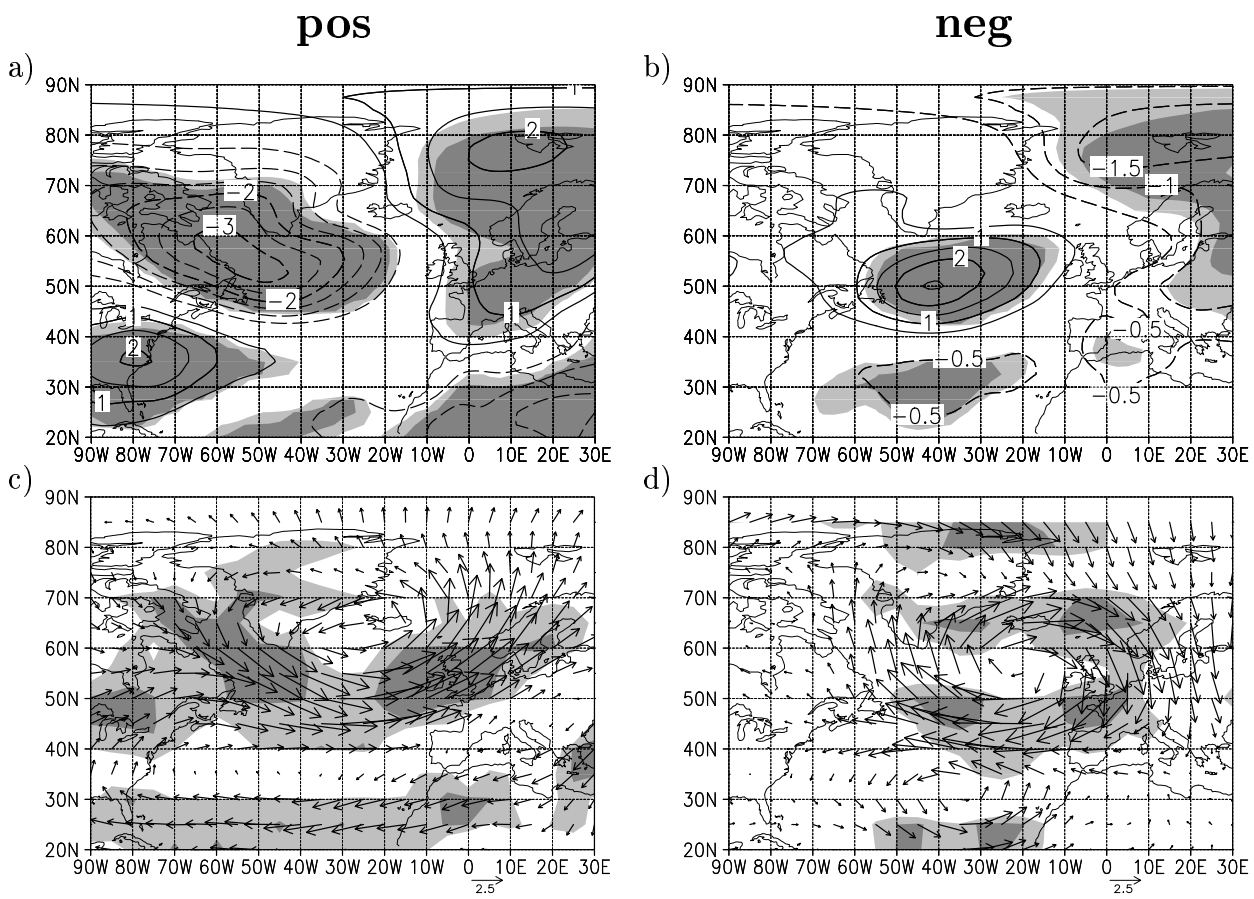

Figure 4.22: *As in Fig. 4.20 but for the NA-SVR pattern.*

positive NA-SVR pattern case, there are large temperature anomalies over the Labrador sea (negative) and over the US east coast (positive). They are related to anomalous westerly flow over the North American continent and anomalous northwesterly flow over the Labrador sea. In the negative index case, the wind and temperature anomalies are weak over North America. A positive temperature anomaly is therefore located over the central North Atlantic where the westerly inflow of cold continental air is reduced.

Over the Nordic Seas and the Fram Strait between Greenland and Svalbard (Spitsbergen), strong meridional wind anomalies can be identified in the composites for the NA-SVR pattern. Positive (negative) index events are associated with southerly (northerly) flow (Fig. 4.22c,d). Although the wind anomalies mainly are not significant above the 95% level, it is obvious that the corresponding anomalies for the eastern NA-WVR pattern are even weaker over the Fram

Strait (Figs. 4.20c,d and 4.21c,d). This inhomogeneity can be related to the fact that the northern center of action of the NA-SVR pattern is associated with larger fluctuations of geopotential height (Fig. 4.16) and extends further to the north near the surface than the corresponding center of the eastern NA-WVR pattern (not shown). Since the 850 hPa wind field exhibits to be mainly similar to the wind field near the surface, one may speculate that the export of sea ice through the Fram Strait may be more strongly influenced in the extreme phases of the NA-SVR pattern than in those of the eastern NA-WVR pattern. Corresponding to this, Vinje (2001) and Hilmer and Jung (2000) found that the wintertime correlation between the volume flux of sea ice through the Fram Strait and a (classic) NAO index is nonstationary: While the correlation over the last 40 to 50 years is close to zero (Vinje, 2001; Hilmer and Jung, 2000), it is strong and significant if only the last 20 to 25 years are examined (Vinje, 2001, Dickson et al., 2000). Cavalieri (2002) argued that, during the period 1958 – 1997, the sea ice export in January is linked with the phase of the zonal wave 1 in sea level pressure (SLP) at 70° to 80°N rather than with the NAO. In particular the zonal wave 1 structure in the troposphere is influenced by the different refraction and transmission of upward propagating waves in the SVR and the WVR (Perlwitz and Graf, 2001a; Castanheira and Graf, 2003). The polar region in the SVR (WVR) reveals to be characterized by a negative (positive) anomaly of SLP east of Greenland (Castanheira and Graf, 2003), i.e. with anomalous northerly (southerly) winds over the Fram Strait. Since heat fluxes and sea ice transports through the Fram Strait may influence the thermohaline circulation at a global scale, the connection between the sea ice flux and the tropospheric flow in the SVR and the WVR should be examined in future studies. We suggest an influence of the strength of the stratospheric polar vortex on these correlations due to the structural changes in the tropospheric mean flow as well as due to the changes in the North Atlantic teleconnection patterns.

Sea surface temperature

It has already been mentioned in the introduction that the North Atlantic Oscillation interacts with the ocean by surface heat and momentum fluxes and, thus, influences the sea surface temperature (SST) in the North Atlantic. Fig. 4.23 displays the correlation of the three tropospheric teleconnection indices derived in this study with the North Atlantic SST, when the atmosphere leads the ocean by one month. The time lag reflects the high frequency stochastic forcing of the oceanic mixed layer by the atmosphere (Deser and Timlin, 1997). Wallace and Jiang (1987) showed that, on a monthly mean data basis, the correlation between the atmospheric circulation and extratropical SST is closest if the atmosphere leads the ocean by one month. This agrees to the results presented here.

In all three cases, a tripole structure emerges which consists of two large areas with negative correlation in the midlatitude and in the tropical North Atlantic and one area with positive correlation in the subtropics. Such a pattern is well known from several studies on the covariation of NAO and SST (e.g. Bjerknes, 1964; Deser and Blackmon, 1993; Kushnir, 1994). Cayan (1992) showed that such a tripole pattern is consistent with anomalous surface heat and momentum fluxes associated with the NAO.

Fig. 4.23 shows that the area with positive correlation between 20° and 40°N is mainly confined to the western North Atlantic for the western NA-WVR and NA-SVR patterns, whereas, for the eastern NA-WVR pattern, the maximum correlation can be detected in the central to eastern North Atlantic. This corresponds to the more easterly position of this teleconnection pattern. The negative correlation in the midlatitude (subpolar) North Atlantic between 40° and 60°N is more emphasized for the NA-SVR pattern than for the two NA-WVR patterns. This may be explained by the larger geopotential height fluctuations in the northern center of action of the NA-SVR pattern (Fig. 4.16) which are associated with large anomalies in near-surface wind over the Labrador sea and the midlatitude North Atlantic (Fig. 4.22). Fluctuations of the NA-SVR pattern index are therefore related to strong anomalous advection of either cold air from the Labrador Sea region or warmer maritime air from the (south)west (Fig. 4.22). It is furthermore obvious that the negative correlation in the tropical North Atlantic is much stronger for the western NA-WVR pattern (maximum about -0.6) and the NA-SVR pattern (maximum about -0.4) than for the eastern NA-WVR pattern. The correlation in the latter case does not even exceed the 95% significance level. This means that, although the eastern NA-WVR and the NA-SVR patterns are not very different at low altitudes, small differences concerning the southern center of action (Fig. 4.8) have an impact on the connection with the SST in the tropical North Atlantic: The southern center of the NA-SVR pattern is broader and located slightly southwest of that of the eastern NA-WVR pattern. Corresponding to the even more westerly position of the western NA-WVR pattern, the maximum anticorrelation in that case can be observed in the western part of the tropical North Atlantic. The index timeseries of the other two teleconnection patterns are relatively stronger anticorrelated with the SST in the central and eastern part of the North Atlantic.

Comparison with the NAO

Fluctuations of a 'classic style' Azores-Iceland NAO index derived from monthly mean 1000 hPa geopotential height (see definition in appendix A) are associated with changes in the strength of the north-south geopotential height gradient over

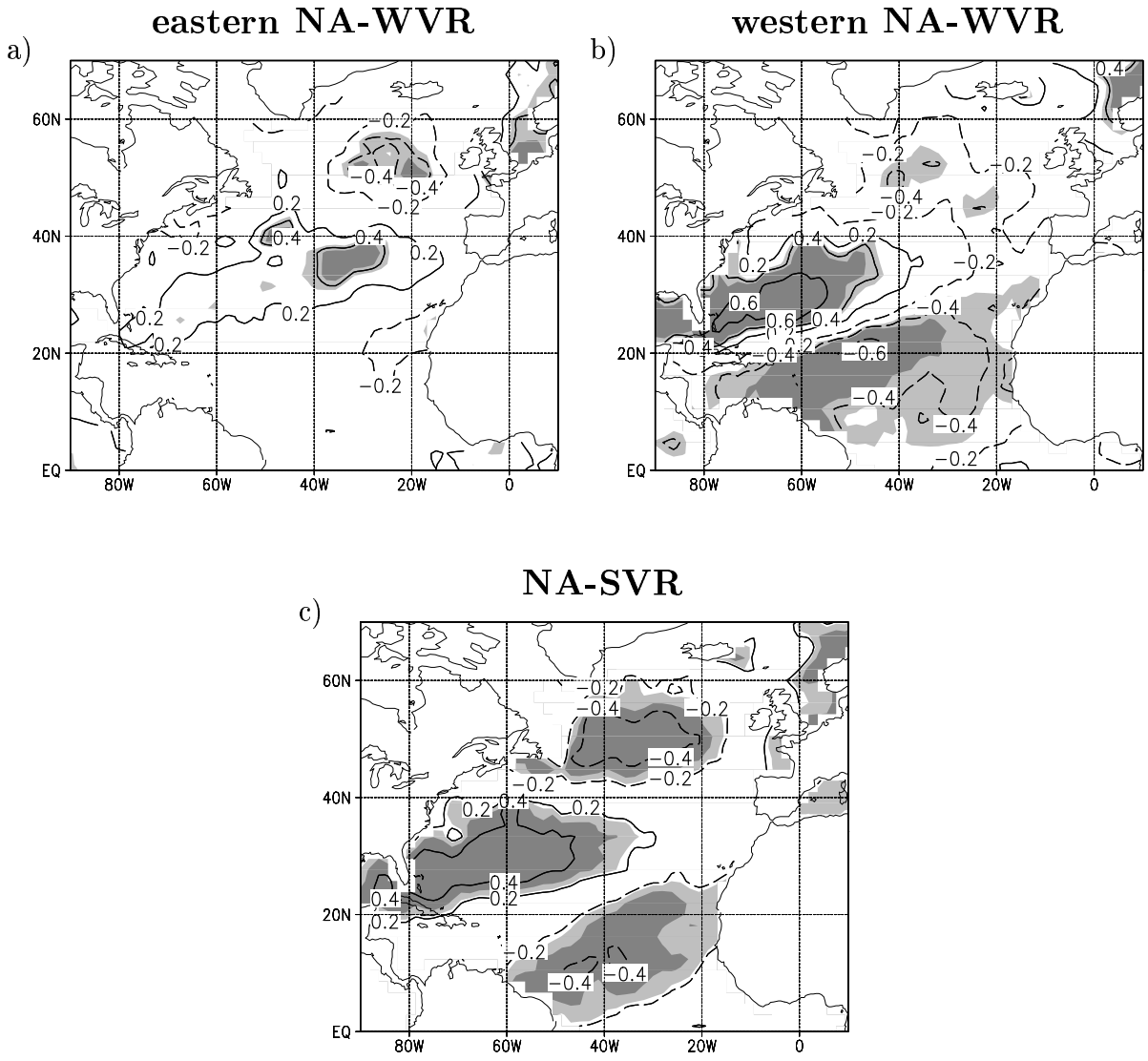

Figure 4.23: *Lagged correlation coefficient of monthly mean sea surface temperature in the North Atlantic sector and the monthly mean (a) eastern NA-WVR index, (b) western NA-WVR index, and (c) NA-SVR index. The index timeseries leads the SST by one month. The isoline interval is 0.2 and the zero contour is omitted. Shadings indicate significance above the 95%- (light) and the 99%-level (dark).*

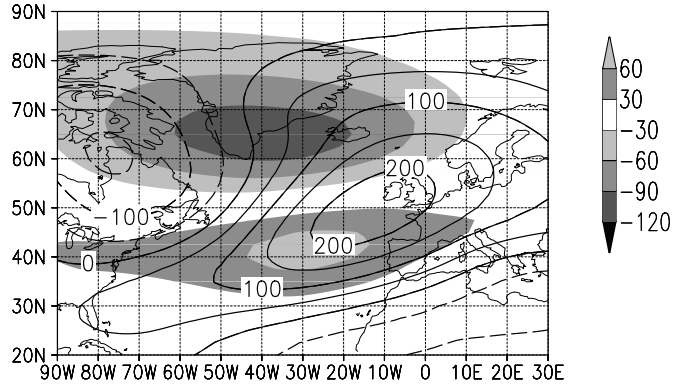

Figure 4.24: *Linear regression coefficient ([gpm]; shadings) of the monthly mean 300 hPa geopotential height in the North Atlantic sector regressed onto the monthly mean NAO index without separating the polar vortex regimes. The isolines represent the deviation of the 1958–1998 time mean geopotential height from its zonal mean [gpm]. The values of the regression coefficients correspond to one standard deviation of the NAO index.*

the central to eastern North Atlantic (Fig. 4.24). The NAO thus influences the tilt of the isohypses in this region. This corresponds to the NA-SVR and eastern NA-WVR patterns (Fig. 4.16a,c) which can therefore be referred to as NAO-like teleconnection patterns. The structure of the 'classic style' NAO mainly represents a blend of the eastern NA-WVR and the NA-SVR patterns. This corresponds to Castanheira et al. (2002) who found that the wintertime NAO can be understood as a barotropic Eigenmode of tropospheric variability whose structure is modulated by the strength of the polar vortex.

Composites for the two phases of the 'classic style' NAO index (Fig. 4.25) show storm track patterns which are qualitatively similar to the positive NA-SVR and the negative eastern NA-WVR pattern composites. The composites are based on 55 (53) months in the positive (negative) NAO index case. In the positive (negative) index case, the storm track is zonally elongated (short) and displaced northward (southward). The precipitation rate anomalies exhibit to be almost linear with the sign of the NAO index, showing enhanced (reduced) precipitation over northwestern Europe and reduced (enhanced) precipitation over southwestern Europe in the positive (negative) index case (Fig. 4.25c,d). Both, the storm track and precipitation patterns associated with the extreme phases of the NAO therefore correspond to the positive NA-SVR phase on the one hand and to the negative phase of the eastern NA-WVR index on the other hand. The blocking situation in the negative NA-SVR index case, however, is not captured. This means, that the classical picture of a uniform NAO is not sufficient

to describe a large part of the storm track and precipitation rate variability over the North Atlantic. The composites are in better agreement with those of the NA-SVR and the eastern NA-WVR pattern if one uses a 'classic style' NAO index but examines the two stratospheric polar vortex regimes separately. Hence, the use of tropospheric data alone ('classic style' NAO index) captures less variability than the combined use of tropospheric and stratospheric data.

Rogers (1997) identified the leading mode of North Atlantic storm track variability by applying rotated EOF analysis to monthly rms fields of 2–8 days filtered sea level pressures (SLP) for the winters 1900–1992. He noted that the classical NAO is not strongly linked to the leading mode, which seemed to be more associated with SLP at the Gulf of Biscay and over northern Scandinavia and the Barents Sea. It turns out that the two extreme phases of the leading mode correspond to the blocking situation described by the negative phase of the NA-SVR pattern on the one hand and and the short (weak) storm track situation described by the negative phase of the eastern NA-WVR pattern on the other hand. As mentioned before, the blocking situations are not captured with a 'classic style' NAO index without separating the two polar vortex regimes. For describing the dominant mode of storm track variability (and the associated precipitation) it is therefore necessary to take into account the state of the polar vortex.

The temperature anomalies associated with the 'classic style' NAO reveal to be almost linear about the sign of the NAO index (Fig. 4.25e,f). The positive and negative NAO composites correspond to the positive NA-SVR and the negative eastern NA-WVR pattern composites, respectively. They also correspond to the two extreme phases of the leading Empirical Orthogonal Function (EOF, appendix B.4) of monthly mean (DJFM) temperature variability in the North Atlantic sector (80°W–30°E, 87.5°–20°N). This leading EOF mode explains 28% of the temperature variability in that region (not shown). The NAO index is thus sufficient to describe the dominant mode of monthly mean temperature variability in the North Atlantic sector. This corresponds to the finding that the structures of the NA-SVR and and the eastern NA-WVR patters are relatively similar at lower altitudes, and the temperature changes associated with the NAO are mainly related to advection of heat by the lower tropospheric flow (Trigo et al., 2002). The structural differences between the NA-SVR and the eastern NA-WVR patterns are larger in the mid to upper troposphere. Thus, the classic NAO is less sufficient to describe a large part of the variability associated with the storm tracks, i.e. precipitation rates.

It has been shown in the preceeding section that the anticorrelation of the eastern NA-WVR pattern index with the SST in the tropical North Atlantic is very weak whereas it is stronger for the NA-SVR pattern index. If a 'classic style' NAO index is used, this anticorrelation (significant above the 99% level) reaches

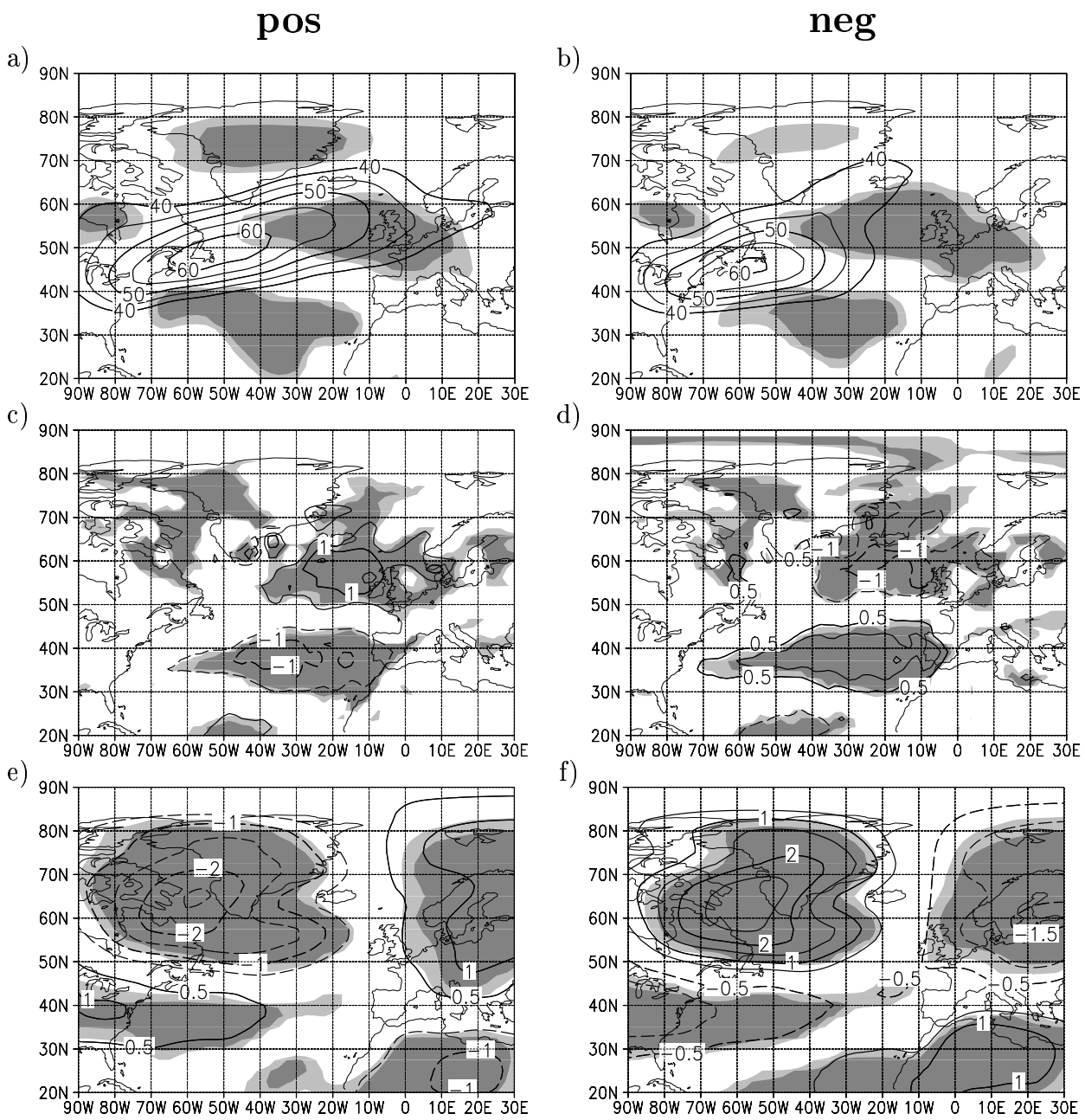

Figure 4.25: *Composites for the positive (left panels) and the negative phase (right panels) of the NAO index without separating the polar vortex regimes. Composite (a,b) monthly rms of band pass filtered 500 hPa geopotential height [gpm] and composite monthly mean anomalies of (c,d) the precipitation rate [mm/d], and of (e,f) the temperature at 850 hPa. The anomalies are deviations from the 1958-to-1998 time mean. The shadings indicate deviations from the time mean above the 95% (light) and the 99% (dark) significance level according to a t-test.*

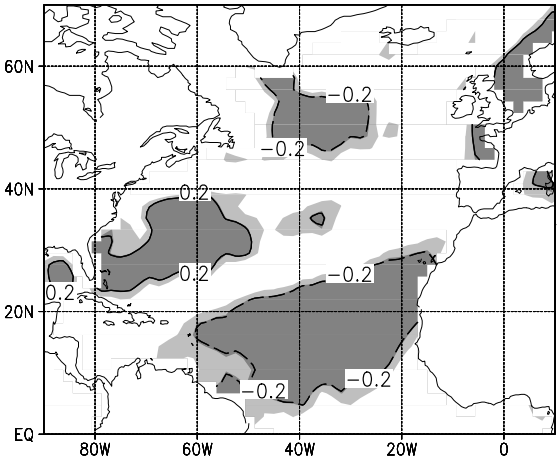

Figure 4.26: *Lagged correlation coefficient of monthly mean sea surface temperature in the North Atlantic sector and the monthly mean NAO index. The index timeseries leads the SST by one month. The isoline interval is 0.2 and the zero contour is omitted. Shadings indicate significance above the 95%- (light) and the 99%-level (dark).*

an intermediate value (Fig. 4.26). The same is true for the area of positive correlation in the midlatitude North Atlantic. This confirms the impression gained from previous results that the NAO represents a blend of the eastern NA-WVR and the NA-SVR pattern.

Some authors (e.g. Jones et al., 2003) argue that a NAO index with Lisbon or Gibraltar as southern station is more appropriate to describe the atmospheric variability over Europe than an index that incorporates data from the Azores. However, the results discussed in this chapter are qualitatively similar for an Iceland-Lisbon NAO index (not shown).

4.4 Summary

Teleconnections of North Atlantic geopotential height were examined separately for winter months (December to March) characterized by either a strong or a weak stratospheric polar vortex. In both cases, the major teleconnection patterns have north-south dipole structures with opposing centers of action in subpolar and subtropic latitudes. The mid to upper troposphere in the strong vortex regime (SVR) is characterized by a single teleconnection pattern over the central North Atlantic with a basically dipolar structure, the NA-SVR pattern. In contrast,

there are two dipole patterns in the weak vortex regime (WVR): One over northeastern Canada and the western North Atlantic (western NA-WVR pattern) and a weaker one over the eastern North Atlantic (eastern NA-WVR pattern). In the lower troposphere, however, the NA-SVR and the eastern NA-WVR patterns are very similar, in particular concerning their northern centers of action.

Fluctuations of the three North Atlantic teleconnection patterns (one in the SVR and two in the the WVR) have typical timescales of about two weeks. Lifecycle analyses of low frequency (periods $\geq$ 10 days) streamfunction anomalies associated with the North Atlantic teleconnection patterns exhibited that the forcing mechanisms dominating the decay phase are basically the same in the two polar vortex regimes. The decay is mainly driven by low frequency divergence whereas synoptic (periods 2.5–6 days) eddy vorticity fluxes act to maintain the anomaly against decay. However, the lifecycle analyses also revealed that, during the growth phase, the relative importance of the forcing mechanisms is very different in the two polar vortex regimes. In the WVR, the anomaly growth is mainly driven by transient eddy vorticity fluxes in particular from the low frequency domain. In the SVR, however, a different forcing mechanism is of similar importance: the forcing related to low frequency advection of (relative) vorticity which results from the interaction of low frequency eddies with the zonally asymmetric part of the time mean flow, i.e. with the stationary eddies. This means, that the different teleconnection structures cannot simply be explained by a reorganization of the transient eddies in the different regimes but are also related to a modified interaction of the transient eddies with the (changed) background flow. The latter can mainly be attributed to different stationary eddy structures in the two polar vortex regimes. Hence, there are fundamental differences in tropospheric dynamics associated with the generation of North Atlantic teleconnection patterns in the two stratospheric polar vortex regimes.

The fluctuations in both, the North Atlantic storm track and the precipitation rates, show significant differences between the two polar vortex regimes. Composites of the winterly North Atlantic storm track and precipitation rates for the two polarities of a 'classic style' NAO index (i.e. without considering the polar vortex regime) mainly correspond to the composites for the positive phase of the NA-SVR pattern index on the one hand and composites for the negative phase of the eastern NA-WVR pattern index on the other hand. However, the composites for the negative NA-SVR phase describe a blocking situation over the North Atlantic with a strong northeastward tilt of the storm track axis and reduced precipitation over western Europe. A comparison with the results presented by Rogers (1997) revealed that one of the two polarities of the leading mode of North Atlantic storm track variability corresponds to such a blocking situation. The latter situation is not captured with composites for the 'classic style' NAO index. As already mentioned by Rogers (1997), it is therefore not

possible to statistically describe the leading mode of North Atlantic storm track variability with a ('classic style') NAO index. However, if strong and weak vortex regimes are examined separately, storm track and precipitation rate composites for the two polarities of a 'classic style' NAO index become more similar to the NA-SVR and eastern NA-WVR pattern composites. This emphasizes the need to consider the state of the polar vortex for describing the atmospheric variability in the North Atlantic region. This is particularly true for the variability related to the flow in the mid to upper troposphere. In the lower troposphere, the NA-SVR and eastern NA-WVR patterns are difficult to distinguish and are quite similar to the classic NAO pattern. As a consequence, a 'classic style' NAO index may be appropriate for a statistical description of fluctuations associated with the leading mode of temperature variability in the lower troposphere, but it does not capture a large part of the atmospheric variability at upper layers.

There are some structural differences in the near-surface geopotential height patterns over the Arctic which have to be examined in the future. The northern center of action of the NA-SVR pattern is associated with larger fluctuations of geopotential height and extends further to the north than the corresponding center of the eastern NA-WVR pattern. The extreme phases of the NA-SVR pattern are therefore associated with stronger anomalies of the meridional flow over the Fram Strait than those of the eastern NA-WVR pattern. This — as well as the different mean flow patterns in the two polar vortex regimes — may have an influence on the ice export from the Arctic to the North Atlantic. Since the heat flux and sea ice transport through the Fram Strait influences the thermohaline circulation at a global scale, the connection between the sea ice flux and the state of the stratospheric polar vortex should be further examined in future studies.

The covariability with the North Atlantic sea surface temperature (SST) appears to be strongly dependent on the teleconnection pattern. The correlation patterns between North Atlantic SST and the NA-WVR and NA-SVR pattern indices all show the typical tripole structure with negative correlation in the midlatitude and the tropical North Atlantic and positive correlation in the subtropics. However, there are also some differences: The SST in the tropical North Atlantic is significantly (anti-)correlated only with the western NA-WVR and the NA-SVR pattern indices but not with the eastern NA-WVR pattern index. This may be explained with the more westerly position of the southern centers of action of the western NA-WVR and the NA-SVR patterns. In the midlatitude North Atlantic south of Greenland, the SST is more strongly (anti-)correlated with the index timeseries of the NA-SVR pattern than with those of the two NA-WVR patterns. This can be explained with the large fluctuations in the tropospheric flow over the midlatitude North Atlantic and the Labrador Sea associated with variations of the NA-SVR pattern index. The covariability between atmospheric circulation and North Atlantic SST will be further discussed in the next chapter.

Chapter 5

Ocean-atmosphere covariability in the North Atlantic region [1]

It has been shown in the previous chapters that atmospheric teleconnection pattern in the North Atlantic region are subject to structural modifications associated with changes in the dynamical coupling between stratosphere and troposphere. The North Atlantic Oscillation thus reveals to be structurally nonstationary. This may have consequences for the interaction with the ocean. The connection between atmosphere and ocean may also be influenced by changes in the temporal variability structure of the atmospheric flow. Due to its longer characteristic timescales, the ocean will react more intensively to very low frequency fluctuations, possibly resulting in a stronger oceanic forcing of the atmosphere.

Concurrent variations in winter mean SST and tropospheric geopotential heights and their relations to the North Atlantic Oscillation are examined in this chapter by means of linear correlation and regression analysis, the first indicating the strength, and the second giving the pattern of a connection. NCEP/NCAR reanalyses as well as the sea surface dataset by Kaplan et al. (1997; 1998) were employed for the analyses. January-to-March (JFM) means are discussed throughout this chapter because the centers of action of the North Atlantic Oscillation are most pronounced during that season. However, the main features discussed in this chapter are the same for December-to-February (DJF) means.

[1] Parts of this chapter have been published as: Walter, K., and H.-F. Graf, 2002: On the changing nature of the regional connection between the North Atlantic Oscillation and sea surface temperature. *J. Geophys. Res.*, **107,** Art. No. 4338, doi:10.1029/2001JD000850.

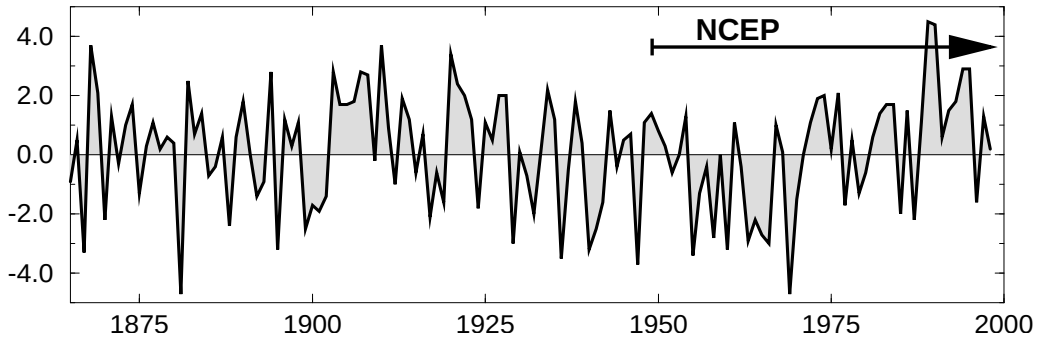

Figure 5.1: *NAO index as the difference between the normalized sea level pressure at Ponta Delgada, Azores and Stykkisholmur/Reykjavik, Iceland, averaged over the JFM season (data from J. Hurrell's website http://www.cgd.ucar.edu/~jhurrell/nao.html). The arrow denotes the period for which NCEP/NCAR reanalysis data is available.*

5.1 Patterns of ocean-atmosphere covariability

Following Hurrell (1995), the polarity and strength of the North Atlantic Oscillation is described in terms of the NAO index, defined as the difference between the normalized sea level pressure anomalies at two stations near the subtropical high and the Icelandic low, respectively (see appendix A). The NAO index used throughout this chapter (Fig. 5.1; data from J. Hurrell's website *http://www.cgd.ucar.edu/~jhurrell/nao.html*) is computed from JFM mean sea level pressure anomalies (relative to the 1865–1984 mean) at Ponta Delgada, Azores, and Stykkisholmur/Reykjavik, Iceland. The pressure anomalies are normalized by division of each JFM mean pressure by the long-term standard deviation (1865–1984).

As mentioned in chapter 1, the atmospheric circulation can interact with the ocean by surface heat and momentum fluxes. The strength of the (concurrent) correlation between the JFM means of NAO index (Azores – Iceland) and reanalyzed North Atlantic SST is presented in Fig. 5.2. The map of correlation coefficients for the period 1949 to 1998 shows the well known tripole structure with maximum correlation coefficients of more than ± 0.5. Between 50°N and 70°N, that is, southeast of Greenland and in the (sub)tropics between 10°N and 30°N the SST is anticorrelated with the NAO index. Between these two centers of negative correlation an area emerges with positive correlation between SST and NAO index. Its center is located in the western North Atlantic between 25° and 40°N, that is, in the subtropical gyre region. There is no significant correla-

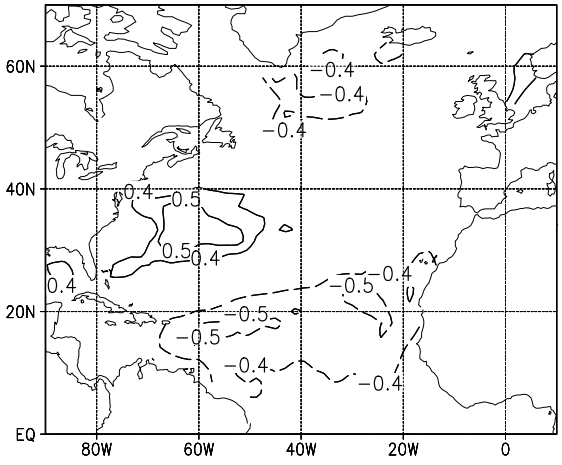

Figure 5.2: *Correlation coefficient between NAO index and reanalyzed SST at each grid point in the North Atlantic region calculated from JFM seasonal means for 1949 – 1998. Only values exceeding ±0.4 are shown.*

tion with South Atlantic SST. (For the significance test please see appendix B.3.) The tripole SST pattern is consistent with the anomalous surface heat and momentum fluxes associated with the NAO (Cayan, 1992). Similar patterns are derived and described in numerous previous studies, e.g. Bjerknes (1964), Deser and Blackmon (1993), Kushnir (1994). The tripole pattern also resembles the leading Empirical Orthogonal Function (EOF, see appendix B.4) mode of North Atlantic SST variability explaining 29.6 % of the total variance (not shown). This indicates that a large fraction of the North Atlantic SST variability is related to the North Atlantic Oscillation. The correlations in Fig. 5.2 are stronger than for monthly means owing to the longer timescales of the ocean.

The variability of the NAO index has not been uniform since the beginning of the observations in the 19th century (Fig. 5.1). We applied a Morlet wavelet analysis (Torrence and Compo, 1998; see appendix B.2) to the JFM mean NAO index. The local wavelet power spectrum is presented in Fig. 5.3. As already mentioned by Appenzeller et al. (1998), the NAO index timeseries reveals to be nearly white. The significance of the local wavelet power spectrum was therefore tested using a white noise background spectrum. Fig. 5.3 shows several peaks of wavelet power for periods between 7–8 years and 20 years. Especially fluctuations with periods around 16 years are pronounced from 1895 to 1920/25. This peak is significant above the 90%-level. From 1965/70 on there are two other peaks for periods around 16 years and 8 years, respectively. The first is not significant above the 90%-level, but may possibly have been artificially reduced by zero padding, as low frequency variability at the end of the timeseries can already

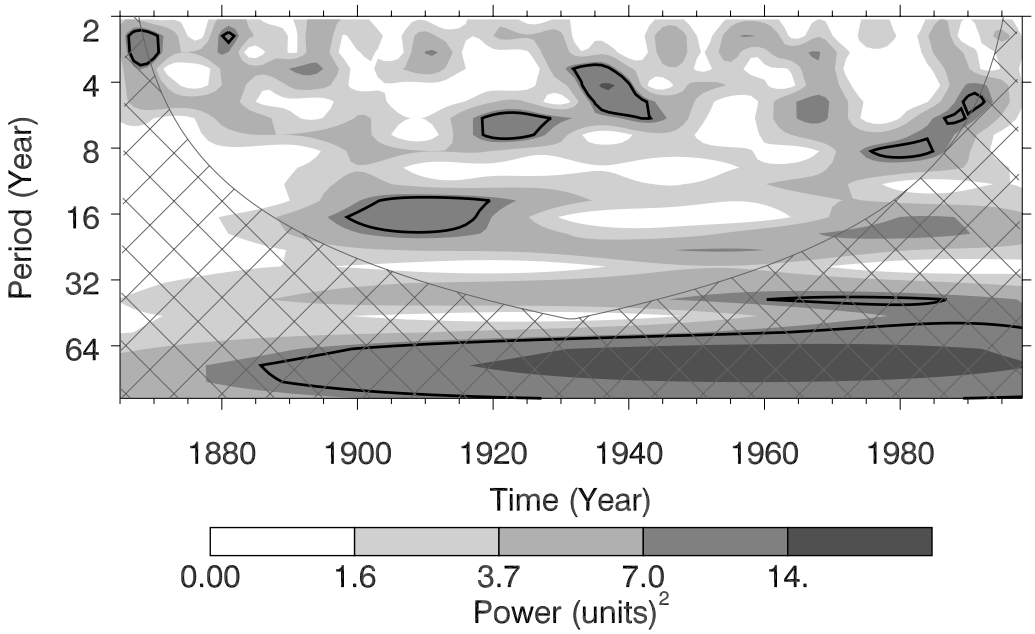

Figure 5.3: *Local wavelet power spectrum of the JFM mean NAO-Index. The analysis is based on a Morlet wavelet with a characteristic frequency of six. The contour levels are chosen so that 70%, 50%, 25%, and 5% of the wavelet power is above each level, respectively. The cross-hatched region corresponds to the cone of influence where zero padding has reduced the variance. The black contour is the 90%-significance level, using a white noise background spectrum. (Software provided by http://www.ResearchSystems.com. Reference: Torrence and Compo (1998).)*

be seen in Fig. 5.1. From 1940 to the mid-1960s there is only little variance for periods between 7–8 and 20 years. This is also true for the second half of the 19th century. In summary, during the first three decades of the 20th century and since the mid-1960s/early 1970s, the NAO index showed pronounced decadal variability. Fig. 5.1 shows that the NAO index was also characterized by mainly positive values during these years. In contrast, the decadal variability was reduced during the second half of the 19th century and from the 1940s to the 1960s. These years are therefore characterized by (relatively) more interannual variability, as there are peaks in the wavelet power spectrum for periods shorter than 6–4 years.

Fig. 5.1 shows that the 1930s to 1960s were additionally characterized by a negative trend of the NAO index, whereas the recent three decades were characterized by a strong positive trend, which is unprecedented in the last few centuries (Appenzeller et al., 1998). These trends correspond to the peak in the wavelet

power spectrum for periods around 64 years (Fig. 5.3) which shall not be further commented.

In the following, two subperiods with lengths of 20 and 30 years are discussed separately in order to take into account the changes in the variability structure of the NAO. One subperiod ranges from 1949 to 1968, characterized by weak decadal and, thus, (relatively) more interannual variability of the NAO index. The second subperiod ranges from 1969 to 1998, characterized by pronounced decadal variability of the NAO index. Linear trends were subtracted prior to the calculation of correlation or regression coefficients. However, correlation maps from raw data are very similar to the ones discussed in this chapter, even concerning the magnitudes of the coefficients. Hence, the changes in correlation and regression presented in the following do not seem to be dependent on linear trends. The 99%-significance level for correlations is ± 0.56 for the 20 year-period and ± 0.46 for the 30 year-period (see appendix B.3).

The change in the variability structure of the NAO in the late 1960s/early 1970s coincided with changes in correlations between NAO index and North Atlantic SST: Separate correlation maps for the two subperiods 1949 – 1968 and 1969 – 1998 show that the correlation between the NAO index and the North Atlantic tripole SST pattern is not stationary. During the first subperiod (1949 – 1968, Fig. 5.4a) the North Atlantic SST is rather weakly correlated to the NAO index. The correlations are not significant above the 99%-level except for the positive midlatitude center, which moved to the central North Atlantic. In contrast, during the second subperiod, 1969 – 1999, the correlation pattern clearly shows the well known tripole structure (Fig. 5.4b). The correlation is stronger in the subtropical as well as in the positive midlatitude center in comparison to the entire period correlations. The maximum correlation in both centers exceeds -0.6 and 0.6, respectively. Especially the subtropical center (of anticorrelation) is broader and stronger than for the entire NCEP/NCAR period. In this region a strong Azores high is related to a strong negative SST anomaly: A strong Azores high corresponds to enhanced northeast trades resulting in both cooling of the sea surface due to heat fluxes and in enhanced upwelling of cold deep water off the North African coast due to anomalously strengthened Ekman-transports. This is reflected by the fact that the subtropical center of strong anticorrelation extends up far to the northeast, i.e. to the upwelling region off the North African west coast.

In summary, the North Atlantic SST is significantly correlated to the NAO index only since the last decades, when the NAO index is characterized by pronounced decadal variability and by mainly positive values. In the subperiod 1969 – 1998 especially the subtropical center of anticorrelation is broader and stronger than for the entire NCEP/NCAR period. Thus, this region is examined in the

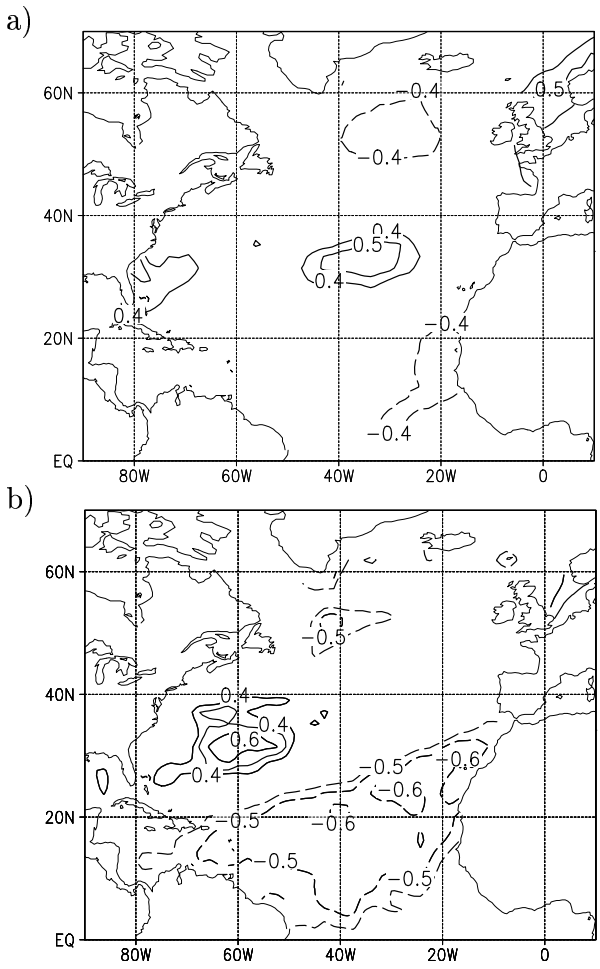

Figure 5.4: *Correlation coefficient between NAO index and reanalyzed SST at each grid point in the North Atlantic region calculated from JFM seasonal means (a) for 1949 – 1968 and (b) for 1969 – 1998. The linear trends are subtracted before calculating the correlation coefficients. Only values exceeding ±0.4 are shown.*

following in order to further document the altered ocean-atmosphere connections. An index for the tropical North Atlantic (TNA) SST is defined as the area average of SST over the grid points in the box 10° – 20°N, 20° – 60°W (see appendix A).

Separate maps of correlation between the TNA index of tropical North Atlantic SST and the 1000 hPa geopotential height at each grid point for the two subperiods 1949 – 1968 (Fig. 5.5a) and 1969 – 1998 (Fig. 5.5b) support the previous conclusion that the correlation between the NAO index and the North Atlantic SST is not stationary. During the first subperiod (1949 – 1968) the TNA SST-index is only weakly correlated with the regional atmospheric circulation in the North Atlantic sector, whereas there is strong correlation with the geopotential height in that region during 1969 – 1998. The latter period is characterized by a dipole structure over the North Atlantic with maximum correlation of more than -0.8 and 0.7, respectively. In the following, we refer to the latter period as the 'regional period' and to the period 1949 – 1968 as the 'global period' because connections with regions outside the North Atlantic region become important then.

The above mentioned analysis was repeated with different mean sea level pressure (SLP) datasets (updates of the dataset by Jones (1987) and of the NCAR dataset described by Trenberth and Paolino (1980)). Both datasets cover the Northern Hemisphere north of 15°N. In that region, the regression and correlation patterns of sea level pressure with SST indices derived from NCEP/NCAR reanalysis and from the Kaplan SST dataset (not shown) are very similar to the corresponding patterns calculated from NCEP/NCAR reanalysis data alone. That is, the results from the NCEP/NCAR reanalysis do not seem to be strongly contaminated by the inconsistencies in that dataset (chapter 2).

'Regional Period'

A map of linear regression coefficients of the 1000 hPa geopotential height regressed onto the TNA SST index (Fig. 5.6b) shows a dipole pattern with a positive pressure anomaly southeast of Greenland and a negative one with center between 20° and 45°N over the subtropical Atlantic. The dipole structure resembles the meridional see-saw pattern associated with the North Atlantic Oscillation (e.g. Barnston and Livezey, 1987). The correlation in both centers of the dipole pattern is significant above the 99%-level.

The correlation between TNA SST index and 1000 hPa geopotential height over the subtropical North Atlantic increases slightly (from about -0.83 to about -0.88) if the TNA SST index of the MAM season is taken and the atmosphere leads the SST by one to two months (not shown), whereas the pattern remains

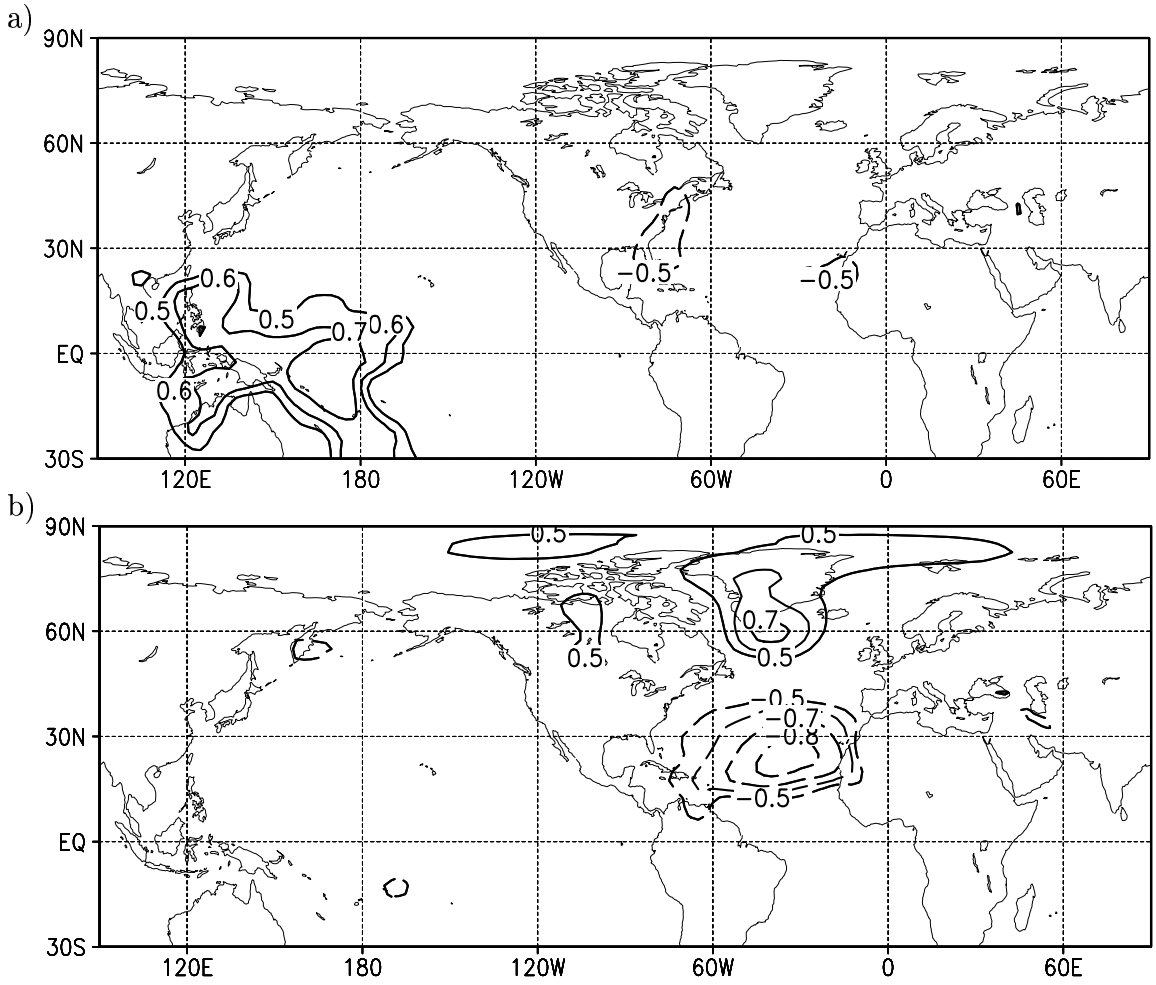

Figure 5.5: *Correlation coefficient between the TNA SST index and the 1000 hPa geopotential height at each grid point calculated from JFM seasonal means of NCEP/NCAR reanalysis data, (a) for 1949 – 1968 and (b) for 1969 – 1998. Only values greater than 0.5 or lower than -0.5 are shown. The linear trends are subtracted.*

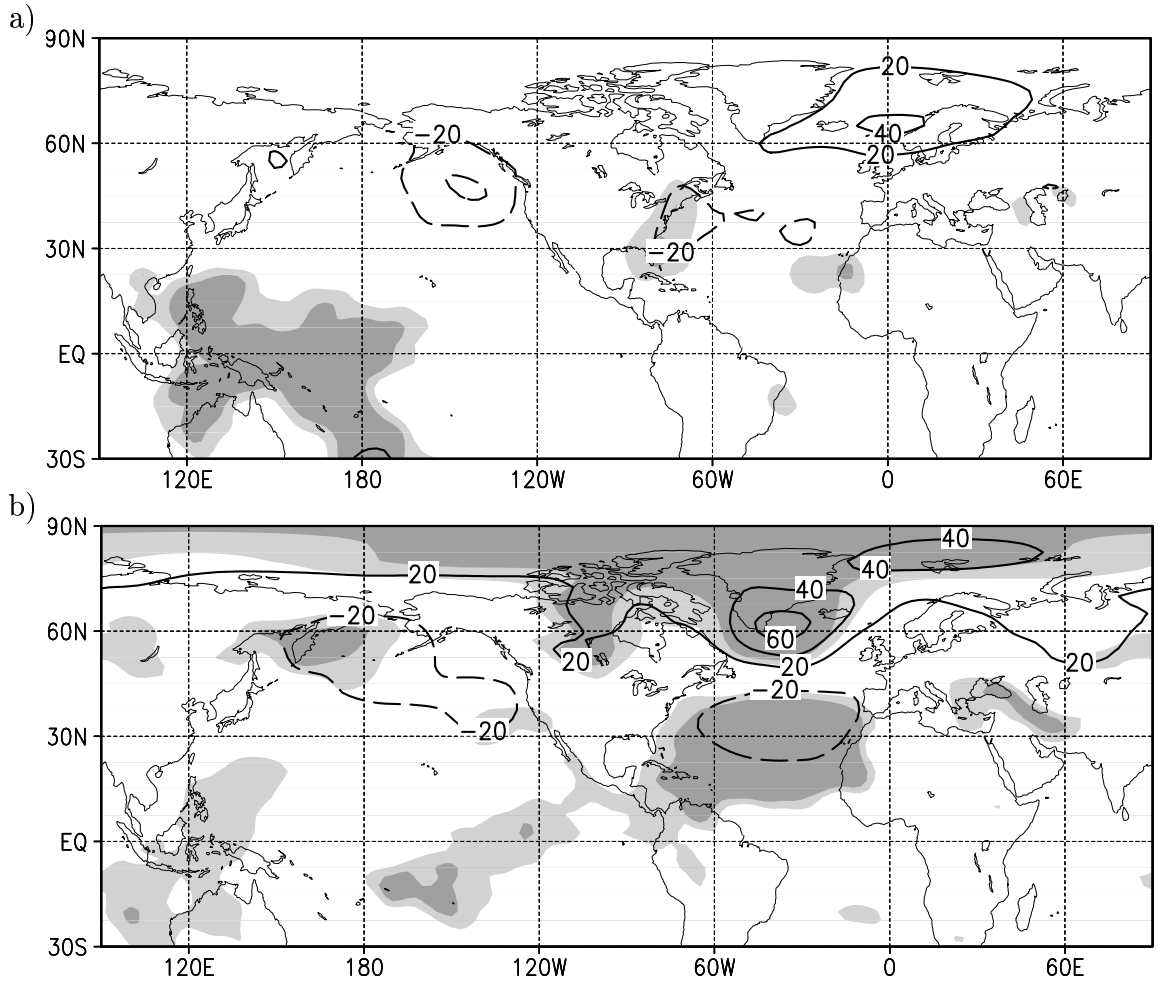

Figure 5.6: *Linear regression coefficient [gpm/K] of the 1000 hPa level geopotential height field regressed onto the TNA SST index calculated from JFM seasonal means of NCEP/NCAR reanalysis data (a) for 1949 – 1968 and (b) for 1969 – 1998. The shading indicates that the correlation is significant above the 95%-(light) and the 99%-level (dark), respectively. The linear trends are subtracted.*

almost unchanged. This indicates an influence of the atmospheric circulation on the SST. Based on weekly mean data, Deser and Timlin (1997) found that the large-scale covariation between wintertime atmospheric circulation and SST over the North Atlantic or the North Pacific is closest if the atmosphere leads the SST by 2–3 weeks. They assume that the 2–3-week timescale reflects the high frequency stochastic forcing of the oceanic mixed layer by the atmosphere. For monthly mean data the maximum correlation between atmospheric circulation and extratropical SST is achieved if the atmosphere leads the ocean by one month (Wallace and Jiang, 1987). However, corresponding to our results from seasonal mean data, they found that the maximum correlations in the North Atlantic region are only slightly stronger than for contemporaneous fields. This is likely to be due to the averaging process.

'Global Period'

During times when the connection between North Atlantic SST and NAO is weak, other — remote — influences become important for the tropical North Atlantic SST: From 1949 to 1968 the TNA SST index is strongly correlated with the 1000 hPa geopotential height over a wide region covering the western tropical Pacific (Fig. 5.5a, 5.6a). The maximum correlation coefficient exceeds 0.7 and is therefore highly significant.

The atmospheric variability in the western tropical Pacific region is strongly influenced by the anomalous Walker Circulation which is involved in the El Niño/Southern Oscillation (ENSO) phenomenon (Bjerknes, 1969): The anomalous Walker Circulation is associated with an east-west surface pressure see-saw across the tropical Pacific consisting of one pressure anomaly over the western tropical Pacific/Indonesia and one of opposite sign over the central/eastern tropical Pacific (Walker, 1924; Walker and Bliss, 1932; Bjerknes, 1969). The connection of this pressure see-saw with the tropical Pacific SST is demonstrated with a correlation map between the NINO3.4 SST index (appendix A) and the 1000 hPa geopotential height (Fig. 5.7). The center of action in the western tropical Pacific corresponds to the area strongly correlated with the TNA SST index (Fig. 5.5a). Remark that, from 1969 to 1998 (Fig. 5.7b), the pressure dipole over the tropical Pacific associated with the NINO3.4 SST emerges more clearly than during the period 1949 – 1968 (Fig. 5.7a). That is, although the Southern Oscillation is more pronounced in the period 1969 – 1998, there is less influence on North Atlantic SST than from 1949 to 1968 (Fig. 5.8).

It is the SST in the western part of the tropical North Atlantic that is especially strongly correlated to the NINO3.4 SST in 1949 – 1968 (Fig. 5.8a), whereas there is weaker correlation with North Atlantic SST in 1969 – 1998 (Fig. 5.8b).

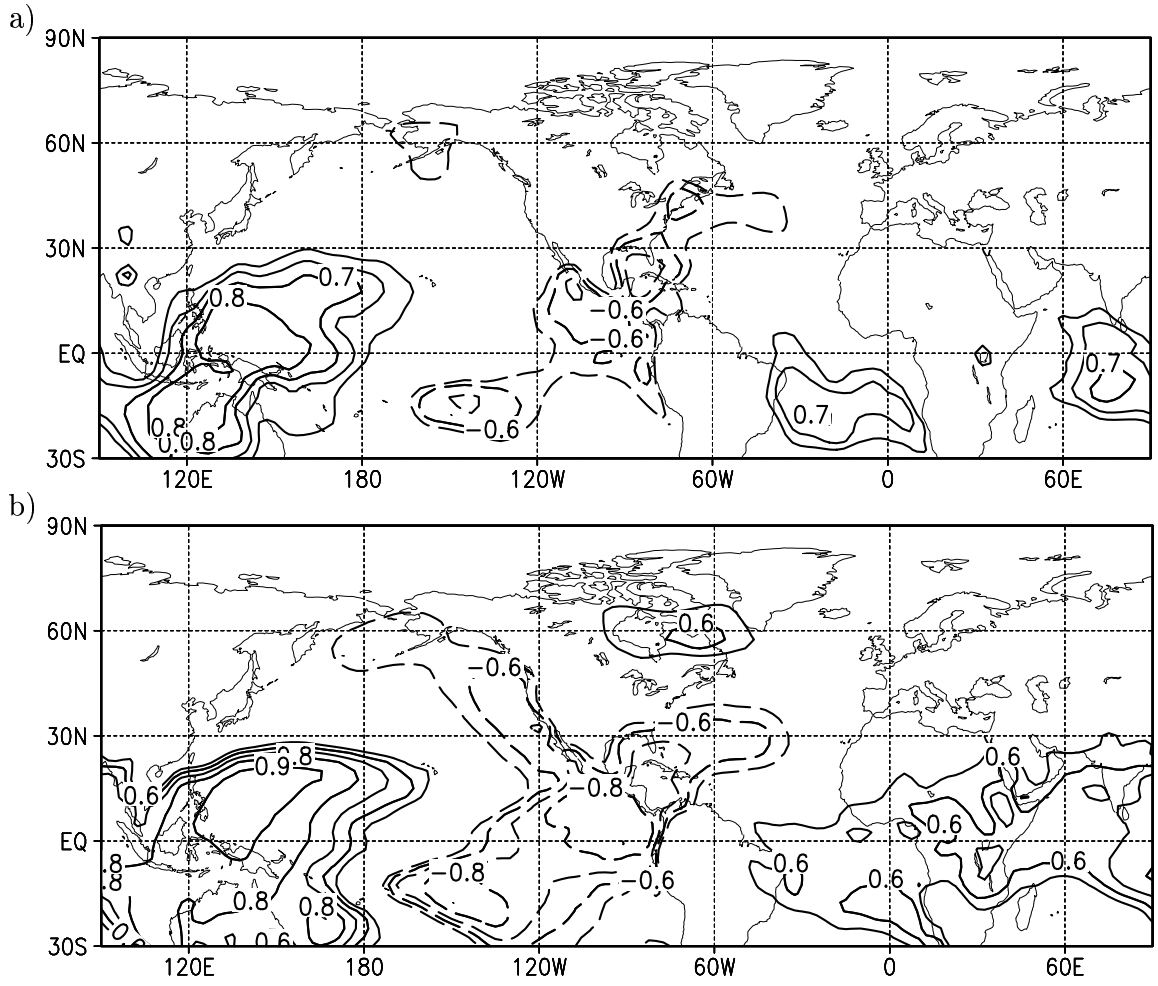

Figure 5.7: *As in Fig. 5.5 but for correlation between the SST averaged over the NINO3.4 region and the 1000 hPa geopotential height at each grid point.*

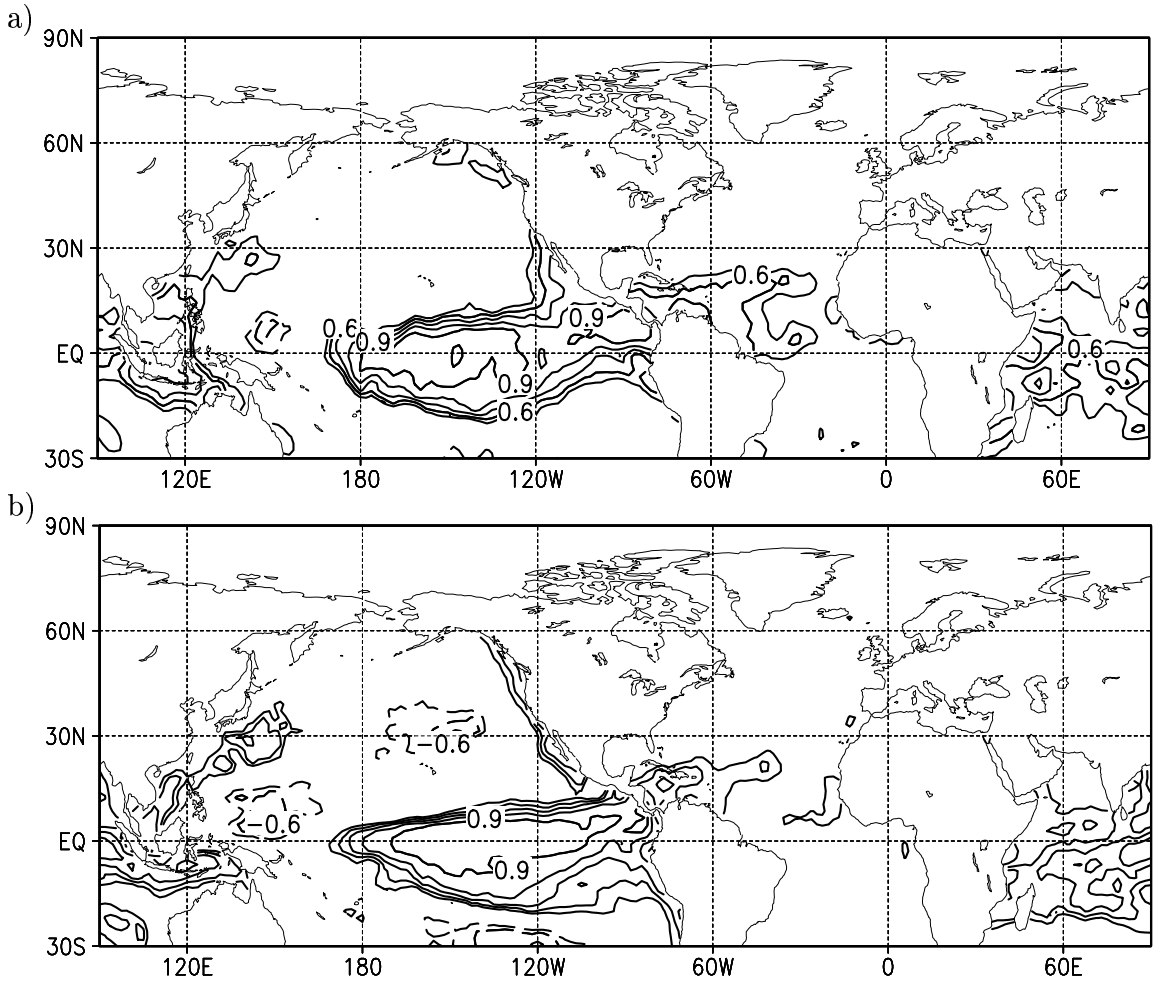

Figure 5.8: *As in Fig. 5.5 but for correlation between the SST averaged over the NINO3.4 region and the SST at each grid point.*

Warm SST events in the tropical Pacific are accompanied by a weakened subtropical high in the western North Atlantic sector/Caribbean region (Fig. 5.7, see also Fig. 5.6a) and therefore by reduced northeast tradewinds over the western tropical North Atlantic (not shown), leading to positive SST anomalies in that region at least in 1949 – 1968 (Fig. 5.8a). As mentioned in the introduction, this feature is described in numerous studies using observational and reanalysis data (e.g. Hastenrath et al., 1987; Curtis and Hastenrath, 1995; Nobre and Shukla, 1996; Enfield and Mayer, 1997; Hastenrath, 2000) and is confirmed by several modeling studies (Hameed et al., 1993; Saravanan and Chang, 2000). However, most of these studies point out that the effects of the ENSO phenomenon on the tropical North Atlantic SST appear to be maximum during the boreal spring season, i.e. several months after the mature phase of ENSO. Corresponding to that, the correlation between NINO3.4 index and the SST increases to more than 0.7 in the western part of the tropical North Atlantic if the SST of the MAM season is employed, that is, if the NINO3.4 index leads the SST by two to three months (not shown). The correlation patterns, however, are not very different and therefore are not discussed in the following.

A remaining question is how the information is transferred from the tropical Pacific to the subtropical Atlantic. Nobre and Shukla (1996) and Hastenrath (2000) present evidence that a wavetrain-like teleconnection pattern, which extends from the tropical Pacific across North America to the North Atlantic, might be involved in connecting the two regions. A map of regression coefficients of the 500 hPa geopotential height onto the TNA SST index (Fig. 5.9a) shows an extratropical wavetrain extending across North America with three major centers of action: A negative one over the southeastern US, a positive one over Canada, and a negative one over the Northern Pacific. This wavetrain-like pattern is reminiscent of the blend of the Pacific/North American (PNA) and the Tropical/Northern Hemisphere (TNH) teleconnection patterns described by Barnston and Livezey (1987). However, in Fig. 5.9a, only the centers of action over Canada and over the southeastern US are significantly correlated with the TNA SST index above the 99%-level and only the latter has a significant imprint on the 1000 hPa geopotential height (Fig. 5.6a). But the strength of the correlations and regression coefficients increases if the geopotential height leads the SST by about one month, i.e. TNA index of the JFM season versus the geopotential height of the DJF season (Fig. 5.10). This is evident even over the midlatitude North Pacific. The latter center of action has also a stronger imprint on the corresponding correlation maps of the 1000 hPa geopotential height, where the correlation with the TNA index is about -0.6.

A map of linear regression coefficients of the 500 hPa geopotential height regressed onto the TNA SST index for the period 1969 – 1998 (Fig. 5.9b) does not show a clearly emerging correlation to a wavetrain-like pattern across North

America. Instead, the regression pattern is again dominated by regional structures over the North Atlantic. Three meridionally arranged centers of action emerge: one over southern Greenland, one over the subtropical North Atlantic and a third one located over the tropical North Atlantic and Northern Africa. Especially the northernmost anomaly is much stronger than any anomaly in the map for the period 1949 – 1968 (Fig. 5.9a). Hence, during the period 1969 – 1998 the regional atmospheric circulation pattern in the North Atlantic sector obviously surpasses a possible imprint of the tropical Pacific variability on the North Atlantic geopotential height (Fig. 5.7b, e.g.). However, an influence from the tropical Pacific is also present during that period. This is revealed by lagged correlations between TNA SST in spring and the 1000 hPa geopotential height in winter showing maxima of more than 0.6 over the western tropical Pacific (not shown). But this influence still appears to be weaker than the one from the regional circulation in late winter (JFM and following months with maximum correlations of more than -0.8 over the subtropical North Atlantic, not shown).

In summary, it is identified from NCEP/NCAR reanalysis data that the wintertime correlation between the North Atlantic SST and the regional atmospheric circulation is not stationary: Since the recent decades (1969 – 1998) the North Atlantic SST is strongly related to the regional circulation in the North Atlantic sector, that is, to the NAO, which is characterized by pronounced decadal variability during this period. In contrast, the period 1949 – 1968 is characterized by a connection of especially the western tropical North Atlantic SST with the atmospheric circulation over the tropical Pacific.

North Atlantic teleconnection patterns

The regression and correlation map between the tropical North Atlantic SST and the 500 hPa geopotential height (Fig. 5.9) shows that, during the 'regional' period 1969 – 1998, the fluctuations of the TNA SST index are mainly associated with a NAO-like dipole structure of geopotential height over the central North Atlantic. This structure resembles the teleconnection pattern identified in chapter 4 for the strong stratospheric polar vortex regime (NA-SVR pattern, Fig. 4.2a). This pattern reveals to be much more closely correlated with North Atlantic SST than the other NAO-like teleconnection pattern in the weak vortex regime (eastern NA-WVR pattern, Fig. 4.2b). It has furthermore been shown in chapter 3 that months with a strong stratospheric polar vortex occurred more frequently during the last decades in comparison to months with a weak polar vortex. Thus, the question arises whether the larger number of strong vortex months can account for the stronger covariance between NAO tropical North Atlantic SST.

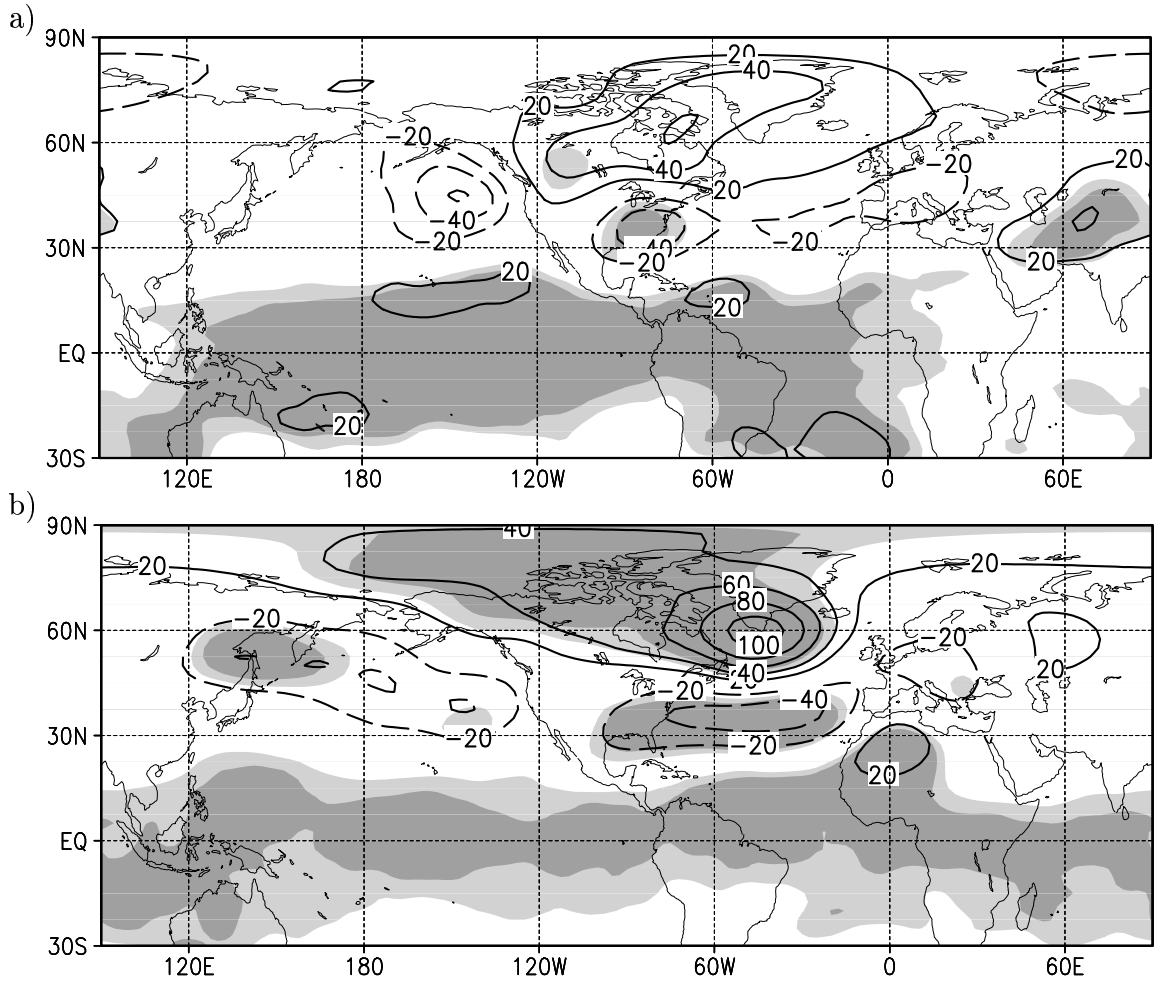

Figure 5.9: *Linear regression coefficient [gpm/K] of the 500 hPa geopotential height field regressed onto the TNA SST index calculated from JFM seasonal means of NCEP/NCAR reanalysis data, (a) for 1949 – 1968 and (b) for 1969 – 1998. The shading indicates that the correlation is significant above the 95%-(light) and the 99%-level (dark), respectively. The linear trends are subtracted. The tropics are shown but are not discussed because of the lack of upper-air observational data in that region before 1958.*

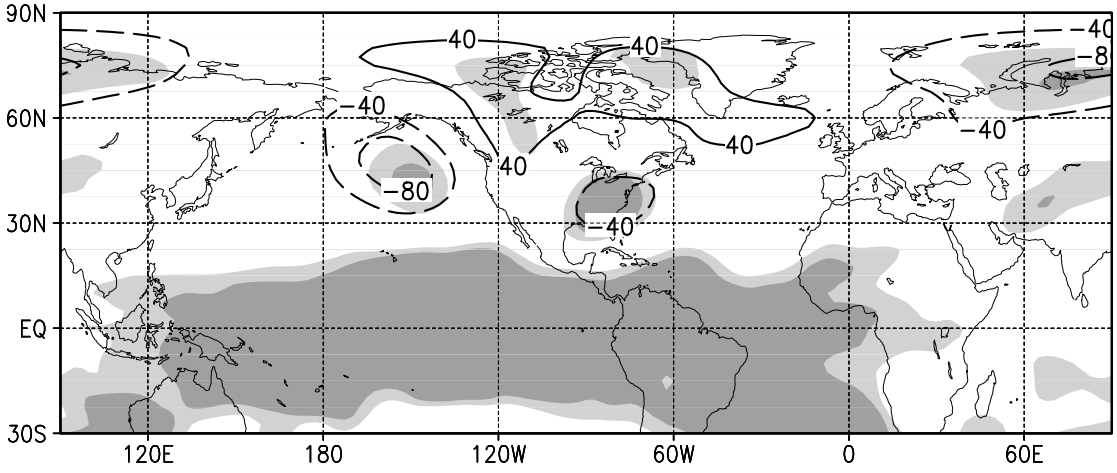

Figure 5.10: *Linear regression coefficient [gpm/K] of the 500 hPa level geopotential height field of the DJF season regressed onto the TNA SST index of JFM season calculated from NCEP/NCAR reanalysis data for 1949 – 1968. The shading indicates that the correlation is significant above the 95%- (light) and the 99%-level (dark), respectively. The linear trends are subtracted.*

It has been shown in chapter 4 that the North Atlantic teleconnection patterns are structurally different in the two regimes of the stratospheric polar vortex strength. Fig. 5.11 displays the teleconnectivity (see chapter 4, section 4.1) of the JFM-mean 500 hPa geopotential height during the global and the regional period. In both periods, a teleconnection dipole over the central North Atlantic can be observed, which resembles the NA-SVR pattern (Fig. 4.2a). The (anti)correlation between the centers of action over the central North Atlantic is almost equal in the two subperiods (-0.8 to -0.85). However, the teleconnection maxima have moved to the west in the last decades. This means, that the western North Atlantic teleconnection pattern in the weak vortex regime (western NA-WVR pattern, Fig. 4.2b) gained more importance in comparison to the period 1949 – 1968. Fluctuations of this pattern appear to be closely correlated with fluctuations in North Atlantic SST (Fig. 4.23b). However, the emphasized western NA-WVR pattern most probably does not account for the stronger covariation between North Atlantic SST and the regional atmospheric circulation: firstly, because variations in tropical North Atlantic SST during 1969 – 1998 are related to geopotential height fluctuations over the *central* North Atlantic (Fig. 5.9) and secondly, because the maximum of the root mean square (rms) of JFM-mean 500 hPa geopotential height is situated over southern Greenland during 1969 – 1998 (Fig. 5.12b), i.e. close to the northern center of the NA-SVR pattern. The

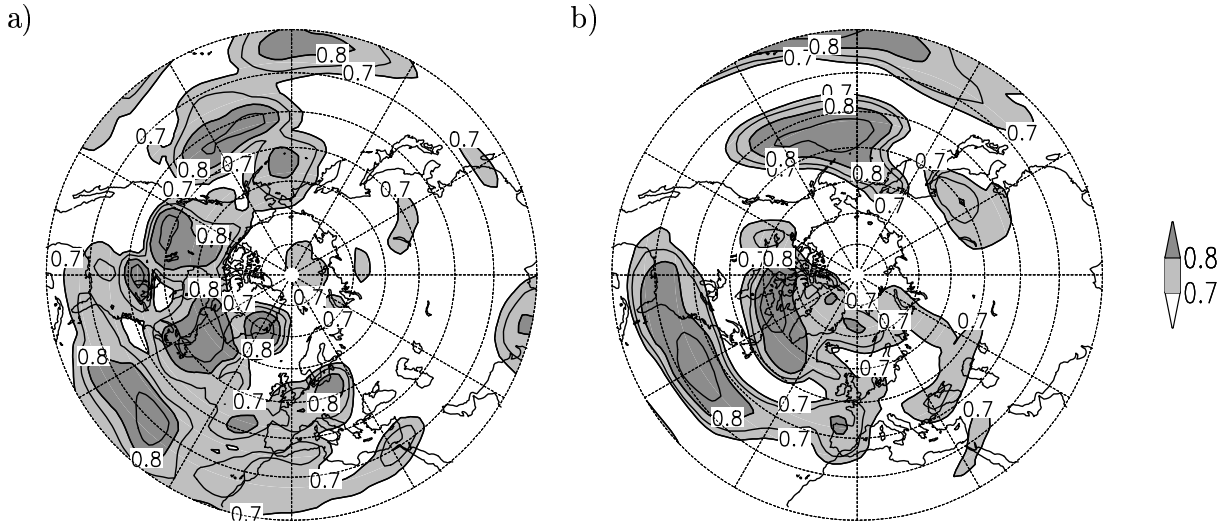

Figure 5.11: *Teleconnectivity of the JFM mean geopotential height of the 500 hPa level for (a) 1949 – 1968 and (b) 1969 – 1998. The isoline interval is 0.05. Only values above 0.7 are shown.*

NA-SVR pattern is thus associated with a larger fraction of variability than the western NA-WVR pattern. The position of the rms maximum corresponds to the more frequent occurrence of months with a strong polar vortex during the last decades (compare Fig. 3.14). During 1949 – 1968 the maximum is located over the Labrador sea (Fig. 5.12b).

The SST in the tropical North Atlantic is mainly related to heat and momentum fluxes associated with the southern center of the North Atlantic teleconnection pattern. The standard deviation of the (detrended) geopotential amplitude at this southern center is almost equal in the 'global' and the 'regional' periods (Fig. 5.12). Together with the small changes in the strength of the teleconnectivity this means, that the NA-SVR-pattern-like teleconnection structure over the central North Atlantic, and in particular its southern center, is almost equally emphasized in both subperiods. It is therefore conceivable that the larger number of months with a strong polar vortex might at least not be the only cause for the closer regional correlation between atmospheric circulation and SST in the North Atlantic.

Another explanation for the closer connection between NAO and SST during the last decades might be that the decadal variability of atmospheric flow over the North Atlantic is intensified during the last three decades. Fluctuations of the teleconnection pattern over the central North Atlantic can be described

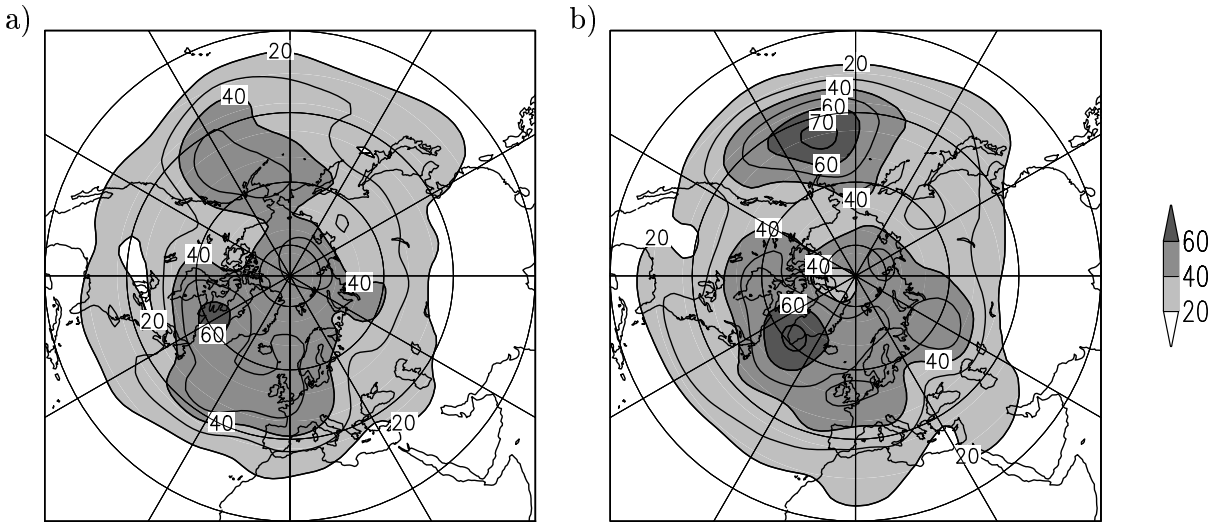

Figure 5.12: *Root mean square of the JFM mean 500 hPa geopotential height [gpm] in (a) 1949 – 1968 and (b) 1969 – 1998. For simplicity, only values above 20 gpm are shown.*

with an index timeseries defined in the same manner as for the NA-SVR pattern (appendix A), but for JFM means from 1949 to 1998. The index time series is well correlated with the NAO index (0.83). It therefore shows the same characteristics as the NAO index: Decadal fluctuations are much more pronounced during 1969 – 1998 than before (not shown). Visbeck et al. (1998) conducted sensitivity experiments with an ocean model driven by NAO-like atmospheric forcing. They found that the SST response is more intense to decadal than to interannual atmospheric forcing.

The question whether it is the more frequent occurrence of the strong vortex regime (and the associated teleconnection pattern) or the enhanced decadal variability that accounts for the closer connection between NAO and SST cannot be answered by examining reanalysis data or observations alone. This issue may be addressed with sensitivity experiments applying ocean models which are driven by the atmospheric circulation patterns identified in chapter 4 with different temporal variability spectra.

5.2 Temporal behavior during the 20th century

In the previous section, two periods of time with fixed boundaries were discussed separately. These periods were found to be characterized by different patterns of North Atlantic ocean-atmosphere covariability. In the following, we examine if these two states inferred from NCEP/NCAR reanalyses can also be identified (in another dataset) if the boundaries of the intervals are moved back or forth in time and if similar periods of covariability already appeared before the beginning of the NCEP/NCAR period. The SST data source used throughout this section is the Kaplan dataset (Kaplan et al., 1997; 1998).

The percentage of variance of the TNA index of tropical North Atlantic SST explained by the either the NAO index or the NINO3.4 index is discussed. Every explained variance (squared correlation coefficient) is computed from a 25 year-window sliding through the data. The linear trends are subtracted from the timeseries for every 25 year-window before calculating the explained variance. However, the features described in the following remain unchanged if trends are included.

Both, the first EOF of North Atlantic SST and the correlation pattern between the NAO index and North Atlantic SST are characterized by a tripole structure (not shown) similar to the corresponding patterns deduced from NCEP/NCAR reanalysis (Fig. 5.2). From 1969 to 1991, the SST in each of the three centers is strongly correlated with the NAO index (± 0.6, not shown). This is reflected by the percentage of variance of the TNA SST index explained by the NAO index. The values for periods starting in even years are shown in Fig. 5.13 (black vertical lines). NAO index and TNA SST index are significantly correlated above the 99%-level in periods comprising the late 1960s/1970s and the subsequent years. Only a rather small fraction (<20%) of the TNA SST index variance can be explained by the variability of the NINO3.4 SST index (gray vertical lines in Fig. 5.13).

In contrast, from the 1930s to the 1960s the NAO index is characterized by weak decadal variability and is — on the average — slightly negative (Fig. 5.1). The correlation between NAO index and TNA SST index is rather weak, i.e. most of the time the explained variance is below 15%, whereas a large fraction of the TNA SST variance can be explained by NINO3.4 SST variability (significant above the 99%-level).

Corresponding to the end of the 20th century, the NAO index is also predominantly positive and characterized by pronounced decadal variability during the first three decades of the 20th century (Figs. 5.1 and 5.3). The fraction of variance explained by fluctuations of the NAO index is most of the time signif-

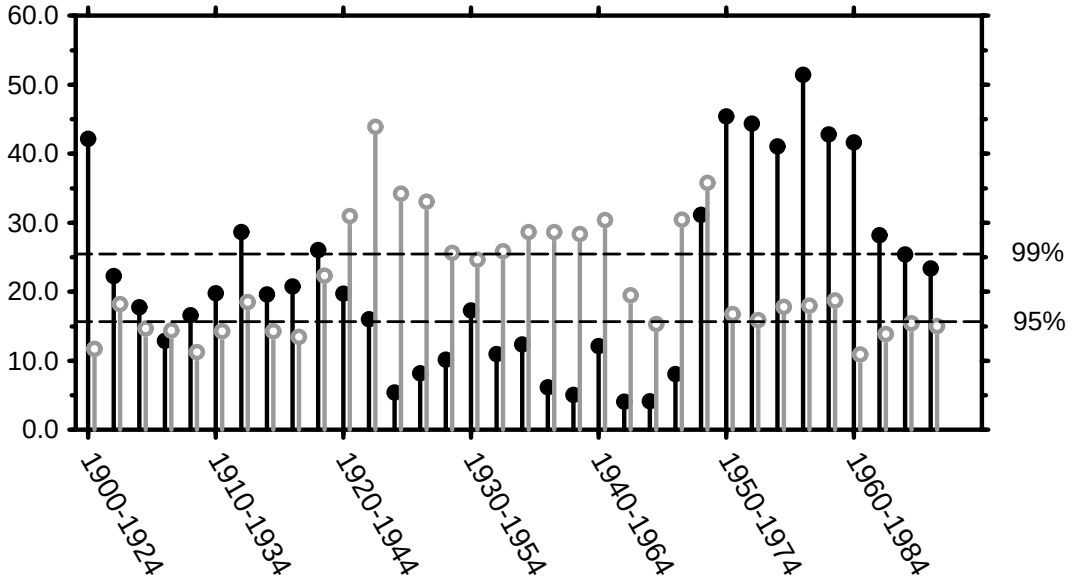

Figure 5.13: *Percentage of variance of the JFM mean TNA SST index explained by the NAO index (black dots/vertical lines), and by the SST averaged over the NINO3.4 region (gray circles/vertical lines). Each value is computed for a 25 year-period. Shown are only the results for periods beginning in even years. The 25 year-linear trends have been subtracted from the time series before calculating each correlation. The 99 and 95% significance levels are also shown (dashed lines). The underlying SST dataset has been derived by Kaplan et al. (1997; 1998).*

icant above the 95%-level, although it is not as large as during the end of the 20th century. For the period 1900 – 1924, the explained variance is about 40%. The fraction of TNA SST variance explained by the NINO3.4 SST fluctuations is most of the time below the 95%-significance level, in contrast to the subsequent decades.

In summary, two periods are identified during which NAO index and tropical North Atlantic (TNA) SST are strongly correlated and influences from the tropical Pacific are weak ('regional periods'): One is from the 1960s/1970s to the end of the data record (1991), and there are indications for another one in the beginning of the 20th century until the 1920s/1930s. During the latter period, however, the correlation with the NAO index is not as strong as in the end of the century. During these two periods, the NAO index shows pronounced decadal variability and is primarily positive. In the ('global') period between, i.e. from the 1930s to the 1960s, when the NAO index is characterized by weak decadal variability, the 'regional' correlation between NAO index and TNA SST is also weak. Correlations with the tropical Pacific SST (in terms of the NINO3.4 SST index) become more important for the tropical North Atlantic SST. Hence, the results from the observational dataset support the hypothesis gained from NCEP/NCAR reanalysis, proposing periods when the North Atlantic sector is dominated by regional correlations between atmospheric and oceanic variables ('regional periods') and others, when remote connections with the tropical Pacific region are preferred ('global periods'). From Fig. 5.13 one cannot infer when exactly, i.e. in which years, the transitions between the periods took place. However, the two transitions must have happened somewhen during the 1920s and 1960s, respectively, possibly over several years.

5.3 Summary

The North Atlantic Oscillation is associated with a basin-wide tripole sea surface temperature (SST) anomaly pattern in the North Atlantic. By means of linear correlation and regression analysis, applied to both, NCEP/NCAR reanalysis and an optimally smoothed SST dataset (Kaplan et al., 1997; 1998), it was inferred that these correlations are not stationary. Two phases were identified, characterized by either a close or weak relationship between the NAO and especially the SST in the tropical North Atlantic ('regional' or 'global' periods). A close relationship ('regional period') can be observed during the recent decades (since the 1960s/1970s) and, in outlines, during the first three decades of the 20th century. The NAO index then shows enhanced variability on the decadal timescale and is predominantly positive. In contrast, the regional circulation over the North Atlantic is of minor importance for the North Atlantic SST from the 1930s to

the early/mid 1960s. Effects from outside the North Atlantic region, particularly from the tropical Pacific, dominate ('global period'). During this period, the SST in the tropical North Atlantic (TNA) is strongly correlated with both the SST in the central/eastern and the (lower tropospheric) geopotential height in the western tropical Pacific. This indicates a connection with the El Niño/Southern Oscillation (ENSO) phenomenon. The tropical North Atlantic SST is then correlated with a wavetrain-like pattern of geopotential height, which extends from the tropical Pacific over the extratropical Northern Pacific and North America to the western part of the tropical North Atlantic region. In years of warm (cold) SST in the tropical Pacific, the latter goes along with a weakening (strengthening) of the North Atlantic subtropical high and, thus, of the northeast tradewinds over the tropical North Atlantic (not shown). The wavetrain-like pattern is reminiscent of a blend of the Pacific/North American (PNA) and the Tropical/Northern Hemisphere (TNH) pattern presented by Barnston and Livezey (1987), who argued that the blend of the mutually independent patterns is an artifact of averaging. Both patterns can be associated with variability in the tropical Pacific region, i.e. also with ENSO (Mo and Livezey, 1986). Although a link via a wavetrain-like teleconnection pattern across North America has also been proposed by Nobre and Shukla (1996) and Hastenrath (2000), additional studies are required on possible mechanisms of transferring information from the tropical Pacific to the North Atlantic.

The SST fluctuations in the tropical North Atlantic during the 'regional' period 1969 – 1998 are mainly related to a NAO-like dipole pattern of midtropospheric geopotential height over the central North Atlantic. This pattern resembles the dominant North Atlantic teleconnection pattern in the strong stratospheric polar vortex regime (see chapter 4). Despite the larger number of months with a strong stratospheric polar vortex in the last decades (see chapter 3), the teleconnection structure over the central North Atlantic is almost equally emphasized in the 'global' and the 'regional' period — in particular concerning its subtropical center of action. Thus, the larger number of months with a strong polar vortex (associated with changes in the teleconnection patterns) might at least not be the only reason for the closer correlation between the NAO index and the tropical North Atlantic SST during the 'regional' period. Another explanation might be the enhanced decadal variability of the NAO (or NAO-like teleconnection patterns) throughout the last decades to which the ocean might react more intensively than to shorter-period fluctuations. This issue, however, has to be further examined with modeling experiments.

Chapter 6

Summary and conclusions

The objective of this thesis was to increase our understanding of the atmospheric variability in the wintertime North Atlantic region with regard to the structural and temporal stationarity of the North Atlantic Oscillation (NAO). The thesis focused on the influence of the interaction between tropospheric and stratospheric variability, the changes in the temporal variability structure of the NAO, and the consequences for the covariability with North Atlantic sea surface temperature (SST). NCEP/NCAR reanalysis data (Kalnay et al., 1996; Kistler et al., 2001) were used for the analyses presented in this thesis, which were, however, supplemented by some analyses with observational data.

Influence of troposphere-stratosphere coupling

It has been shown in numerous publications that the low-frequency variability in the stratosphere and the troposphere are strongly coupled in winter (e.g. Baldwin et al., 1994; Perlwitz and Graf, 1995; Perlwitz, 2000). A large part of the tropospheric flow in the Northern Hemisphere reveals to be connected with the strength of the stratospheric polar vortex. The strength of the stratospheric polar vortex in turn is characterized by two regimes in which the vortex is either primarily strong or weak (Christiansen, 2003; Perlwitz and Graf, 2001b). Analyses presented in this thesis were therefore conducted separately for strong and weak polar vortex regimes (SVR and WVR) in the winter months December to March.

Changes in the strength of the stratospheric polar vortex are associated with changes in the strength of the zonal wind and its vertical profile. These changes affect the reflection/transmission properties for upward propagating planetary waves from the troposphere. During times when the polar vortex is strong, ultra-

long planetary waves are more effectively reflected downward while less wave activity is getting absorbed in the stratosphere (Charney and Drazin, 1961; Hu and Tung, 2002; Perlwitz and Harnik, 2003). This has consequences for the planetary wave structure in the troposphere as well as for the stratospheric circulation. Analyses of the Eliassen-Palm fluxes (E-P fluxes; Edmon et al., 1980) and their divergence exhibited that the westerly flow in the lower stratosphere is less counteracted by stationary eddy fluxes in the SVR than in the WVR. Hence, the potential for a strong vortex to stay strong is enhanced, whereas a weak vortex is further disturbed and, thus, stays weak. The anomalous stationary eddy fluxes thus support the persistence of a strong or weak polar vortex. The persistence of the polar vortex is, however, counteracted by anomalous transient eddy fluxes from the low frequency domain (periods $\geq$ 10 days), but the stationary eddy forcing dominates. In the upper to middle troposphere, a discussion of E-P fluxes and an analysis of single terms of the time mean streamfunction tendency equation (Cai and van den Dool, 1994; Feldstein, 1998) revealed that both, stationary and transient eddy fluxes, are responsible for maintaining different parts of the time mean geopotential height difference between SVR and WVR. Transient eddy fluxes, mainly from the low frequency domain, act to maintain the anomalous low over the Arctic and the anomalous high over western Europe. In contrast, the strong anomalous low over southern Greenland is mainly sustained by anomalous forcing by stationary eddy fluxes with a small contribution from synoptic eddy fluxes (periods 2.5–6 days). This means that both, stationary and transient eddies make important contributions to the mean flow difference between the two polar vortex regimes.

The largest differences in the tropospheric mean flow between the two stratospheric polar vortex regimes can be observed in the North Atlantic sector. This means that this region is most sensitive to changes the strength of the polar vortex. The mid-to-upper tropospheric geopotential height in the North Atlantic sector is characterized by teleconnection patterns with basically north-south dipole structures which consist of opposing centers of action in subpolar and subtropical latitudes. However, there are large differences between the two polar vortex regimes: The strong vortex regime is characterized by a single teleconnection pattern (NA-SVR pattern) which is situated over the central North Atlantic. Its northern center of action is located south of Greenland, the opposing center over the subtropical North Atlantic. In contrast, the weak vortex regime is characterized by two teleconnection dipoles. One is located in the western North Atlantic region with centers over northeastern Canada/Labrador sea and the western subtropical North Atlantic (western NA-WVR pattern). The fluctuations in the amplitude of this pattern exhibit to be related to fluctuations in the strength of the stratospheric polar vortex. The other teleconnection dipole is situated over the eastern North Atlantic (eastern NA-WVR pattern). It resembles very much the NAO, but is associated with a smaller fraction of low frequency

geopotential height variability than the western NA-WVR pattern.

Geopotential height fluctuations associated with the three North Atlantic teleconnection patterns (one in the SVR and two in the the WVR) have typical timescales of about two weeks. Their lifecycles were examined by analyzing the forcing mechanisms which contribute to the streamfunction tendency during the growth and decay of a low frequency streamfunction (or geopotential height) anomaly (Cai and van den Dool, 1994; Feldstein, 1998). It has been shown that the decay phase is characterized by similar processes in both stratospheric regimes: The anomaly decay is mainly related to negative forcing by low frequency divergence, whereas synoptic eddy vorticity fluxes act to maintain the anomaly against decay. However, there are fundamental differences between SVR and WVR concerning the forcing mechanisms responsible for the anomaly growth. In the WVR, the dominant forcing mechanism is related to transient eddy vorticity fluxes, in particular from the low frequency domain. In the SVR, however, another forcing term is equally important: forcing by vorticity advection resulting from the interaction of low frequency eddies with the zonally asymmetric part of the time mean flow, i.e. with the stationary eddies. Hence, the different teleconnection structures in the SVR and the WVR are not just originating from a reorganization of transient eddies in the two regimes but are also related to a modified interaction of the transient eddies with the (changed) background flow. The latter can mainly be attributed to the different stationary eddy structures in the two polar vortex regimes. In summary, the generation of tropospheric teleconnection patterns in the two polar vortex regimes is related to fundamentally different dynamical processes in the troposphere.

The teleconnection patterns in the two regimes are associated with very different structures of atmospheric variability over the North Atlantic, in particular in the middle to upper troposphere. This becomes apparent for fluctuations in strength and direction of the North Atlantic storm track and for precipitation rates in the North Atlantic sector. The negative phase of the NA-SVR pattern, e.g., is associated with blocking situations over the North Atlantic with a strong northeastward tilt of the storm track axis and reduced precipitation over western Europe. Blocking situations correspond to neither polarity of the two NA-WVR patterns and cannot be identified with a 'classic style' NAO index (e.g. defined as the difference of normalized near-surface geopotential heights at the Azores and Iceland — without considering the polar vortex regime). A comparison with Rogers (1997) revealed that the blocking situation corresponds to one polarity of the leading mode of storm track variability in the North Atlantic region. As already mentioned by Rogers (1997), it is therefore not possible to (statistically) describe the leading mode of North Atlantic storm track variability with a 'classic style' NAO index. However, if strong and weak vortex regimes are treated separately, the variability structures corresponding to the two polarities of a 'classic

style' NAO index become more similar to those described by the two polarities of the NA-SVR and the (eastern) NA-WVR patterns. This emphasizes the need to consider the state of the stratospheric polar vortex for describing the atmospheric variability in the North Atlantic region.

In summary, a 'classic style' NAO index, i.e. without considering the polar vortex strength, is not appropriate for a statistical description of a large part of tropospheric variability within the two polar vortex regimes — in particular in the mid to upper troposphere. For an adequate representation of the weather conditions over Europe and the eastern North Atlantic it is necessary to take into account the state of the polar vortex. Although it is not yet possible to predict the sign and strength of a teleconnection anomaly within the regimes, one can say that the probability for a certain circulation pattern (e.g. a blocking situation) depends on the state of the stratospheric polar vortex.

Covariability of NAO and North Atlantic SST

It has been shown in this thesis that changes in the stratospheric polar vortex regime are related to changes in the structure of tropospheric circulation modes in the North Atlantic sector. It has furthermore been shown that the number of months with a strong polar vortex is increased since the 1970s in comparison to the number of months with a weak polar vortex. Corti et al. (1999) found that the years 1949–1970 were dominated by different modes of winterly 500 hPa geopotential height variability than the years 1971–1994. Graf and Castanheira (2001) showed that these two sets of variability modes can be related to regimes with either a strong or a weak stratospheric polar vortex. However, not only the structure of the NAO (or NAO-like teleconnection patterns) but also its temporal behavior has a nonstationary character (Appenzeller et al., 1998). It is conceivable that changes in the spatial structure as well as in the temporal variability of the tropospheric circulation patterns may have an impact on the interaction between ocean and atmosphere.

On the average, the North Atlantic Oscillation is associated with a basin-wide tripole anomaly pattern of North Atlantic sea surface temperature (SST). It has been shown that the correlation between NAO index and sea surface temperature (SST) in the North Atlantic is not constant in time. Two phases have been identified, characterized by either a close or weak relationship between winter means (January to March) of the NAO and the SST especially in the tropical North Atlantic ('regional' or 'global' periods). A close relationship ('regional period') can be observed during the recent decades (since the 1960s/1970s) and, in outlines, during the first three decades of the 20th century. During these pe-

riods, the NAO index shows enhanced variability on the decadal timescale and is predominantly positive. In contrast, the regional circulation over the North Atlantic is of minor importance for the North Atlantic SST from the 1930s to the early/mid 1960s. During this period, influences from outside the North Atlantic region, particularly from the tropical Pacific, dominate ('global period'). The tropical North Atlantic SST is then correlated with a wavetrain-like pattern of tropospheric geopotential height, which extends from the tropical Pacific over the extratropical Northern Pacific and North America to the western part of the tropical North Atlantic region. The wavetrain-like pattern is reminiscent of a blend of the Pacific/North American (PNA) and the Tropical/Northern Hemisphere (TNH) pattern presented by Barnston and Livezey (1987), who argued that the blend of the mutually independent patterns is an artifact of temporal averaging. Both patterns can be associated with variability in the tropical Pacific region, i.e. also with the El Niño/Southern Oscillation (ENSO) phenomenon (Mo and Livezey, 1986). Although a link via a wavetrain-like teleconnection pattern across North America has also been proposed by Nobre and Shukla (1996) and Hastenrath (2000), additional studies are required on possible mechanisms of transferring information from the tropical Pacific to the North Atlantic.

The time period covered by the datasets used for this study is too short to prove that the identified periods are atmospheric regimes. But findings by Raible et al. (2001), who examined a 600 year experiment with the coupled general circulation model ECHAM4/HOPE, agree to our results. They identified two regimes of North Atlantic atmosphere–ocean interaction which are connected with the decadal variability of the NAO: Periods of enhanced decadal variability of the NAO index were characterized by strong correlation of the North Atlantic SST and the NAO index whereas periods of low decadal variability of the NAO index were characterized by a dominant PNA pattern linking the tropical Pacific and the North Atlantic region. Our results together with the findings of Raible et al. (2001) indicate that the atmosphere–ocean covariability in the North Atlantic sector may not be regarded as stationary.

The periods we found to be characterized by different SST-atmosphere covariation match exactly with the periods of interdecadal North Atlantic SST variability defined by Kushnir (1994). He remarked that the middle and high latitude North Atlantic SST is characterized by cold anomalies before 1920 and during the 1970s and 1980s, and by warm anomalies from about 1930 to 1960. This interdecadal fluctuation is associated with a basin-scale pattern, which is largely of one polarity, and has maxima near Iceland, in the Labrador Sea, and northeast of Bermuda. Kushnir (1994) found that the atmosphere mostly damps the local interdecadal SST anomalies, except in the northern part of the North Atlantic, where the atmospheric circulation acts to maintain the SST anomalies. He argued that the interdecadal SST variability therefore may be governed by

large-scale ocean dynamics. However, as discussed in the introduction, the role of oceanic forcing for the midlatitude atmospheric circulation is not yet clear.

A shift in remote teleconnections during the late 1960s to early 1970s was also detected by Rimbu et al. (2003). They examined oxygen isotope records generated from Red sea corals (as a measure for temperature in that area) and found that the correlation with the NINO3 index changed from negative to positive during that time. Nonstationarity of circulation regimes and associated modulations of teleconnections on interdecadal timescales thus limit the ability to predict or reconstruct remote climate phenomena from proxy data.

Is the shift in NAO-SST covariability associated with the structural changes in tropospheric teleconnection patterns related to stratosphere-troposphere coupling?

If tropospheric circulation patterns change in the North Atlantic sector, it is feasible that the oceanic feedback to the atmosphere might be influenced. This may result in a stabilization (destabilization) of atmospheric Eigenmodes and in an increase (reduction) of their variance. Such a behavior would be associated with a stabilization (destabilization) and a strengthening (weakening) of the regional atmosphere-ocean interaction in the North Atlantic sector so that influences from the tropical Pacific become less (more) important. It has been shown in chapter 4, that the NA-SVR teleconnection pattern is more closely correlated with the North Atlantic SST than the eastern NA-WVR pattern — especially in the tropical North Atlantic. Moreover, the tropical North Atlantic SST after 1969 is indeed correlated with a geopotential height pattern over the central North Atlantic resembling very much the NA-SVR pattern. Maps of 500 hPa geopotential height teleconnectivity, however, exhibit that this teleconnection pattern — and in particular the center of action over the subtropical North Atlantic — is almost equally emphasized before and after the late 1960s. Furthermore, a first inspection of the coupled modeling experiment discussed by Raible et al. (2001) did not reveal a significant relationship between an extraordinarily strong (weak) vortex and phases of close (weak) NAO-SST covariability.

Another possible explanation for the changes in the atmosphere-ocean covariability may be attributed to changes in the frequency spectrum of the atmospheric fluctuations. Visbeck et al. (1998) conducted experiments with an ocean general circulation model coupled with a atmospheric boundary layer model. The model system was driven by a NAO-like wind forcing with different interannual to multidecadal fluctuations. Visbeck et al. (1998) found that, overall in the entire North Atlantic basin, the SST response was stronger for decadal and interdecadal than for interannual NAO-like forcing. If the atmospheric circulation shows pronounced decadal (or longer) variability the covariation with the SST might thus be more intense due to the thermal inertia of the ocean. The ocean is then able to develop larger SST anomalies reaching into deeper layers. The SST

anomalies may therefore be long-living, i.e. persist for several winters. Several observational as well as modeling studies show that the atmospheric flow is able to generate such large-scale and long-living SST anomalies, e.g. Wallace and Jiang (1987), Luksch and von Storch (1992), Luksch (1996). Decadal cycles as described by Grötzner et al. (1998) or proposed by Visbeck et al. (1998), involving the subtropical and subpolar gyre, respectively, may be generated resulting in a decadal forcing of the atmosphere.

It is not yet clear what causes decadal (or longer) variability in the atmosphere. Ultra-low frequency variability may be generated by feedback processes within the atmosphere (James and James, 1989). However, decadal variability may also evolve from feedback processes between climate subsystems, e.g. with the ocean (Latif and Barnett, 1994; 1996). Feser et al. (1999) found decadal to secular variability of the stratospheric polar vortex in a coupled run with an atmosphere-ocean general circulation model without incorporation of external forcing. However, as discussed in the introduction, external factors such as changes in the solar radiation, injection of volcanic gases and aerosols and anthropogenic emission of greenhouse gases may also give rise to long periodic fluctuations in the stratosphere and troposphere.

Outlook

The reanalyzed and observational datasets used in this thesis only reach back until the middle of the 20th and 19th century, respectively. Thus, the findings about the modification of reflection/transmission properties in the two stratospheric polar vortex regimes and their effect on the structure of the NAO should be tested with modeling experiments. This can be achieved by examining long-term model runs as well as by sensitivity experiments with a prescribed or forced strong or weak polar vortex. It has been shown in chapter 3 and 4 that eddy-eddy and eddy-mean-flow interactions are vitally important for the generation of tropospheric flow patterns. Thus, in order to capture eddy-related processes, a sufficient horizontal resolution of the models is required. It is furthermore of crucial importance for modeling studies on the troposphere-stratosphere interaction that the strength of the polar vortex and the related reflection/transmission properties are properly represented. However, many general circulation model (GCM) experiments are characterized by a too strong polar vortex ('cold bias'; Perlwitz, 2000) so that the mean modeled circulation in the troposphere mainly corresponds to SVR conditions. The strength of the polar vortex is better represented in GCMs with a high resolution of the upper stratosphere or even higher levels (Shindell, 1999). Modeling studies dealing with stratosphere-troposphere interaction should better employ these high resolution models. Such models,

however, need a lot of computing time and memory. It is therefore reasonable to conduct sensitivity experiments with simplified global circulation models (SGCM) which have both, a high vertical resolution and the dynamical core of a GCM.

Experiments with high resolution models may also help to improve our understanding of external influences on the stratosphere and their impact on the troposphere (Shindell, 1999). Moreover, the transitions between the stratospheric regimes have not been examined in this thesis but they should also be subject of future studies since they might have a strong direct impact on the tropospheric flow (Baldwin and Dunkerton, 2001). It has been shown by Perlwitz (2000) that the forecast potential of the NAO from the coupled stratospheric-tropospheric circulation mainly results from transitions between the polar vortex regimes.

From reanalyses and observations alone we cannot determine the physical mechanisms leading to a transition between the two phases of North Atlantic atmosphere-ocean covariability or what the role of external influences like the solar cycle or the greenhouse effect is. It is necessary to examine whether the observed changes in the atmospheric circulation patterns and/or the different timescales of the NAO variability can change the oceanic response in a way that can account for the different phases of covariation. Both topics can be addressed for example with experiments applying ocean models forced by the different observed atmospheric circulation patterns with different temporal variability spectra. On interannual timescales, the SST variability can mainly be described as the response of the upper layers of the ocean to atmospheric fluctuations (Bjerknes, 1964). Moreover, Visbeck et al. (1998) found that the response of the tropical North Atlantic SST is almost in phase with the forcing. They concluded that this indicates a fast response with only little contribution from slow ocean dynamics. Thus, models of the oceanic mixed layer may be sufficient if one focuses on interannual to decadal variability. Experiments with the high-vertical-resolution SGCM as well as with a full GCM, both coupled with a oceanic mixed layer model may be appropriate for studying the feedback between ocean, troposphere and stratosphere.

It has been discussed in chapter 4 that the extreme phases of the NA-SVR pattern index are associated with large anomalies of the near-surface meridional wind over the Fram Strait, whereas this is not so for the eastern NA-WVR pattern. This suggests that the above mentioned teleconnection patterns might exert a different influence on the ice export through the Fram Strait. Cavalieri (2003) showed that the ice export during 1958 – 1997 is linked with the phase of zonal wave 1 in high latitude sea level pressure. In particular the zonal wave 1 structure in the troposphere is influenced by the different downward reflection properties for waves in SVR and WVR (Perlwitz and Graf, 2001a; Castanheira and Graf, 2003). Since ice export through the Fram Strait is an important source of fresh water

in the subpolar North Atlantic (Vinje, 2001), variations in ice export may have an impact on the thermohaline circulation. The possible influence of the polar vortex strength on the ice export due to structural changes in the high latitude tropospheric flow should therefore be examined in the future.

Appendix A

Index timeseries

Index timeseries have to be defined in order to describe the temporal behavior of low-frequency teleconnection patterns in the North Atlantic sector and associations between fluctuations in different variables or in remote areas.

Teleconnections within the polar vortex regimes

In chapter 4, three teleconnection patterns of mid to upper tropospheric height were identified in the North Atlantic region: The strong stratospheric polar vortex regime (SVR) is characterized by one pattern over the central North Atlantic, the weak stratospheric polar vortex regime (WVR) by two patterns over the western and the eastern North Atlantic, respectively. These teleconnection patterns have mainly north-south dipole structures with centers of action in subpolar and subtropical latitudes. Index timeseries for these teleconnection patterns were defined in a manner similar to Wallace and Gutzler (1981), i.e. as the difference of normalized anomalous geopotential heights in the centers of action of the respective teleconnection pattern:

$$Index(t) = \left(\frac{\widehat{Q'_S}(t)}{\sigma(\widehat{Q'_S})} \right) - \left(\frac{\widehat{Q'_N}(t)}{\sigma(\widehat{Q'_N})} \right), \tag{A.1}$$

where the hat denotes an area average and the prime the deviation from the long term mean, so that $\widehat{Q'_S}$ represents the timeseries of the area averaged (geopotential height) anomalies at the southern center of action, and $\widehat{Q'_N}$ the corresponding timeseries at the northern center. σ denotes the root mean square (rms) of a timeseries. The sign of such an index is positive if there is lower-than-normal

Teleconnection pattern	Level [hPa]	Area averages over northern center	Area averages over southern center	Index defined for
NA-SVR	300	55°–60°N, 32.5°–42.5°W	30°–32.5°N, 37.5°–45°W	SVR
eastern NA-WVR	300	65°–70°N, 27.5°–35°W	37.5°–40°N, 15°–22.5°W	WVR
western NA-WVR	300	62.5°–65°N, 77.5°–82.5°W	35°–37.5°N, 55°–62.5°W	WVR
NAO ('classic style')	1000	62.5°–67.5°N, 17.5°–22.5°W	32.5°–37.5°N, 22.5°–27.5°W	entire period 1958–1998

Table A.1: *Teleconnection indices derived from reanalyzed NCEP/NCAR geopotential height data (December to March, 1958–1998) following equation A.1.*

pressure (or geopotential height) at the northern center of action and higher-than-normal pressure (or geopotential height) at the southern center.

The indices for the three teleconnection patterns examined in chapter 4 were calculated from 300 hPa geopotential heights in the winter months December to March. The data were taken from from NCEP/NCAR reanalyses for the years 1958 to 1998 (see chapter 2). The geopotential heights were area averaged over the centers of action given in table A.1. The long term means and the rms values were calculated only for the polar vortex regime in which the corresponding teleconnection pattern emerges. The index timeseries are therefore only defined for a specific polar vortex regime. Several index timeseries were calculated from daily means, low pass filtered data (see appendix B.1), and monthly means, respectively.

North Atlantic Oscillation indices

An index for the North Atlantic Oscillation was derived in a similar manner as in equation A.1 from monthly mean 1000 hPa geopotential heights (from NCEP/NCAR reanalyses for December to March), averaged over 9 grid points close to Iceland and the Azores, respectively (see table A.1). This 'classic style' NAO index is defined for the entire NCEP/NCAR period from 1958 to 1998, i.e. it is not restricted to a certain polar vortex regime. It is positive if the Icelandic low and the Azores high are both strengthened so that the geopotential height difference between them is anomalously large.

The above index definition corresponds to the Hurrell (1995) station-based NAO index describing the polarity and strength of the North Atlantic Oscillation. That index is defined as the difference between normalized anomalies of sea level pressure at two stations near the subtropical high and the Icelandic low, respectively. In chapter 5, the connection between NAO index and sea surface temperature (SST) is examined in different datasets. Therefore, a NAO index based on station data was employed instead of an index derived from NCEP/NCAR reanalysis data. The NAO index used in chapter 5 was computed from January-to-March (JFM) mean sea level pressure anomalies (relative to the 1865–1984 mean) at Ponta Delgada, Azores, and Stykkisholmur/Reykjavik, Iceland. The pressure anomalies were normalized by division of each JFM mean pressure by the long-term standard deviation (1865–1984). The data were taken from J. Hurrell's website *http://www.cgd.ucar.edu/~jhurrell/nao.html*)

Some authors (e.g. Jones et al., 2003) suggested that a NAO index which uses Lisbon or Gibraltar as southern station instead of the Azores reflects more directly the strength of large scale fluctuations of the geostrophic wind over western Europe. They therefore recommended that, if the atmospheric circulation over Europe has to be examined, an Iceland-Lisbon or Iceland-Gibraltar NAO index would possibly take better into account the tilt in the streamlines over western Europe. However, the results presented in chapter 4 do not change much if a Lisbon-Iceland NAO index is used. The discussion in chapter 5 furthermore exhibits that the SST in the tropical North Atlantic is strongly connected to the geopotential height over the central subtropical North Atlantic. Hence, for the analyses in this thesis, it was appropriate to use NAO indices which incorporate data from the Azores.

Sea surface temperature indices

Two index timeseries for the (January-to-March mean) SST variability were used in chapter 5 in order to examine the covariability between atmosphere and ocean:

- The tropical North Atlantic region is known to be strongly influenced by both the NAO and the ENSO phenomenon. Therefore, an index for the tropical *North Atlantic (TNA) SST* was defined as the area average of SST over 10° – 20°N, 20° – 60°W in the NCEP/NCAR reanalysis dataset and over 12.5° – 22.5°N, 20° – 60°W in the Kaplan dataset.
- The SST anomaly averaged over the *NINO3.4* region (5°N – 5°S, 120° – 170°W) was used as an index for the ENSO phenomenon.

Appendix B

Analysis tools

B.1 Filter

The midlatitude atmospheric circulation is characterized by transient eddies and their interaction with the mean flow. In order to isolate eddies from different frequency domains, two types of filters were used: The 21-point filters introduced by Blackmon and Lau (1980) and a Fourier low pass filter. The filtering procedures were applied to the November-to-April data. In order to omit spurious fluctuations resulting from jumps in the data between two winters, the months November and April were discarded afterwards. Finally, the time mean over the discussed period was subtracted from the filtered data.

Blackmon and Lau (1980) filters

In order to isolate fluctuations from different frequency domains we used two so-called 21-point filters introduced by Blackmon and Lau (1980):

- a band pass filter leaving fluctuations with periods of 2.5 to 6 days (synoptic eddies) and
- a low pass filter leaving fluctuations with periods $\geq$ 10 days, i.e. more precisely, periods from 10 to 90 days (low frequency eddies).

These filters do not capture fluctuations with periods between 6 and 10 days. It is thereby possible to distinctly separate synoptic and low frequency eddies.

With the 21-point filters, each member of the filtered timeseries of a variable X at a certain gridpoint is calculated from 21 members of the unfiltered timeseries:

$$\tilde{X}(t_i) = a_0 X(t_i) + \sum_{p=1}^{10} a_p \left[X(t_{i+p}) + X(t_{i-p}) \right],$$

where $\tilde{X}(t)$ is the filtered timeseries, and $X(t)$ the unfiltered timeseries. The timestep of the timeseries is 24 hours, corresponding to the use of daily mean data. The filter weights a_i are listed in Blackmon and Lau (1980).

Fourier filter

Not only the Blackmon and Lau (1980) filters were applied in this thesis but also Fourier filters, by which the timeseries $X(t)$ is transformed into Fourier space by the finite Fourier transform

$$\tilde{X}(\nu) = \frac{1}{\sqrt{n}} \cdot \sum_{t=1}^{n} X(t) \cdot e^{-i2\pi\nu t} \qquad with \quad \frac{1}{2n} \leq \nu \leq \frac{1}{2},$$

where ν is a frequency component and n the length of the timeseries. The filtered timeseries is reconstructed using the inverse Fourier transform with each frequency weighted by the filter window $G(\nu)$

$$X'(t) = \frac{1}{\sqrt{n}} \cdot \sum_{1/\nu=2}^{2n} G(\nu)\tilde{X}(\nu) \cdot e^{i2\pi\nu t} \qquad with \quad 1 \leq t \leq n\,.$$

The filter window $G(\nu)$ is defined by the delimiting periods

$$\begin{array}{rcll} \text{PMAX} & = & 1/\nu_{max} & = \text{ real maximum filter period,} \\ \text{PMIN} & = & 1/\nu_{min} & = \text{ real minimum filter period,} \end{array}$$

such that

$$G(\nu) = \begin{cases} 0 & : \quad \nu < \nu_{max} \\ 1 & : \quad \nu_{max} \leq \nu \leq \nu_{min} \\ 0 & : \quad \nu_{min} < \nu \end{cases}.$$

In the examinations presented, the low frequency variability revealed to be well captured with a Fourier filter that removes fluctuations with periods shorter

than 15 days. This was tested with several low pass filters with different PMIN. Hence, for this thesis, a low pass Fourier filter with PMAX=2×n and PMIN=15 was applied. One may additionally introduce a smoothing to $G(\nu)$ in order to suppress secondary maxima that might occur for a pure rectangular filter, in particular in the case of a pulse which may then be falsely interpreted as an oscillation in the dataset. This problem is particularly important for a very narrow filter window. However, for the low pass filter used here it turned out that smoothing, e.g. by introduction of cosine tails of different widths, only had a weak influence on the features discussed in this thesis.

B.2 Wavelet analysis

The wavelet transform is a useful method to analyze timeseries that contain non-stationary power at different frequencies. Wavelet analysis decomposes a time-series into time/frequency space simultaneously. In contrast to classical Fourier analysis, the wavelet transform provides information on both, the amplitude of any (quasi-)periodic signals within the timeseries, and how this amplitude varies with time.

Assume that we have a timeseries X_n with equal time spacing δt and the time steps n=0, ..., N-1. Also assume that we have a wavelet function $\phi_0(\eta)$ that depends on a nondimensional time parameter η. The wavelet function must have zero mean and must be localized in both time and frequency space (Farge, 1992). A Morlet wavelet was applied for the wavelet analysis presented in chapter 5. However, also other types of functions may be used. An overview over possible wavelet functions is given by Torrence and Compo (1998). The Morlet wavelet consists of a plane wave modulated by a Gaussian:

$$\phi_0(\eta) = \pi^{-1/4} e^{i\omega_0\eta} e^{-\eta^2/2}, \tag{B.1}$$

where ω_0 is a nondimensional frequency. Corresponding to Torrence and Compo (1998), this frequency is taken to be 6 in order to satisfy the above mentioned admissibility condition for wavelets (Farge, 1992).

The continuous wavelet transform of a discrete timeseries X_n is defined as the convolution of X_n with ϕ^*, a scaled and translated version of $\phi_0(\eta)$:

$$W_n(s) = \sum_{m=0}^{N-1} X_m \phi^* \left[\frac{(m-n)\delta t}{s} \right], \tag{B.2}$$

where the asterisk indicates the complex conjugate of equation B.1. ϕ^* is normalized to have unit energy at each scale s so that the wavelet transforms at each scale s are directly comparable to each other and to the transforms of other timeseries. The scaling procedure was explained in detail by Torrence and Compo (1998). By varying the wavelet scale s and translating along the localized time index n, one can construct a picture showing both the amplitude of fluctuations versus the scale and how this amplitude varies with time. As suggested by Torrence and Compo (1998) the wavelet in chapter 5 was calculated in Fourier space. The wavelet function $\psi(\eta)$ is in general complex. Thus, the wavelet transform $W_n(s)$ is also complex and can be divided into its real and imaginary parts or into amplitude and phase. In this thesis, however, the wavelet power spectrum $\mid W_n(s) \mid^2$ is discussed.

Once a wavelet function is chosen, it is necessary to choose a set of scales s to use in the wavelet transform. It is convenient to write the scales as fractional powers of two (Torrence and Compo, 1998)

$$s_j = s_0 2^{j\delta j}, \qquad j = 0, 1, ..., J \ , \tag{B.3}$$

$$J = \delta j^{-1} log_2(N\delta t/s_0), \tag{B.4}$$

where s_0 is the smallest recoverable scale and J determines the largest scale. s_0 should be chosen so that the equivalent Fourier period (see Torrence and Compo, 1998) is approximately $2\delta t$. For the wavelet analysis presented here, we used N = 134, $\delta t = 1$ yr, $s_o = 2$ yr, $\delta j = 0.25$, J = 24. The value of δj appears adequate to provide a smooth picture of wavelet power.

Since one is dealing with timeseries of finite length, errors will occur at the (temporal) beginning and end of the wavelet power spectrum. This is due to the Fourier transform used to solve equation B.2 which assumes that the data is cyclic. The end of the timeseries may therefore be padded with zeroes before computing the wavelet transform in order to bring the total length of the timeseries N up to the next-higher power of two. Zero padding, however, introduces discontinuities at the endpoints of the wavelet power spectrum and decreases the amplitude near the edges. This becomes more evident as one goes to larger scales because more zeroes enter the analysis. The cross-hatched area in Fig. 5.3, the so-called cone of influence, indicates the regions of the wavelet power spectrum in which the above-mentioned edge effects become important. It is defined here as the e-folding time for the autocorrelation of wavelet power at each scale.

A more detailed description of the wavelet analysis concept is given by Torrence and Compo (1998).

B.3 Significance tests

In this thesis, anomalies from long term means or differences between the two stratospheric polar vortex regimes are discussed as well as correlation and regression coefficients. The methods for testing their statistical significance are described in the following.

t-Test

When discussing anomalies from long term means or differences between the two stratospheric polar vortex regimes, the question arises if these deviations are reliable or just random. In order to check this, it is hypothesized that the averages of the compared variables are similar:

$$\bar{x}_1 = \bar{x}_2 \ . \tag{B.5}$$

This hypothesis is referred to as the 'null hypothesis'. It will be verified by applying a so-called *t-test*. $\bar{x}_1$ and $\bar{x}_2$ are the average values of two random samples $X_1(x_{11}, x_{12}, ...x_{1n_1})$ and $X_2(x_{21}, x_{22}, ...x_{2n_2})$ of sample size n_1 and n_2, respectively. It is assumed that each sample realization x_{ij} is independent from the other realizations and that the universe from which the samples are extracted is normally distributed. In this thesis, the samples consist of either monthly means from the strong or weak polar vortex regime or of (persistent) episodes selected with the method described in chapter 4, section 4.2. With some justification these 'sample realizations' may be regarded as statistically independent.

Assuming that the variances of the universes are unknown but equal, the following test statistic is calculated:

$$t = \frac{\bar{x}_1 - \bar{x}_2}{\sqrt{\left(\frac{n_1+n_2}{n_1 n_2}\right)\left(\frac{(n_1-1)s_1^2+(n_2-1)s_2^2}{n_1+n_2-2}\right)}} \ , \tag{B.6}$$

where s_1 and s_2 are the standard deviations of the random samples. Under the assumption that the null hypothesis is true, the test statistic t is student-t distributed with $\nu = n_1 + n_2 - 2$ degrees of freedom.

However, the variances of universes are often not equal. In this case, a modified test statistic is calculated (e.g. Press et al., 1980):

$$\hat{t} = \frac{\bar{x}_1 - \bar{x}_2}{\sqrt{\frac{s_1^2}{n_1} + \frac{s_2^2}{n_2}}} \ . \tag{B.7}$$

The distribution of $\hat{t}$ is named Behrens-Fisher distribution if the null hypothesis is true. It may be regarded as approximately student-t distributed with $\hat{\nu}$ degrees of freedom, where

$$\hat{\nu} = \frac{\left(\frac{s_1^2}{n_1} + \frac{s_2^2}{n_2}\right)^2}{\frac{s_1^4}{n_1^2(n_1-1)} + \frac{s_2^4}{n_2^2(n_2-1)}} \,. \tag{B.8}$$

In this thesis, the null hypothesis was tested with the modified test statistic $\hat{t}$. The test statistic is compared with a critical value $t_{\hat{\nu},\alpha}$. The latter value depends on the degree of freedom $\hat{\nu}$ of the student-t distribution and on the selected significance level $(1-\alpha)$. Critical values are e.g. listed in Sachs (1997; chapter 15, section 141). If $|\hat{t}| \geq t_{\hat{\nu},\alpha}$, then the null hypothesis is rejected with a probability of error of $\alpha \cdot 100\%$, i.e. the averages $\bar{x}_1$ and $\bar{x}_2$ are not equal with a probability of $(1-\alpha) \cdot 100\%$. Their difference is significant above the $(1-\alpha) \cdot 100\%$-level.

Significance of correlations

For mapping correlations which clearly stand out of noise null hypothesis testing as described by Fisher (1958) was applied. Under the assumption that each realization of the two samples from which the correlation coefficient is computed is independent from the other realizations, the critical value for significant correlation only depends on the degrees of freedom and on the selected significance level. For the 20 or 30 year periods of January-to-March (JFM) means discussed in chapter 5, a correlation coefficient larger than ± 0.56 or ± 0.46, respectively, is significantly different from zero above the 99%-level under the assumption that each season is independent of the rest. The corresponding thresholds for the monthly means of December to March during 1958 to 1998 are about ± 0.2 for the entire period, about ± 0.3 for the months of the strong vortex regime, and ± 0.45 for the months of the weak vortex regime. While monthly means may still be regarded as independent from each other with some justification, this is not as clear for daily means or band and low pass filtered daily data. Such correlations can therefore not be tested with the method introduced above. Instead, their robustness was examined in this thesis by recalculating the correlations after applying different time filters.

However, as discussed by Nicholls (2001), the above mentioned method of testing the significance of correlations as well as the t-test described further above have to be applied very cautiously. One reason is that the significance levels are chosen arbitrarily and that the threshold values corresponding to them depend on the sample size. Thus, even physically reasonable correlations or anomalies can be ignored as nonsignificant if the sample size is small. However, Nicholls (2001)

also admits that plotting confidence levels, e.g., would result in very complex maps. Therefore, as also proposed by Nicholls (2001), our figures showing regression coefficients or anomalies display also the values in regions where the null hypothesis (correlation or anomaly not different from zero) could not be rejected. However, figures which only display the correlation coefficient revealed to be very complex. Thus, in order to keep the figures as simple as possible the zero contour as well as very small correlations are not displayed. This is admissible because we only discuss large-scale features (in the regions of interest).

B.4 Empirical Orthogonal Functions

Empirical Orthogonal Function (EOF) analysis is a linear multivariate method commonly used in meteorology and oceanography for isolating variability patterns that most efficiently explain the temporal variance of a geophysical field (von Storch and Zwiers, 1999).

Consider a geophysical data field $s(x,t)$ with values at N_s grid points for T observation times. This leads to a $T \times N_s$ data Matrix S in which each column contains the timeseries at one grid point. Let us further assume that the time mean at each grid point is zero and that the observations at each grid point are statistically independent. The $N_s \times N_s$ (co)variance matrix is then

$$C_{ss} = \frac{1}{T} S'S\,, \tag{B.9}$$

where the prime indicates the transpose. EOF analysis transforms the data into into a set of (time-invariant) orthonormal functions which completely span the real space. This is achieved by expanding the data matrix S by a set of linear combinations of the form

$$S \equiv \vec{s}(t) = \sum_{i=1}^{N_s} a_i(t)\, \vec{p_i}\,, \tag{B.10}$$

with the real vectors $\vec{p_i}$ with length N_s, and $a_i(t) = \vec{p_i}'\, \vec{s}(t)$ representing a temporal expansion coefficient with length T. EOF analysis determines the set of linear combinations that describe maximum variance, while the $\vec{p_i}$ are subject to the orthonormality constraint

$$\vec{p_i}'\vec{p_j} = \begin{cases} 1 & if \quad i = j \\ 0 & if \quad i \neq j \end{cases}\,. \tag{B.11}$$

The procedure is equivalent to maximizing the (co)variance $\langle a_i(t)\, a_j(t)\rangle_t = \frac{1}{T}\vec{p_i}'S'S\vec{p_i}$ for $i,j = 1,...,N_s$, where $\langle\ \ \rangle_t$ denotes a time mean. This leads to the eigenvalue problem

$$C_{ss}\vec{p_i} = \lambda_i\vec{p_i} \qquad or \qquad (C_{ss} - \lambda I)\,\vec{p_i} = 0, \tag{B.12}$$

where the vector $\vec{p_i}$ is the eigenvector associated with the eigenvalue λ_i of the matrix C_{ss}. I is the unit diagonal matrix of order N_s. λI then forms a diagonal matrix with the eigenvalues λ_i as diagonal elements. Since the covariance matrix C_{ss} is symmetric and positive definite, the eigenvalues $\lambda_1, ..., \lambda_{N_s}$ are real and positive. Each eigenvalue λ_i explains a fraction $\lambda_i / \sum_{j=1}^{N_s}\lambda_j$ of the total (explained) variance. The eigenvalues are arranged $\lambda_1 \geq \lambda_2 \geq ... \geq \lambda_{N_s}$ so that the first eigenvector $\vec{p_1}$ explains the largest fraction of variance. The eigenvectors $\vec{p_i}$ are referred to as EOF modes. The temporal expansion coefficients $a_i(t)$ are often called Principal Components (PCs) since EOF analysis is also often referred to as Principal Component analysis (PCA). The orthonormality constraint requires that the PCs are uncorrelated and that the variance of each PC is equal to the corresponding eigenvalue λ_i.

EOF analysis extracts the most efficient patterns for explaining the temporal variance integrated over the analysis domain within the constraints of spatial and temporal orthogonality (Cheng and Dunkerton, 1995). However, real dynamical processes are not necessarily associated with spatially orthogonal patterns or uncorrelated timeseries. Thus, patterns derived by EOF analysis do not necessarily display the real dynamical structure or the physical processes associated with it. This is particularly true for second and higher order modes, whereas it is often possible to relate the first EOF mode to a known physical process. However, as shown by Dommenget et al. (2002), this may also fail. Furthermore, the EOFs often reveal to be sensitive to the spatial domain selected for the analysis (Richman, 1986). Moreover, since EOFs are based on a finite number of realizations, it may well be that eigenvectors are mixed and the true eigenvector is a linear combination of two or more EOFs (North et al., 1982). According to North's 'Rule of Thumb' two eigenvectors may be regarded as well separated if the difference between the corresponding eigenvalue λ_i and its neighboring eigenvalue is larger than the sampling error $\Delta\lambda_i \approx \sqrt{\frac{2}{T}}\lambda_i$. Modes derived by EOF analysis should therefore be interpreted with caution. The EOF modes discussed and presented in this thesis significantly reappear in simple point-to-point correlation analyses and are well separated from other EOF modes.

In order to identify the leading coupled mode of North Atlantic storm track variability Rogers (1997) applied 'rotated EOF analysis'. This method linearly transforms (rotates) a subset of (lower order) EOFs (e.g. Richman, 1986) in order to obtain statistically robust regional patterns of variability. However, like the EOFs isolated with 'simple' EOF analysis, the rotated EOFs do not necessarily

correspond to a real physical process (Dommenget et al., 2002).

B.5 Singular Value Decomposition

Singular Value Decomposition (SVD) analysis was used for this thesis in order to investigate coherent structures of covariance between the atmospheric circulation in the troposphere and the stratosphere. SVD analysis is a linear multivariate analysis method like the EOF analysis (appendix B.4) and can be understood as a generalization of the latter (Bretherton et al., 1992; Wallace et al., 1992). SVD maximizes the covariance between two (geophysical) fields subjected to the constraint of spatial orthogonality.

Following Bretherton et al. (1992), a 'left' field $s(x,t)$ and a 'right' field $z(y,t)$ with values at N_s and N_z grid points, respectively, are given for T observation times. The time averages $\langle s(x,t)\rangle_t$ and $\langle z(y,t)\rangle_t$ over all T are assumed to be zero at every grid point x and y, respectively, and the observations at each grid point are assumed to be statistically independent from each other. The two datasets can be viewed as a $T \times N_s$ matrix S and a $T \times N_z$ matrix Z where the grid points are represented by columns and the timesteps by rows. The covariance matrix C_{sz} is then

$$C_{sz} = \frac{1}{T} S'Z \qquad (N_s \times N_z)\,, \tag{B.13}$$

where the prime indicates the transpose. SVD analysis determines linear combinations of the form $S \equiv \vec{s}(t) = \sum_{i=1}^{d} a_i(t)\,\vec{p_i}$ and $Z \equiv \vec{z}(t) = \sum_{i=1}^{d} b_i(t)\,\vec{q_i}$ for i=1,2,...,d , where $d = min(N_s, N_z)$. $\vec{p_i}$ and $\vec{q_i}$ are real vectors ('patterns') with length N_s and N_z, respectively. $a_i(t)$ and $b_i(t)$ represent temporal expansion coefficients with length T. The linear combinations are selected such that the covariance between the new variables

$$\langle a_i(t)\,b_i(t)\rangle_t = \vec{p_i}'\,C_{sz}\,\vec{q_i}\,, \qquad for \quad i = 1, ..., d\,, \tag{B.14}$$

is maximized regarding the orthonormality constraint

$$\vec{p_i}'\,\vec{p_j} = \vec{q_i}'\,\vec{q_j} = \begin{cases} 1 & if \quad i = j \\ 0 & if \quad i \neq j \end{cases}\,. \tag{B.15}$$

The application of a Lagrange multiplier σ leads to the following set of equations:

$$\begin{aligned} C_{sz}\vec{q_i} &= \sigma\vec{p_i}\,, \\ C_{sz}\vec{p_i} &= \sigma\vec{q_i}\,. \end{aligned} \tag{B.16}$$

Following Bretherton et al. (1992), the constrained maximizing problem is then uniquely solved by singular value decomposition of the covariance matrix C_{sz}:

$$C_{sz} = P\Lambda Q'\,, \tag{B.17}$$

where $P(N_s \times r)$ and Q $(N_z \times r)$ are column orthonormal matrices, and r is the rank of the covariance matrix C_{sz}. Λ is a $N_s \times N_z$ matrix whose elements are equal to zero except for the first r diagonal values $\sigma_1, ...\sigma_r$. The σ_i are nonnegative numbers called 'singular values'. Their square values, ${\sigma_i}^2$, are the r nonzero eigenvalues of $C'_{sz}C_{sz}$ and $C_{sz}C'_{sz}$ and, thus,

$$\langle a_i(t)\, b_i(t)\rangle_t = \sigma_i\,. \tag{B.18}$$

The first r column vectors of P and Q, i.e. the variability patterns $\vec{p_1}, ..., \vec{p_r}$ and $\vec{q_1}, ..., \vec{q_r}$, are the left and right 'singular vectors'. If the σ_i are ordered such that that $\sigma_1 \geq \sigma_2 \geq ... \geq \sigma_r$ then the first mode with the right singular vector $\vec{p_1}$ and the left singular vector $\vec{q_1}$ describes the largest fraction of covariance between the two fields. The temporal expansion coefficients can be determined by projecting the original data onto the singular vectors of the corresponding field

$$\begin{aligned} a_i(t) &= \vec{p_i}'\,\vec{s}(t)\,, \\ b_i(t) &= \vec{q_i}'\,\vec{z}(t)\,. \end{aligned} \tag{B.19}$$

The total (squared) covariance explained by a single pair of patterns $(\vec{p_i}\ \vec{q_i})$ is ${\sigma_i}^2$, so that the squared covariance fraction explained by a the ith pair of patterns is (Bretherton et al., 1992):

$$SFC_i \equiv \frac{{\sigma_i}^2}{\sum_{j=1}^{r} {\sigma_j}^2}\,. \tag{B.20}$$

In order to simplify the physical interpretation of the statistical results gained by an SVD analysis, homogeneous and heterogeneous regression maps may be generated following Bretherton et al. (1992). The i th left (right) homogeneous regression pattern represents a map of regression coefficients derived from regressing the timeseries of field $s(x,t)$ $(z(y,t))$ at every grid point x (y) onto the i th left (right) expansion coefficient $a_i(t)$ $(b_i(t))$. The map thus describes the covarying part of the left (right) field. The i th left (right) heterogeneous regression map is in turn defined as the regression map of the timeseries of the left (right) field at every grid point onto the i th right (left) expansion coefficient $b_i(t)$ $(a_i(t))$. This map describes, how the variability in one field is related to fluctuations of the expansion coefficient of the other field. For this thesis, the timeseries at each grid point of field $s(x,t)$ and $z(y,t)$ were regressed onto standardized expansion coefficients. Hence, the regression coefficients display mean anomalies occurring if the anomaly of the temporal expansion coefficient is equal to one standard deviation.

Corresponding to the EOF analysis method, the variability modes isolated by SVD analysis do not necessarily represent real physical modes. This is particularly true for higher order modes. Hence, variability modes derived by methods like EOF or SVD analysis have to be interpreted with caution.

B.6 Eliassen-Palm flux

Interactions between eddy fluxes and the mean flow can be described with the Eliassen-Palm flux (Eliassen and Palm 1961; Edmon et al. 1980). This so-called E-P flux is defined as a fictious vector in the meridional-vertical plane, with the eddy momentum flux as the meridional component and the meridional eddy flux of sensible heat as the vertical component. In case of a beta-plane geometry with pressure p as vertical component, the E-P flux $\vec{F} = (F_\phi, F_p)$ is given in the quasigeostrophic approximation by

$$F_\phi = -R\,cos\Phi\,[u^* v^*]\,, \tag{B.21}$$

$$F_p = f\,R\,cos\Phi\,\frac{[v^*\theta^*]}{\frac{\partial\theta_R}{\partial p}}\,, \tag{B.22}$$

where square brackets and asterisks denote zonal means and departures therefrom, R is the Earth's radius, Φ the latitude, u and v are the zonal and meridional wind, f is the Coriolis parameter, and θ is the potential temperature. θ_R is the zonal and time mean potential temperature. For the derivation of the equations

see e.g. Edmon et al. (1980) or Peixoto and Oort (1992). Due to the quasi-geostrophic approximation, the version of the E-P flux used in this thesis is not valid in the tropics.

The net effects of the eddies on the mean flow can be studied through the divergence of the E-P flux. In order to clarify these eddy effects, Andrews and McIntyre (1976) introduced the transformed Eulerian mean flow equations by applying a 'residual mean circulation'. The 'residual mean circulation' $(\tilde{v}, \tilde{\omega})$ can be understood as that part of the mean meridional circulation which is not balanced by the convergence of the eddy enthalpy flux. This concept will not be further discussed here. The transformed mean flow equations reduce in the quasigeostrophic framework to

$$\frac{\partial [u]}{\partial t} - f\tilde{v} - [\tilde{F}r] = \frac{1}{R\,cos\Phi} \nabla \cdot \vec{F}\,, \tag{B.23}$$

$$\frac{\partial [\theta]}{\partial t} + \tilde{\omega}\frac{\partial \theta_R}{\partial p} = [\tilde{Q}]\,, \tag{B.24}$$

$$\frac{1}{R\,cos\Phi}\frac{\partial\,(\tilde{v}\,cos\Phi)}{\partial \Phi} + \frac{\partial \tilde{\omega}}{\partial p} = 0\,, \tag{B.25}$$

where $[\tilde{F}r]$ and $[\tilde{Q}]$ are Eulerian mean friction and heating, respectively. $\tilde{v}$ and $\tilde{\omega}$ are the meridional and vertical components of the residual circulation

$$\tilde{v} = [v] - \frac{\partial}{\partial p}\left(\frac{[v^*\theta^*]}{\partial \theta_R / \partial p}\right)\,, \tag{B.26}$$

$$\tilde{\omega} = [\omega] + \frac{1}{R\,cos\Phi}\frac{\partial}{\partial \Phi}\left(\frac{[v^*\theta^*]\,cos\Phi}{\partial \theta_R / \partial p}\right)\,. \tag{B.27}$$

Within the quasigeostrophic framework, the E-P flux divergence $\nabla \cdot \vec{F}$ represents the only internal forcing of the mean state by the eddies. A divergent E-P flux would therefore exert a westerly forcing on the zonal mean zonal wind, whereas convergence is associated with easterly forcing. The E-P flux divergence is zero for steady, conservative wave-like disturbances of the zonal wind.

Edmon et al. (1980) showed that the E-P flux vectors are parallel to the projection of the local group velocity onto the meridional-vertical plane. This

approximation, however, is only valid for conditions, under which the group velocity concept is meaningful, i.e. if one is dealing with planetary waves of small enough meridional and vertical wavelength (Lighthill, 1978).

In order to obtain a graphical representation of the E-P flux and its divergence, the following procedure given by Edmon et al. (1980) was applied. Instead of the divergence of $\vec{F}$, the divergence weighted by the mass $\Delta m = 2\pi R^2 cos\Phi d\Phi(dp/g)$ of an annular ring $d\Phi dp$ was derived:

$$\int \nabla \cdot \vec{F} dm = \int\int \Delta d\Phi dp \,, \tag{B.28}$$

where g is the gravitational acceleration and Δ is the natural form of the E-P flux divergence

$$\Delta = \frac{\partial}{\partial \Phi}\left(\frac{2\pi R}{g} cos\Phi \, F_\Phi\right) + \frac{\partial}{\partial p}\left(\frac{2\pi R^2}{g} cos\Phi \, F_p\right) . \tag{B.29}$$

The corresponding version of the E-P flux is then

$$\hat{F_\Phi} = \frac{2\pi R}{g} cos\Phi \, F_\Phi = -\frac{2\pi R^2}{g} cos^2\Phi \, [u^* v^*] \,, \tag{B.30}$$

$$\hat{F_p} = \frac{2\pi R^2}{g} cos\Phi \, F_p = \frac{2\pi R^3}{g} f \, cos^2\Phi \, [v^* \theta^*] \, (\partial \theta_R / \partial p)^{-1} \,. \tag{B.31}$$

Since only long term means are discussed in this thesis, the E-P fluxes can be separated into their transient and stationary components. Within the (quasi-)geostrophic framework, u, v, and θ can be approximated by derivatives of the geopotential height z

$$u = -\frac{g}{f}\frac{1}{R}\frac{\partial z}{\partial \Phi} \,, \qquad v = \frac{g}{f}\frac{1}{R \, cos\Phi}\frac{\partial z}{\partial \varphi} \,, \qquad \theta = -\frac{g}{h(p)}\frac{\partial z}{\partial p} \,, \tag{B.32}$$

where φ is the longitude and $h(p)$ the static stability parameter

$$h(p) = \frac{R_{gas}}{p}\left(\frac{p}{p_R}\right)^\kappa \,, \tag{B.33}$$

with the gas constant R_{gas} for dry air 287 $\mathrm{Jkg^{-1}K^{-1}}$, the standard reference pressure $p_R = 1000$ hPa, and the adiabatic exponent $\kappa = 0.286$. This approximation

was used for this thesis because of the enormously large amount of data which would be associated with daily data records for the three variables u, v, and θ on all pressure levels. This method may reduce the accuracy of E-P fluxes and their divergence. Stationary E-P fluxes calculated from monthly means of u, v, and θ, however, show the same major characteristics as those derived by using the above approximations.

In chapter 3, E-P fluxes and their divergences (Eq. B.29 to B.31) are discussed for the strong and the weak vortex regime as well as the differences between the two regimes. Horizontal and vertical derivations were approximated by centered differences. Since vertical derivatives are influenced by boundary effects the at the surface and at the upper boundary layer of the reanalysis model, the figures in chapter 3 therefore only display values for the layers between 700 hPa and 30 hPa.

B.7 Maximum Eady growth rate

The growth rate of the most unstable wave in the Eady model (Eady, 1949; see also James, 1994) is a measure for the baroclinic production of transient eddies and is therefore used or explaining the storm track behavior in this thesis. It is more briefly named the (maximum) Eady growth rate σ_{BI} and describes the degree of baroclinic instability of flows and, thus, the disposition for wave-like disturbances to grow.

$$\sigma_{BI} = 0.31 \cdot f \cdot \left| \frac{\partial \vec{v}}{\partial z} \right| \cdot N^{-1} \; . \tag{B.34}$$

where f is the Coriolis parameter, $\vec{v}$ the horizontal wind (u, v) of the mean flow, and N the Brunt-Väisällä frequency

$$N = \sqrt{\frac{g}{\theta} \frac{\partial \theta}{\partial z}} \, , \tag{B.35}$$

with the gravitational acceleration g and the potential temperature θ. The growth rate of baroclinic eddies depends on the static stability and on the vertical wind shear or, in the framework of the thermal wind balance, on the meridional temperature gradient.

The (maximum) Eady growth rate was calculated for the lower troposphere (700 hPa) for this study, because it is a precondition for the growth of baroclinic wave-like disturbances that an increased vertical wind shear (or meridional temperature gradient) reaches down to the surface (James, 1994). The vertical derivatives were approximated by centered differences between the 500 hPa and the 925 hPa levels.

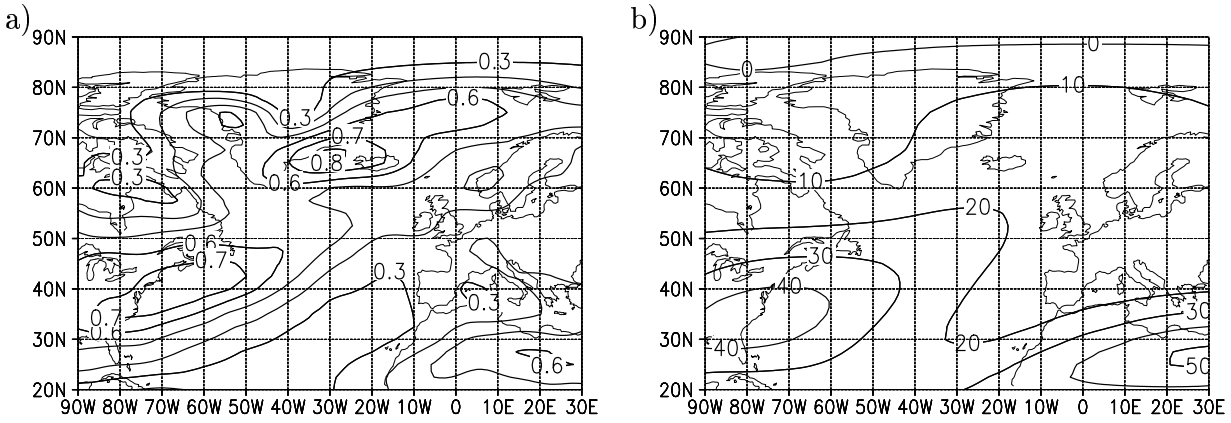

Figure B.1: *Time mean (a) maximum Eady growth rate at 700 hPa [d^{-1}] and (b) zonal wind at 200 hPa [m/s] calculated from NCEP/NCAR reanalysis data for the years 1958 – 1998.*

Fig. B.1a shows that the mean Eady growth rate at 700 hPa has three major maxima in the North Atlantic sector. One is located between 35°N and 45°N off the North American east coast. This coincides with the position of the North Atlantic subtropical jet (Fig. B.1b). Most of the storms crossing the North Atlantic develop in this area. Another maximum of the growth rate is located in the North African jet region. The third maximum is situated over the Denmark Strait between Greenland and Iceland. This region is characterized by strong meridional winds in the upper troposphere. It turns out that, in all cases discussed in chapter 3, the anomalies of the Eady growth rate are structurally similar to the anomalies of the upper tropospheric zonal wind. This may be explained by the strong association of the Eady growth rate with the vertical wind shear.

Bibliography

[1] Ambaum, M. H. P., and B. J. Hoskins, 2002: The NAO troposphere-stratosphere connection. *J. Climate*, **15,** 1969–1978.

[2] Andrews, D. G., and M. E. McIntyre, 1976: Planetary waves in horizontal and vertical shear: The Generalized Eliassen-Palm relation and mean zonal acceleration. *J. Atmos. Sci.*, **33,** 2031–2048.

[3] Andrews, D. G., J. R. Holton, and C. B. Leovy, 1987: *Middle Atmosphere Dynamics*. Academic Press, Orlando, 487 pp.

[4] Appenzeller, C., T. F. Stocker, and M. Anklin, 1998: North Atlantic Oscillation dynamics recorded in Greenland ice cores. *Science*, **282,** 446–449.

[5] Baldwin, M. P., X. H. Cheng, and T. J. Dunkerton, 1994: Observed correlations between winter-mean tropospheric and stratospheric circulation anomalies. *Geophys. Res. Lett.*, **21,** 1141–1144.

[6] Baldwin, M. P., and T. J. Dunkerton, 1999: Propagation of the Arctic Oscillation from the stratosphere to the troposphere. *J. Geophys. Res.*, **104,** 30,937–30,946.

[7] Baldwin, M. P., and T. J. Dunkerton, 2001: Stratospheric harbingers of anomalous weather regimes. *Science*, **294,** 581-584.

[8] Barnston, A. G., and R. E. Livezey, 1987: Classification, seasonality and persistence of low-frequency atmospheric circulation patterns. *Mon. Wea. Rev.*, **115,** 1083–1126.

[9] Barsugli, J. J., and D. S. Battisti, 1998: The basic effects of atmosphere-ocean thermal coupling on midlatitude variability. *J. Atmos. Sci.*, **55,** 477–493.

[10] Bjerknes, J., 1964: Atlantic air-sea interaction. *Adv. Geophys.*, **10,** 1–82.

[11] Bjerknes, J., 1969: Atmospheric teleconnections from the equatorial Pacific. *Mon. Wea. Rev.*, **97,** 163–172.

[12] Black, R. X., 2002: Stratospheric forcing of surface climate in the Arctic Oscillation. *J.Climate*, **15,** 268-277.

[13] Blackmon, M. L., and N.-C. Lau, 1980: Regional characteristics of the Northern Hemisphere wintertime circulation: A comparison of the simulation of a GFDL general circulation model with observations. *J. Atmos. Sci.*, **37,** 497–514.

[14] Bretherton, C. S., C. Smith, and J. M. Wallace, 1992: An intercomparison of methods for finding coupled patterns in climate data. *J. Climate*, **5,** 541–560.

[15] Bretherton, C. S., and D. S. Battisti, 2000: An interpretation of the results from atmospheric general circulation models forced by the time history of the observed sea surface temperature distribution. *Geophys. Res. Lett.*, **27,** 767–770.

[16] Cai, M., and H. M. van den Dool, 1994: Dynamical decomposition of low-frequency tendencies. *J. Atmos. Sci.*, **51,** 2086–2100.

[17] Castanheira, J. M., H.-F. Graf, C. C. DaCamara, and A. Rocha, 2002: Using a physical reference framework to study global circulation variability. *J. Atmos. Sci.*, **59,** 1490–1501.

[18] Castanheira, J. M., and H.-F. Graf, 2003: North Pacific-North Atlantic relationships under stratospheric control? *J. Geophys. Res.*, **108**, Art. No. 4036, doi:10.1029/2002JD002754.

[19] Cayan, D. R., 1992: Latent and sensible heat flux anomalies over the northern oceans: The connection to monthly atmospheric circulation. *J. Climate*, **5,** 354–370.

[20] Cavalieri, D. J., 2002: A link between Fram Strait sea ice export and atmospheric planetary wave phase. *Geophys. Res. Lett.*, **29,** Art. No. 1614, doi:10.1029/2002GL014684.

[21] Charney, J. G., and P. G. Drazin, 1961: Propagation of planetary-scale disturbances from the lower into the upper atmosphere. *J. Geophys. Res.*, **66,** 83–109.

[22] Chen, W., H.-F. Graf, and M. Takahashi, 2002: Observed interannual oscillations of planetary wave forcing in the Northern Hemisphere winter. *Geophys. Res. Lett.*, **29,** Art. No. 2073, doi:10.1029/2002GL016062.

[23] Cheng, X. H., and T. J. Dunkerton, 1995: Orthogonal rotation of spatial patterns derived from singular-value decomposition analysis. *J. Climate*, **8,** 2631–2643.

[24] Christiansen, B., 2003: Evidence for nonlinear climate change: Two stratospheric regimes and a regime shift. *J. Climate*, submitted. [Available online at http://dmiweb.dmi.dk/fsweb/solar-terrestrial/staff/boc/publist.html]

[25] Corti, S., F. Molteni, and T. N. Palmer, 1999: Signature of recent climate change in frequencies of natural atmospheric regimes. *Nature*, **398,** 799–802.

[26] Cubasch,U., R. Voss, G. C. Hegerl, J. Waskewitz, and T. J. Crowley, 1997: Simulation of the influence of solar radiation variations on the global climate with an ocean-atmosphere general circulation model. *Climate Dynamics*, **13,** 757–767.

[27] Curtis, S., and S. Hastenrath, 1995: Forcing of anomalous surface temperature evolution in the tropical Atlantic sector during Pacific warm events. *J. Geophys. Res.*, **100,** 15,835–15,847.

[28] Delworth, T. L., and K. W. Dixon, 2000: Implications of the recent trend in the Arctic/North Atlantic Oscillation for the North Atlantic thermohaline circulation. *J. Climate*, **13,** 3721–3727.

[29] Deser, C., 2000: On the teleconnectivity of the 'Arctic Oscillation'. *Geophys. Res. Lett.*, **27,** 779–782.

[30] Deser, C., and M. L. Blackmon, 1993: Surface climate variations over the North Atlantic Ocean during winter: 1900–1989. *J. Climate*, **6,** 1743–1753.

[31] Deser, C., and M. S. Timlin, 1997: Atmosphere-ocean interaction on weekly timescales in the North Atlantic and Pacific. *J. Climate*, **10,** 393–408.

[32] Dickson, R. R., T. J. Osborn, J. W. Hurrell, J. Meincke, J. Blindheim, B. Adlandsvik, T. Vinje, G. Alekseev, and W. Maslowski, 2000: The Arctic Ocean response to the North Atlantic oscillation. *J. Climate*, **13,** 2671-2696.

[33] Dommenget, D., and M. Latif, 2002: A cautionary note on the interpretation of EOFs. *J. Climate*, **15,** 216–225.

[34] Eady, E. T., 1949: Long waves and cyclone waves. *Tellus*, **1,** 33–52.

[35] Edmon, H. J., B. J. Hoskins, and M. E. McIntyre, 1980: Eliassen-Palm cross-sections for the troposphere. *J. Atmos. Sci.*, **37,** 2600–2616.

[36] Eliassen, A., and E. Palm, 1961: On the transfer of energy in stationary mountain waves. *Geofys. Publ.*, **22,** 1–23.

[37] Enfield, D. B., and D. A. Mayer, 1997: Tropical Atlantic sea surface temperature variability and its relation to El Niño–Southern Oscillation. *J. Geophys. Res.*, **102,** 929–945.

[38] Farge, M., 1992: Wavelet transforms and their applications to turbulence. *Ann. Rev. Fluid Mech.*, **24,** 395–457.

[39] Feldstein, S., 1998: The growth and decay of low-frequency anomalies in a GCM. *J. Atmos. Sci.*, **55,** 415–428.

[40] Feldstein, S. B., 2000: The timescale, power spectra, and climate noise properties of teleconnection patterns. *J. Climate*, **13,** 4430–4440.

[41] Feldstein, S. B., 2002: Fundamental mechanisms of the growth and decay of the PNA teleconnection pattern *Quart. J. Roy. Met. Soc.*, **128,** 775–796.

[42] Feldstein, S. B., 2003: The dynamics of NAO teleconnection pattern growth and decay. *Quart. J. Roy. Met. Soc.*, **129,** 901–924.

[43] Feldstein, S., and S. Lee, 1996: Mechanisms of zonal index variability in an aquaplanet GCM. *J. Atmos. Sci.*, **53,** 3541–3555.

[44] Feser, F., H.-F. Graf, and J. Perlwitz, 2000: Secular variability of the coupled tropospheric and stratospheric circulation in the GCM ECHAM 3/LSG. *Theoret. Appl. Meteor.,* **65,** 1–15.

[45] Fisher, R. A., 1958: *Statistical Methods for Research Workers.* 13th rev. ed., Oliver and Boyd, Edinburgh and London, 356 pp.

[46] Glowienka-Hense, R., 1990: The North Atlantic Oscillation in the Atlantic-European SLP. *Tellus*, **42,** 497–507.

[47] Graf, H.-F., J. Perlwitz, and I. Kirchner, 1994: Northern Hemisphere tropospheric mid-latitude circulation after violent volcanic eruptions. *Contrib. Atmos. Phys.*, **67,** 3–13.

[48] Graf, H.-F., J. Perlwitz, I. Kirchner, and I. Schult, 1995: Recent northern winter climate trends, ozone changes and increased greenhouse gas forcing. *Contrib. Atmos. Phys.*, **68,** 233–248.

[49] Graf, H.-F., J. Perlwitz, and I. Kirchner, 1997: Coupled modes of tropospheric and stratospheric circulation in nature and in models. In: *Stratospheric Processes and their Role in Climate (SPARC). Proceedings of the First SPARC General Assembly,* Vol. I, WMO/TD-No. 814, 129–132.

[50] Graf, H.-F., I. Kirchner, and J. Perlwitz, 1998: Changing lower stratospheric circulation: The role of ozone and greenhouse gases. *J. Geophys. Res.*, **103,** 11,251–11,261.

[51] Graf, H.-F., and J. M. Castanheira, 2001: Structural changes of climate variability. Report No. 330, Max-Planck-Institut für Meteorologie, Hamburg, 14pp. [Available online at http://www.mpimet.mpg.de]

[52] Grötzner, A., M. Latif, and T. P. Barnett, 1998: A decadal climate cycle in the North Atlantic Ocean as simulated by the ECHO coupled GCM. *J. Climate*, **11**, 831–847.

[53] Hameed, S., K. R. Sperber, and A. Meinster, 1993: Teleconnections of the Southern Oscillation in the tropical Atlantic sector in the OSU Coupled Upper Ocean–Atmosphere GCM. *J. Climate*, **6,** 487–498.

[54] Hartley, D. E., J. T. Villarin, R. X. Black, and C. A. Davies, 1998: A new perspective on the dynamical link between the stratosphere and troposphere. *Nature*, **391,** 471–474.

[55] Hastenrath, S., 2000: Upper air mechanisms of the Southern Oscillation in the tropical Atlantic sector. *J. Geophys. Res.*, **105,** 14,997–15,009.

[56] Hastenrath, S., L. C. de Castro, and P. Aceituno, 1987: The Southern Oscillation in the tropical Atlantic sector. *Contrib. Atmos. Phys.*, **60,** 447–463.

[57] Hilmer, M., and T. Jung., 2000: Evidence for a recent change in the link between the North Atlantic Oscillation and Arctic sea ice export. *Geophys. Res. Lett.*, **27,** 989-992.

[58] Hines, C. O., 1974: A possible mechanism for the production of sun-weather correlations. *J. Atmos. Sci.*, **31,** 589–591.

[59] Hoskins, B. J., and D. J. Karoly, 1981: The steady linear response of a spherical atmosphere to thermal and orographic forcing. *J. Atmos. Sci.*, **38,** 1179–1196.

[60] Hoskins, B. J., I. N. James, and G. H. White, 1983: The shape, propagation and mean-flow interaction of large-scale weather systems. *J. Atmos. Sci.*, **40,** 1595–1612.

[61] Hu, Y. Y., and K. K. Tung, 2002: Interannual and decadal variations of planetary wave activity, stratospheric cooling, and Northern Hemisphere Annular mode. *J. Climate*, **15,** 1659-1673.

[62] Hurrell, J. W., 1995: Decadal trends in the North Atlantic Oscillation: Regional temperatures and precipitation. *Science*, **269,** 676–679.

[63] Hurrell, J. W., and H. van Loon, 1997: Decadal variations in climate associated with the North Atlantic Oscillation. *Clim. Change*, **36,** 301–326.

[64] James, I. N., 1994: *Introduction to Circulating Atmospheres.* Cambridge University Press, Cambridge, 422 pp.

[65] James, I. N. and P. M. James, 1989: Ultra-low frequency variability in a simple atmospheric circulation model. *Nature*, **342,** 53–55.

[66] Jones, P. D., 1987: The early twentieth century Arctic high — Fact or fiction? *Clim. Dyn.*, **1,** 63–75.

[67] Jones, P. D., T. J. Osborn, and K. R. Briffa, 2003: Pressure-based measures of the North Atlantic Oscillation (NAO): A comparison and an assessment of changes in the strength of the NAO and its influence on surface climate parameters. In: *The North Atlantic Oscillation: Climatic Significance and Environmental Impact,* J. W. Hurrell, Y. Kushnir, G. Ottersen, and M. Visbeck, Eds., American Geophysical Union, Washington D.C., Geophysical Monograph 134, 51–62.

[68] Kalnay, E., M. Kanamitsu, R. Kistler, W. Collins, D. Deaven, L. Gandin, M. Iredell, S. Saha, G. White, J. Woollen, Y. Zhu, M. Chelliah, W. Ebisuzaki, W. Higgins, J. Janowiak, K. C. Mo, C. Ropelewski, J. Wang, A. Leetmaa, R. Reynolds, R. Jenne, and D. Joseph, 1996: The NCEP/NCAR 40-year reanalysis project. *Bull. Amer. Meteor. Soc.*, **77,** 437–472.

[69] Kaplan, A., Y. Kushnir, M. A. Cane, and M. B. Blumenthal, 1997: Reduced space optimal analysis for historical data sets: 136 years of Atlantic sea surface temperatures. *J. Geophys. Res.*, **102,** 27,835–27,860.

[70] Kaplan, A., M. A. Cane, Y. Kushnir, A. C. Clement, M. B. Blumenthal, and B. Rajagopalan, 1998: Analyses of global sea surface temperature 1856–1991. *J. Geophys. Res.*, **103,** 18,567–18,589.

[71] Kistler, R., E. Kalnay, W. Collins, S. Saha, G. White, J. Woollen, M. Chelliah, W. Ebisuzaki, M. Kanamitsu, V. Kousky, H. van den Dool, R. Jenne, M. Fiorino, 2001: The NCEP–NCAR 50-year reanalysis: Monthly means CD-ROM and documentation. *Bull. Amer. Meteor. Soc.*, **82,** 247–268.

[72] Kodera, K., M. Chiba, H. Koide, A. Kitoh, and Y. Nikaidou, 1996: Interannual variability of the winter stratosphere and troposphere in the Northern Hemisphere. *J. Meteor. Soc. Japan*, **74,** 365–382.

[73] Kodera, K., and H. Koide, 1997: Spatial and seasonal characteristics of recent decadal trends in the northern hemispheric troposphere and stratosphere. *J. Geophys. Res.*, **102,** 19,433–19,447.

[74] Kushnir, Y., 1994: Interdecadal variations in the North Atlantic sea surface temperature and associated atmospheric conditions. *J. Climate*, **7,** 141–157.

[75] Kushnir, Y., and I. M. Held, 1996: Equilibrium atmospheric response to North Atlantic SST anomalies. *J. Climate*, **9,** 1208–1220.

[76] Labitzke, K., 1987: Sunspots, the QBO, and the stratospheric temperature in the North Polar-region. *Geophys. Res. Lett.*, **14,** 535–537.

[77] Labitzke, K., and H. van Loon, 1988: Associations between the 11-year solar cycle, the QBO and the atmosphere. Part I: The troposphere and stratosphere in the Northern Hemisphere winter. *J. Atmos. Terr. Phys.*, **50,** 197–206.

[78] Labitzke, K., and H. van Loon, 1996: The effect on the stratosphere of three tropical volcanic eruptions. In: *The Mount Pinatubo Eruption. Effects on the Atmosphere and Climate,* G. Fiocco, D. Fuá, and G. Visconti, Eds., NATO ASI Series I, Vol. 42, Springer Verlag, Berlin/Heidelberg, 113–125.

[79] Labitzke, K., 1999: *Die Stratosphäre. Phänomene, Geschichte, Relevanz.* Springer-Verlag, Berlin/Heidelberg, 177 pp.

[80] Latif, M., and T. P. Barnett, 1994: Causes of decadal climate variability over the North Pacific and North America. *Science*, **266,** 634–637.

[81] Latif, M., and T. P. Barnett, 1996: Decadal climate variability over the North Pacific and North America: Dynamics and predictability. *J. Climate*, **9,** 2407–2423.

[82] Latif, M., K. Arpe, and E. Roeckner, 2000: Oceanic control of decadal North Atlantic sea level pressure variability in winter. *Geophys. Res. Lett.*, **27,** 727–730.

[83] Lighthill, M.J., 1978: *Waves in Fluids.* Cambridge University Press, Cambridge, 504 pp.

[84] Limpasuvan, V., and D. L. Hartmann, 2000: Wave-maintained annular modes of climate variability. *J. Climate*, **13,** 4414–4429.

[85] Luksch, U., 1996: Simulation of North Atlantic low-frequency SST variability. *J. Climate*, **9,** 2083–2092.

[86] Luksch, U., and H. von Storch, 1992: Modeling the low-frequency sea-surface temperature variability in the North Pacific. *J. Climate*, **5,** 893–906.

[87] Matsuno, T., 1970: Vertical propagation of stationary planetary waves in the winter Northern Hemisphere. *J. Atmos. Sci*, **27,** 871–883.

[88] Mehta, V. M., M. J. Suarez, J. V. Manganello, and T. L. Delworth, 2000: Oceanic influence on the North Atlantic Oscillation and associated Northern Hemisphere climate variations: 1959–1993. *Geophys. Res. Lett.*, **27,** 121–124.

[89] Mo, K. C., and R. E. Livezey, 1986: Tropical-extratropical geopotential height teleconnections during the Northern Hemisphere winter. *Mon. Wea. Rev.*, **114,** 2488–2515.

[90] Nicholls, N., 2001: The insignificance of significance testing. *Bull. Amer. Met. Soc.*, **81,** 981–986.

[91] Nobre, P., and J. Shukla, 1996: Variations of sea surface temperature, wind stress, and rainfall over the tropical Atlantic and South America. *J. Climate*, **9,** 2464–2479.

[92] North, G. R., T. L. Bell, R. F. Cahalan, and F. J. Moeng, 1982: Sampling errors in the estimation of Empirical Orthogonal Functions. *Mon. Wea. Rev.*, **110,** 699–706.

[93] Orlanski, I., 1998: Poleward deflection of storm tracks. *J. Atmos. Sci.*, **55,** 2577–2602.

[94] Pawson, S., K. Labitzke, R. Lenschow, B. Naujokat, B. Rajewski, M. Wiesner, and R.-C. Wohlfahrt, 1993: Climatology of the Northern Hemisphere stratosphere derived from Berlin analysis. Part 1: Monthly means. Meteorologische Abhandlung der FU Berlin, Serie A, Band 7, Heft 3.

[95] Pawson, S., and M. Fiorino, 1999: A comparison of reanalyses in the tropical stratosphere. Part 3: Inclusion of the pre-satellite data era. *Clim. Dyn.*, **15,** 241–250.

[96] Peixoto, J. P. and A. H. Oort, 1992: *Physics of Climate*. American Institute of Physics, New York, 520 pp.

[97] Peng, S., W. A. Robinson, and M. P. Hoerling, 1997: The modeled atmospheric response to midlatitude SST anomalies and its dependence on background circulation states. *J. Climate*, **10,** 971–987.

[98] Peng, S., and J. S. Whitaker, 1999: Mechanisms determining the atmospheric response to midlatitude SST anomalies. *J. Climate*, **12,** 1393–1408.

[99] Perlwitz, J., 2000: The dynamical link between the troposphere and stratosphere and its potential to affect climate. Ph.D. thesis, Examensarbeit No. 74, Max-Planck-Institut für Meteorologie, 147 pp.

[100] Perlwitz, J., and H.-F. Graf, 1995: The statistical connection between tropospheric and stratospheric circulation of the Northern Hemisphere in winter. *J. Climate*, **8,** 2281–2295.

[101] Perlwitz, J., H.-F. Graf, and R. Voss, 2000: The leading variability mode of the coupled troposphere-stratosphere winter circulation in different climate regimes. *J. Geophys. Res.*, **105,** 6915–6926.

[102] Perlwitz, J., and H.-F. Graf, 2001a: Troposphere-stratosphere dynamic coupling under strong and weak polar vortex conditions. *Geophys. Res. Lett.*, **28,** 271–274.

[103] Perlwitz, J., and H.-F. Graf, 2001b: The variability of the horizontal circulation in the troposphere and stratosphere — a comparison. *Theor. Appl. Climatol.*, **69,** 149–161.

[104] Perlwitz, J., and N. Harnik, 2003: Observational evidence of a stratospheric influence on the troposphere by planetary wave reflection. *J. Climate*, **16,** 3011–3026.

[105] Press, W. H., S. A. Teukolsky, W. T. Vetterling und B. P. Flannery, 1986: *Numerical Recipes: The Art of Scientific Computing.* Cambridge University Press (Cambridge), 818pp.

[106] Ramaswamy, V., M. D. Schwarzkopf, and W. J. Randel, 1996: Fingerprint of ozone depletion in the spatial and temporal pattern of recent lower-stratospheric cooling. *Nature*, **382,** 616–618.

[107] Raible, C. C., U. Luksch, K. Fraedrich, and R. Voss, 2001: North Atlantic decadal regimes in a coupled GCM simulation. *Clim. Dyn.*, **18,** 321–330.

[108] Reid, P. A., P. D. Jones, O. Brown, C. M. Goodess, and T.D. Davies, 2001: Assessments of the reliability of NCEP circulation data and relationships with surface climate by direct comparisons with station based data. *Clim. Res.*, **17,** 247–261.

[109] Richman, M. B., 1986: Rotation of Principal Components. *J. Climatol.*, **6,** 293–335.

[110] Rimbu, N., G. Lohmann, T. Felis, and J. Pätzold, 2003: Shift in ENSO teleconnections recorded by a northern Red Sea coral. *J. Climate*, **16,** 1414–1422.

[111] Rodwell, M. J., D. P. Rowell, and C. K. Folland, 1999: Oceanic forcing of the wintertime North Atlantic Oscillation and European climate. *Nature*, **398,** 320–323.

[112] Rogers, J. C., 1990: Patterns of low-frequency monthly sea-level pressure variability (1899–1986) and associated wave cyclone frequencies. *J. Climate*, **3,** 1364–1379.

[113] Rogers, J. C., 1997: North Atlantic storm track variability and its association to the North Atlantic Oscillation and climate variability of Northern Europe. *J. Climate*, **10,** 1635–1647.

[114] Sachs, L., 1999: *Angewandte Statistik. Anwendung statistischer Methoden.* Springer-Verlag, Berlin/Heidelberg, 884 pp.

[115] Saravanan, R., and P. Chang, 2000: Interaction between tropical Atlantic variability and El Niño–Southern Oscillation. *J. Climate*, **13,** 2177–2194.

[116] Shindell, D. T., R. L. Miller, G. A. Schmidt, and L. Pandolfo, 1999: Simulation of recent winter climate trends by greenhouse-gas forcing. *Nature*, **399,** 452–455.

[117] Thompson, D. W. J., and J. M. Wallace, 1998: The Arctic Oscillation signature in the wintertime geopotential height and temperature fields. *Geophys. Res. Lett.*, **25,** 1297–1300.

[118] Thompson, D. W. J., and J. M. Wallace, 2000: Annular modes in the extratropical circulation. Part I: Month-to-month variability. *J. Climate*, **13,** 1000–1016.

[119] Timmermann, A., M. Latif, R. Voss, and A. Grötzner, 1998: Northern Hemisphere interdecadal variability: A coupled air-sea mode. *J. Climate*, **11,** 1906–1931.

[120] Torrence, C., and G. P. Compo, 1998: A practical guide to wavelet analysis. *Bull. Amer. Met. Soc.*, **79,** 61–78.

[121] Trenberth, K. A., and D. A. Paolino, 1980: The Northern Hemisphere sea-level pressure data set: Trends, errors and discontinuities. *Mon. Wea. Rev.*, **108,** 855–872.

[122] Trigo, R. M., T. J. Osborn, and J. M. Corte-Real, 2002: The North Atlantic Oscillation influence on Europe: Climate impacts and associated physical mechanisms. *Clim. Res.*, **20,** 9–17.

[123] von Storch, H. and F. W. Zwiers, 1999: *Statistical Analysis in Climate Research.* Cambridge University Press, Cambridge, 494pp.

[124] Vinje, T., 2001: Fram Strait ice fluxes and atmospheric circulation: 1950-2000. *J. Climate*, **14,** 3508–3517.

[125] Visbeck, M., H. Cullen, G. Krahmann, and N. Naik, 1998: An ocean model's response to North Atlantic Oscillation-like wind forcing. *Geophys. Res. Lett.*, **25,** 4521–4524.

[126] Walker, G. T., 1924: Correlations in seasonal variations of weather. *IX. Mem. Ind. Meteorol. Dept.*, **24,** 275–332.

[127] Walker, G. T., and E. W. Bliss, 1932: World weather V. *Mem. Roy. Meteorol. Soc.*, **4,** 53–84.

[128] Wallace, J. M., and D. S. Gutzler, 1981: Teleconnections in the geopotential height field during the Northern Hemisphere winter. *Mon. Wea. Rev.*, **109,** 784–812.

[129] Wallace, J. M., and Q. Jiang, 1987: On the observed structure of the interannual variability of the atmosphere/ocean climate system. In: *Atmospheric and Oceanic Variability*, H. Cattle, Ed., Roy. Meteor. Soc., Reading, 17–43.

[130] Wallace, J. M., C. Smith, and, C. S. Bretherton, 1992: Singular value decomposition of wintertime sea-surface temperature and 500-mb height anomalies. *J. Climate*, **5,** 561–576.

[131] Walter, K., U. Luksch, and K. Fraedrich, 2001: A response climatology of idealized midlatitude thermal forcing experiments with and without a stormtrack. *J. Climate*, **14,** 467–484.

[132] Walter, K., and H.-F. Graf, 2002: On the changing nature of the regional connection between the North Atlantic Oscillation and sea surface temperature. *J. Geophys. Res.*, **107,** Art. No. 4338, doi:10.1029/2001JD000850.

Danksagung (Acknowledgements)

Zunächst möchte ich mich bei Hans-F. Graf für die Ermöglichung dieser Arbeit sowie für sein großes Interesse, zahlreiche fruchtbare Diskussionen und wertvolle Anregungen bedanken.

Mein Dank geht weiterhin an Herrn Prof. Dr. Klaus Fraedrich für sein Interesse und seine freundliche Bereitschaft, diese Arbeit zu begutachten.

Ein besonderer Dank geht an Ute Luksch, Judith Perlwitz und Christoph Raible für die konstruktive Kritik sowie für die vielen hilfreichen Diskussionen und Anregungen.

I would also like to thank José Castanheira and José Silvestre for scientifically inspiring discussions.

Den Kolleginnen und Kollegen am Max-Planck-Institut für Meteorologie und insbesondere der „Schlump-WG" gilt mein Dank für ihre stete Hilfsbereitschaft und die super Arbeitsatmosphäre.

Zu guter Letzt möchte ich mich bei meinen Eltern und bei Hinrich für die seelisch-moralische Unterstützung — vor allem während der Endphase dieser Arbeit — bedanken.